MICROSEISMIC MONITORING OF CHOCOLATE BAYOU TEXAS THE PLEASANT BAYOU NO. 2 GEOPRESSURED/GEOTHERMAL ENERGY TEST WELL PROGRAM

1981 ANNUAL PROGRESS REPORT

Microseismic Monitoring of
Chocolate Bayou Texas
The Pleasant Bayou No. 2
Geopressured/Geothermal Energy
Test Well Program

1981 Annual Progress Report

Prepared by
Frederick J. Mauk, Ph.D.
Teledyne Geotech

DISCLAIMER

This report has been produced directly from the best available copy.

Available from the National Technical Information Service, U. S. Department of Commerce, Springfield, Virginia 22161.

Price: Printed Copy A05
Microfiche A01

Codes are used for pricing all publications. The code is determined by the number of pages in the publication. Information pertaining to the pricing codes can be found in the current issues of the following publications, which are generally available in most libraries: Energy Research Abstracts (ERA): Government Reports Announcements and Index (GRA and I); Scientific and Technical Abstract Reports (STAR); and publication NTIS-PR-360, available from NTIS at the above address.

TABLE OF CONTENTS

ILLUSTRATIONS

TABLES

TR82-2

INTRODUCTION

Commercial utilization of the geopressured brines underlying the Gulf Coast
as unconventional geothermal-methane energy sources is dependent upon high
volumetric production rates. The production requirements for effective
withdrawal and disposal of these highly saline brines is believed to be near
3×10^4 bbl/day/well. Such high volumetric productions can alter substan-
tially the ambient state of stress of the local geological column potentially
resulting in reactivation of preexisting zones of weakness as well as causing
new fracture development.

To investigate normal ambient seismicity as well as potentially enhanced
seismic activity induced by brine production, Teledyne Geotech, with the
authorization of the Texas Bureau of Economic Geology, has conducted a seismic
monitoring program in the vicinity of the Chocolate Bayou geopressured test
well (the Pleasant Bayou No. 2) since September 1978. The Pleasant Bayou No.
2 well has been completed and perforated at depths of 14,467 - 14,707 feet
(4464.4 - 4482.7m). The brines produced from the Pleasant Bayou No. 2 well
are reinjected at a depth of 6226 - 6538 feet (1897.7 - 1992.8m) in the
Pleasant Bayou No. 1 well. This report describes the seismic monitoring net-
work and results obtained from January through November 1981.

THE BRAZORIA SEISMOGRAPH STATION DESIGN SPECIFICATIONS

The detection and analysis of seismic signals recorded by arrays or networks of seismographs ultimately depend upon the design specifications of the instrumentation. Although earth movements can cover a spectrum of frequencies from DC to kilohertz with amplitudes which may range over many orders of magnitude, seismic instruments are capable of faithfully reproducing amplified replicas of these movements only over a finite spectral window with limited dynamic range. The conclusions drawn from the data collected, therefore, will have finite spectral and dynamic range limitations imposed by the selection of the seismograph response characteristics. The rationale for, and limitations of, the Brazoria seismograph station will be discussed next.

The basic resolution limitations of the Brazoria seismograph station can be discussed most easily with the three illustrations of figure 1. The first two diagrams illustrate the static end members (a. before, b. after) for a displacement, S, of one block with respect to the other. It is assumed that the displacement is confined to the fault plane and that no separation of the blocks normal to that plane (dilatancy) occurs ($W \approx 0$). Figure 1c illustrates the important dynamic characteristics of this displacement. If the time rate of displacement, $\dot{S}$, is nearly equivalent to the shear wave velocity of the medium, β, the earth movement would be referred to as a normal earthquake. If the time rate of displacement is much slower than the shear wave velocity of the medium, the earth movement would be referred to as a slow earthquake. If the time rate of displacement is very long (i.e., minutes or more) the observable earth movement would be referred to as creep. Finally, if the displacement S is accomplished in two or more temporally discrete intervals, the earth movement would be referred to as a multiple event or swarm. Whether or not the seismograph is capable of faithfully reproducing amplified versions of these displacements is dependent on the magnification and frequency response of the instrument. Useful limiting parameters to know, therefore, are (1) the minimum displacement observable above the ambient noise, (2) the maximum displacement observable without the signal being distorted or clipped, and (3) the range of time rate behavioral characteristics resolvable.

These three reliable data acquisition limitations for the Brazoria seismograph station are determined by operational characteristics which are specified in terms of the instrumental response curves. In practice, these limits are established from empirical studies of the ambient noise characteristics and source spectral characteristics for typical regional earthquakes.

First, we will consider the source spectral characteristics which are expected to be encountered for normal earthquakes. Examination of any seismicity map for the United States clearly indicates that the largest earthquake to occur in the Gulf Coast has never exceeded a magnitude 5.5; so, the upper bound on the size we need consider is certainly less than that. Source spectra from central United States earthquakes which have had magnitudes less than 5.5 are illustrated in figure 2. One measure of size, the magnitude, is given on the right-hand logarithmic ordinate. Although magnitudes are physically meaningless, they do provide a means of ranking the
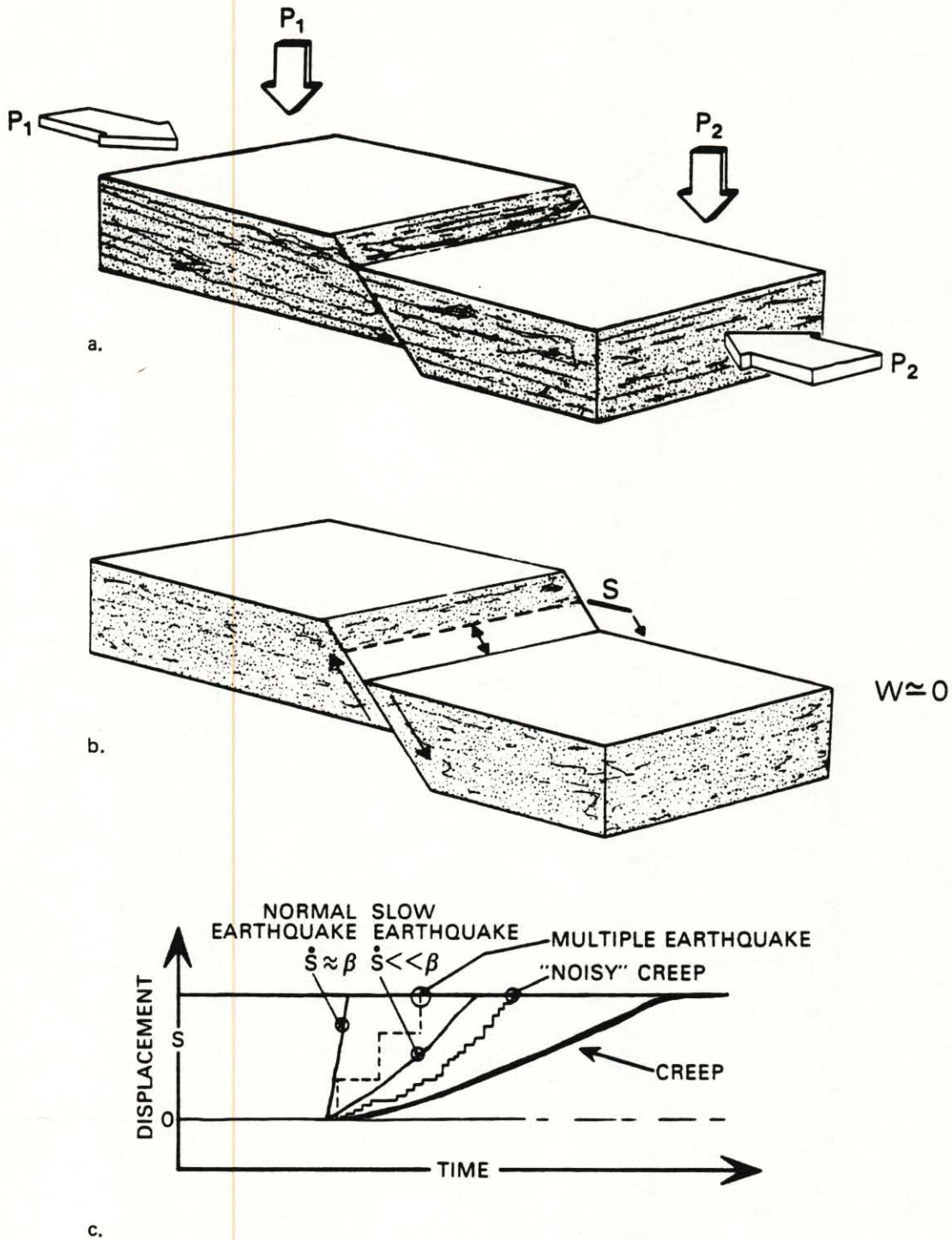
-3-

FIGURE 1. a. BLOCK DIAGRAM OF EARTH PRIOR TO SLIP DISPLACEMENT
b. BLOCK DIAGRAM OF EARTH FOLLOWING SLIP DISPLACEMENT
ASSUMING NO FRACTURE DILATANCE
c. POSSIBLE DISPLACEMENT TIME HISTORIES TO PROCEED FROM a TO b.

G.12323

-4-
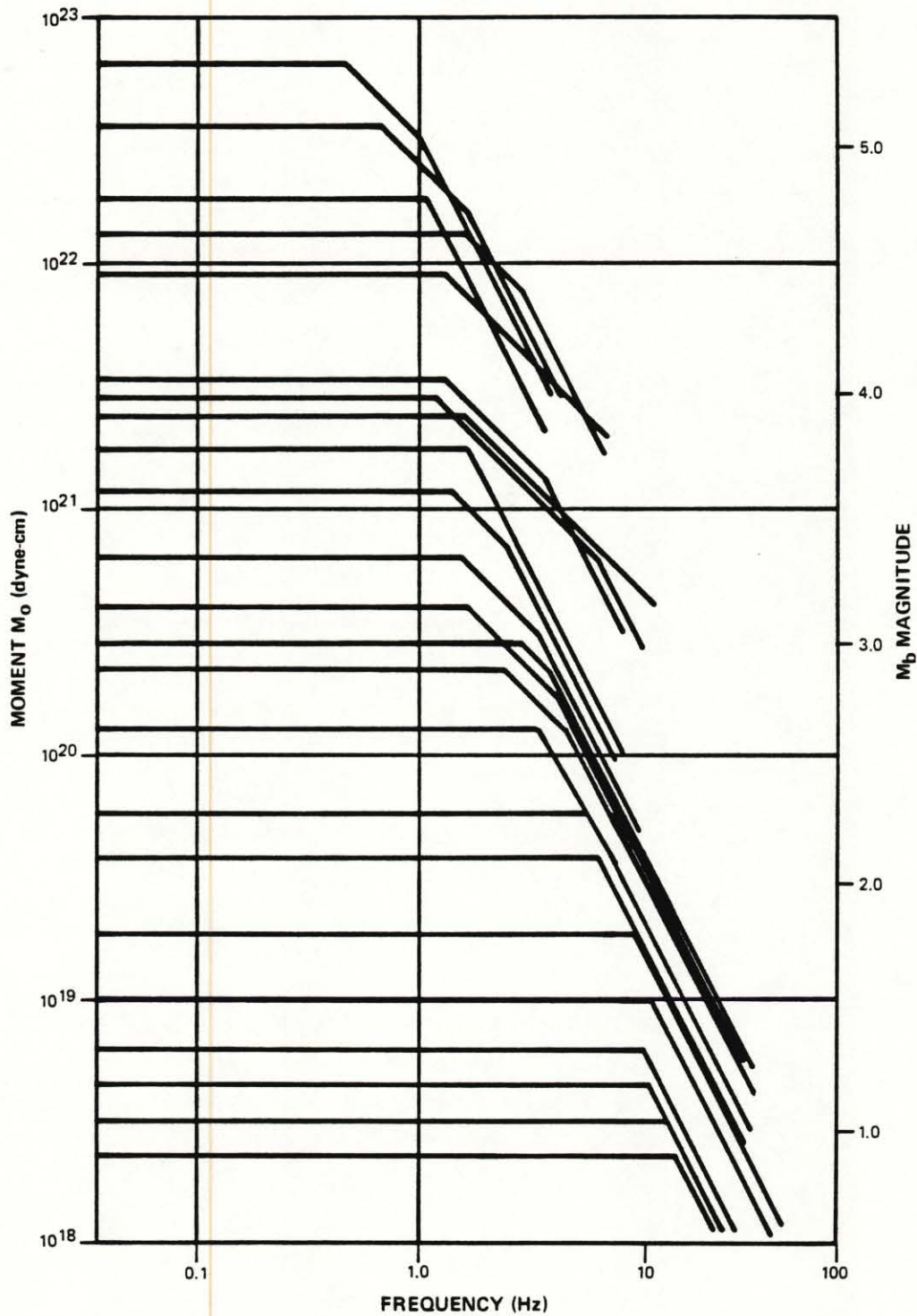
FIGURE 2. SOURCE SPECTRAL CHARACTERISTICS FROM L_g FOR CENTRAL UNITED STATES
EARTHQUAKES (AFTER STREET, HERRMANN, AND NUTTLI, 1975)

G 12318

TR82-2

relative sizes of the earthquakes. A recent alternative, physically meaningful, measure of size, the moment (product of the stress drop and fault area), is given on the left-hand logarithmic ordinate in units of dyne-centimeters. The logarithmic abscissa is frequency of ground vibration. The source spectra for the central United States earthquakes are generally composed of two segments, one with constant moment as a function of frequency and the other with moment which decreases as the square of the increasing frequency. The frequency where these two asymptotes join is called the corner frequency and is related to the physical dimensions of the fault area. The flat or low frequency asymptote of the spectrum clearly is a measure of the size of the earthquake, and the high frequency asymptote is related to the stress drop time history and some other geometric parameters. The significance of figure 2 is that, as the size of the earthquakes in the central United States decrease, the corner frequency shifts to higher frequencies. This relationship is illustrated more clearly in figure 3 which demonstrates a logarithmic-linear increase in corner frequency as a logarithmic-decrement in size. The implication of these studies to the performance of the Brazoria seismic array is that if earthquakes smaller than magnitude 3.0 and larger than magnitude 0.0 are to be recorded, the spectral band of dominant interest is from 2 to 20 hertz. Accordingly, figure 4 illustrates the relative amplitude frequency response of the seismograph station selected for the Brazoria array.

This response curve provides a well-calibrated, relatively flat response over the spectral band of interest and simultaneously rapidly decreases the sensitivity at frequencies above one hertz where earth noise becomes a problem particularly near coastal regions.

Returning to the problem of maximum resolution, or alternatively the smallest event resolvable by the Brazoria array, it is next necessary to determine the ambient noise conditions for Chocolate Bayou in the spectral band of interest. This is an empirical measurement which is both temporally and spatially highly variable. That means that the ultimate sensitivity of the spatially fixed array to detect signals will vary with time according to weather conditions, cultural noise, etc. By measuring the recorded amplitude of ground displacements at various frequencies at various times, it was determined that the average ambient background noise level was 4.5×10^{-9} meters. Design specifications for the S-500 seismometer used as the ground sensor for the Brazoria array rate the typical instrumental noise level as 2.5×10^{-9} m (0-P). Thus, the typical ground noise at Chocolate Bayou is a factor of approximately two above the inherent instrumental noise level.

From other empirical studies, it is known that the displacement amplitude for earthquakes decreases as the square of the distance increases. Similarly, it is possible from many studies to establish displacement amplitude versus distance curves for specified magnitudes. One such set of curves is illustrated in figure 5 for magnitudes 0.5, 1.0, and 1.5. The average observed ambient noise level for Chocolate Bayou is illustrated as a change from unshaded to shaded background. Signal amplitudes which fall in the shaded portion of the diagram can be considered unrecognizable from noise. What this figure diagramatically illustrates is that, during average conditions, any earthquake with magnitude larger than 1.25 within the dimensions of the array will be recorded by all seismographs of the array. Under

-6-
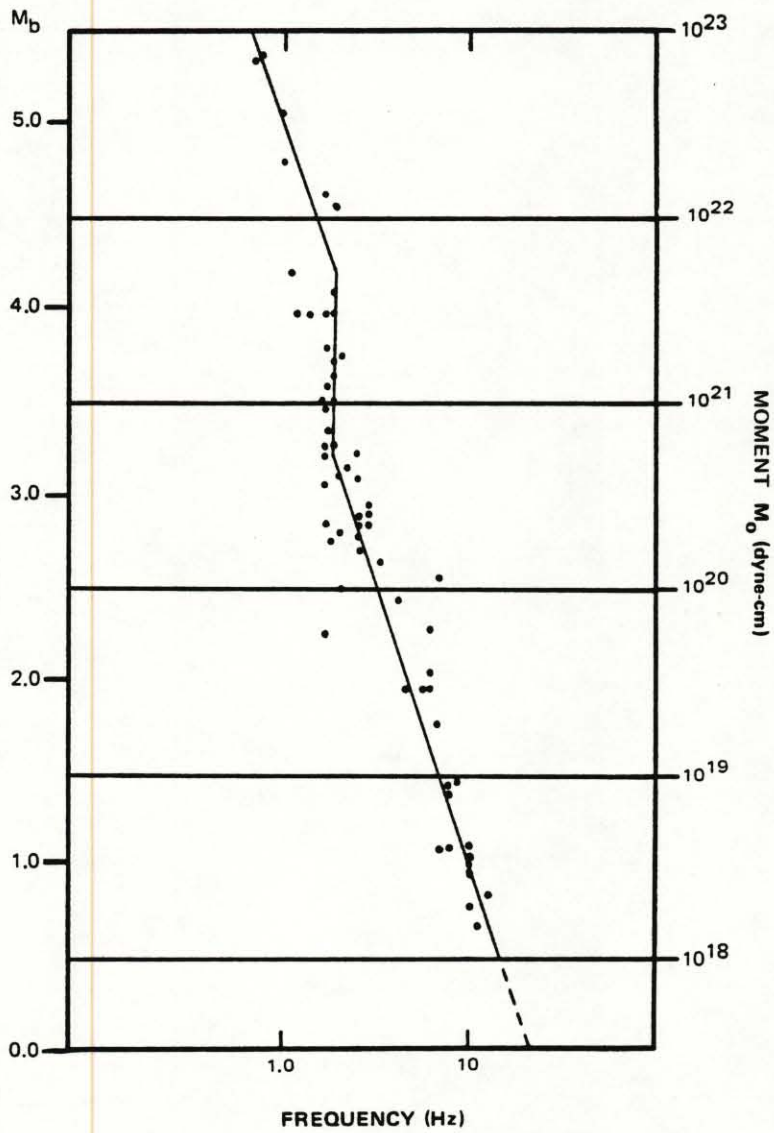
FIGURE 3. CORNER FREQUENCY VERSUS SEISMIC MOMENT FOR CENTRAL UNITED STATES
EARTHQUAKES (AFTER STREET, HERRMANN, AND NUTTLI, 1975)

G 12321

-7-
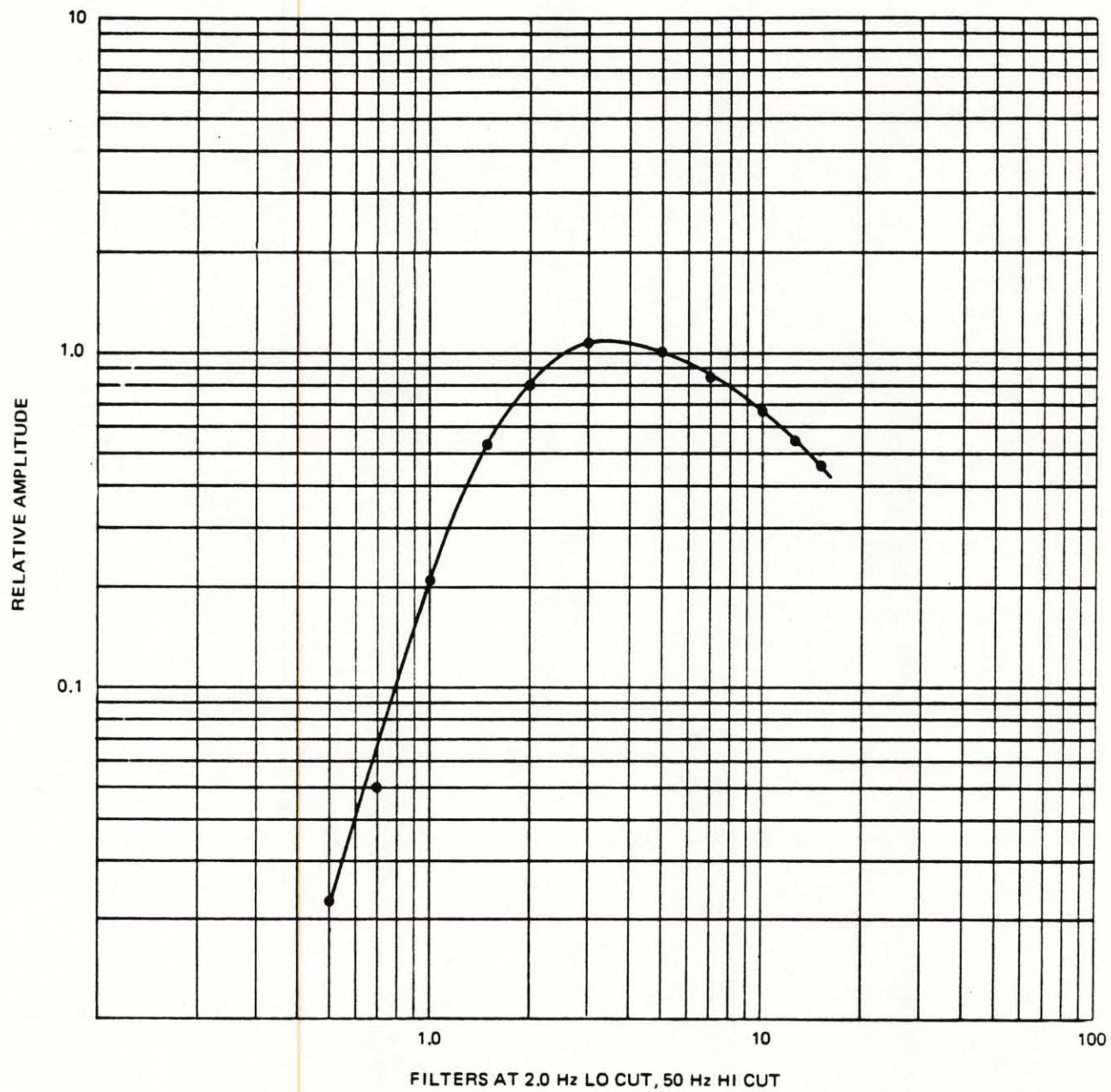
FIGURE 4. SYSTEM FREQUENCY RESPONSE

FILTERS AT 2.0 Hz LO CUT, 50 Hz HI CUT

G 11147C

-8-
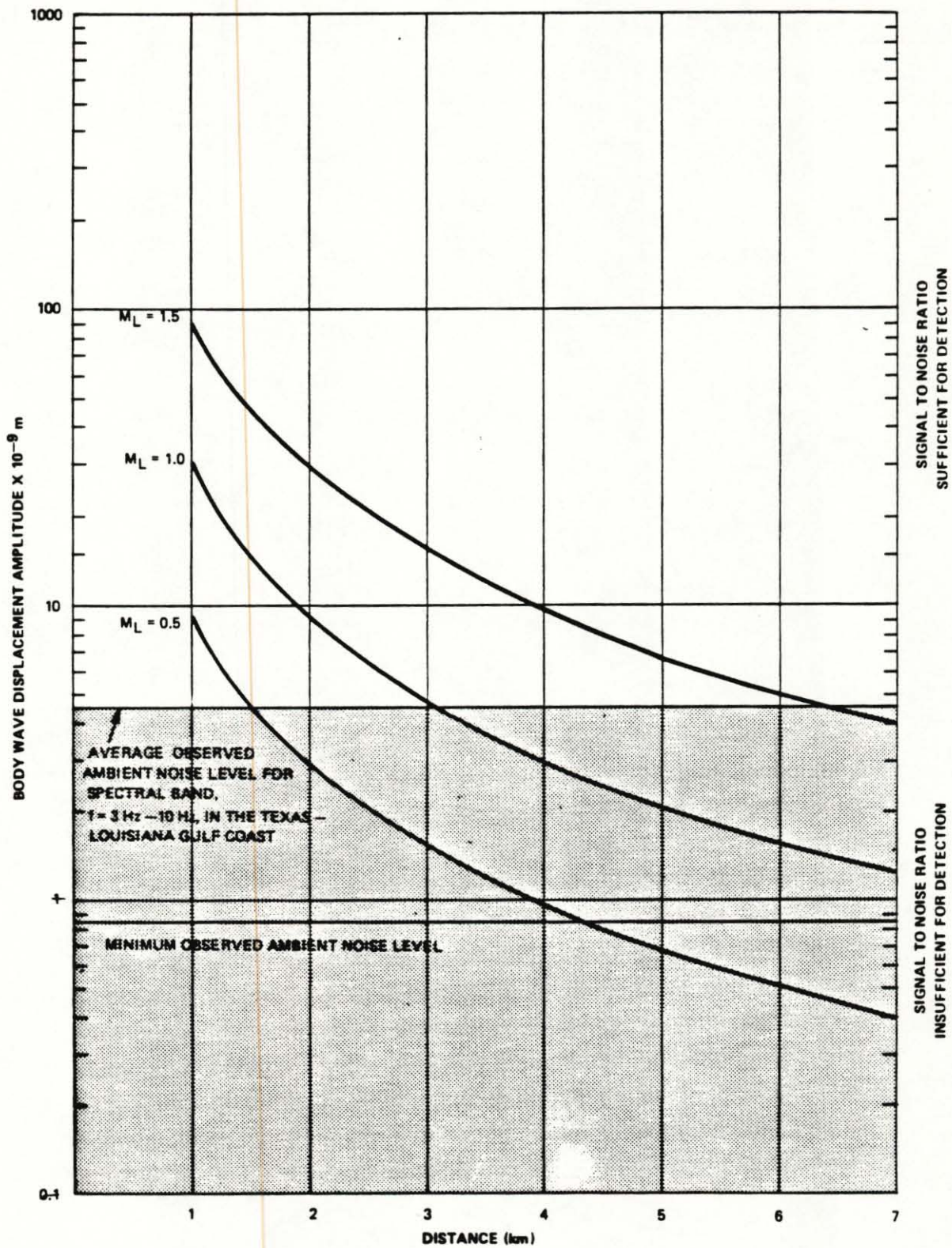
FIGURE 5. THEORETICAL P-WAVE AMPLITUDE (O-P) VERSUS DISTANCE FOR SMALL MAGNITUDE EARTHQUAKES

-9-

exceptionally quiet conditions, earthquakes with magnitudes as low as 0.5 will be recorded adequately by all stations.

The maximum signal observable without significant distortion or clipping is complicated by a number of factors such as the frequency of the signal, the proximity of the source, and the band limiting nature of the electronics. Thus, it is not generally possible to specify a maximum magnitude observable without distortion unless some additional parameters are specified, e.g., the distance and specific frequency to be observed. The maximum (O-P) ground displacements observable with the Brazoria seismograph instrumentation at one, five, and ten hertz are respectively 7.43×10^{-5}, 2.6×10^{-6}, and 1.2×10^{-6} meters.

Having defined the operational limitations of the Brazoria seismograph systems, it is now possible to place confidence constraints on the data acquired by any of the stations and thus on conclusions which can be drawn from the data. In summary, any earth movement occurring within six kilometers of any station having displacement amplitudes greater than 5×10^{-9} meters and less than 5×10^{-6} meters with frequencies between one and twenty hertz will be recorded without distortion and have signal-to-noise ratios of at least 1:1. In other words, all of the signal types identified on figure 1c with the exception of creep could be recognizably recorded by the Brazoria seismographs providing that the signal-to-noise ratio is greater than 1:1.

TR82-2

THE BRAZORIA NETWORK DESIGN AND LIMITATIONS

The utility of the data recorded is not only limited by the performance characteristics of the individual stations, but also by the performance of the entire network. In this section, we will examine the limitations imposed on the data and the conclusions drawn by the array or network design.

The Brazoria seismic array consists of five individual seismograph stations which are schematically illustrated in figure 6. Each station consists of a Geotech S-500 seismometer, 42.50 amplifier with signal conditioners, a voltage-controlled oscillator (VCO) and discriminator, and a dual-recording medium on magnetic tape and 16 millimeter film. The function of the seismometer is to sense the earth vibrations in vertical mode and convert the vertical ground motion to an electrical voltage proportional to the amplitude of the ground motion. The function of the amplifier is to amplify the voltages produced by the seismometer and shape the frequency response of the system through filtration. The function of the voltage-controlled oscillator (VCO) is to convert the amplified voltages to deviations of a central carrier frequency (frequency modulated, FM, signals) which can be transmitted over telephone lines. This permits transmission of several signals over the same pair of wires for very long distances without introducing additional noise produced by the long transmission path. The FM signals from the individual Brazoria stations are transmitted over individual voice-grade (unconditioned) telephone lines to Liverpool, Texas. At Liverpool, the individual signals are added together or multiplexed for transmission to Garland, Texas, using AT&T long-line services. At Garland, Texas, the multiplexed FM signals are separated and demodulated from their respective carrier frequencies by the Geotech 46.12 discriminators. Some additional filtration of the signals, which contributes to the shaped response illustrated in figure 4, is also performed by the discriminators. The signals from the individual stations at this point have been returned to voltage deviations on individual pairs of wires. Thus, the purpose of the VCO, multiplexer and discriminator electronics is to permit remote recording of several simultaneous data channels as if the recording equipment were at the individual sites. The signals from the seismograph stations are recorded then at the Teledyne Geotech laboratory in Garland in analog form on magnetic tape and on 16mm microfilm together with encoded time information.

The distribution of the five seismograph stations in the Brazoria array is illustrated in figure 7 as solid triangles. The location of the Pleasant Bayou No. 2 well is identified by a divided circle, and known growth faults are identified at the 15000 feet depth as shaded lines. The locations of the individual stations, elevations of the S-500 sensors below mean sea level, magnification factor at five hertz and VCO center frequency are listed in table 1. All seismometers are in boreholes one hundred feet deep.

Given the distribution of stations with known response characteristics, we are now ready to evaluate the constraints which the network design places on the data recovered. This, in part, depends on what the function of the array is to be. If the function of the array is detection, then the capabilities of the network depend only on the sum of the detection probabilities of the individual stations. If, on the other hand, location of the source of the signals is an important function, the joint probabilities of detection by

-11-
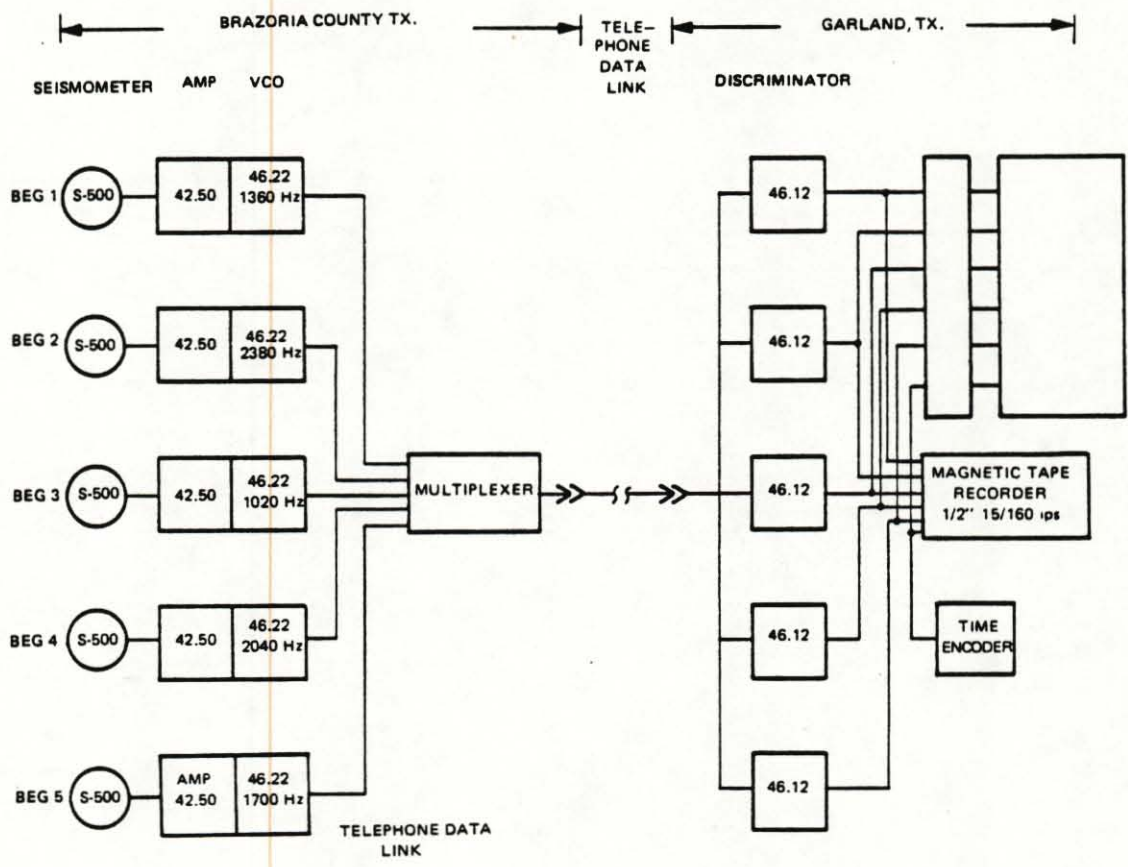
FIGURE 6. BLOCK DIAGRAM OF BRAZORIA COUNTY SEISMIC ARRAY
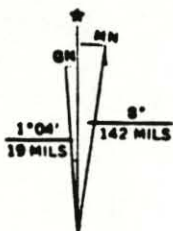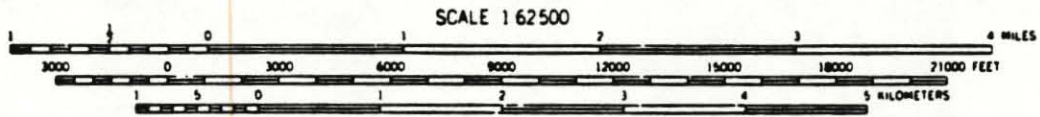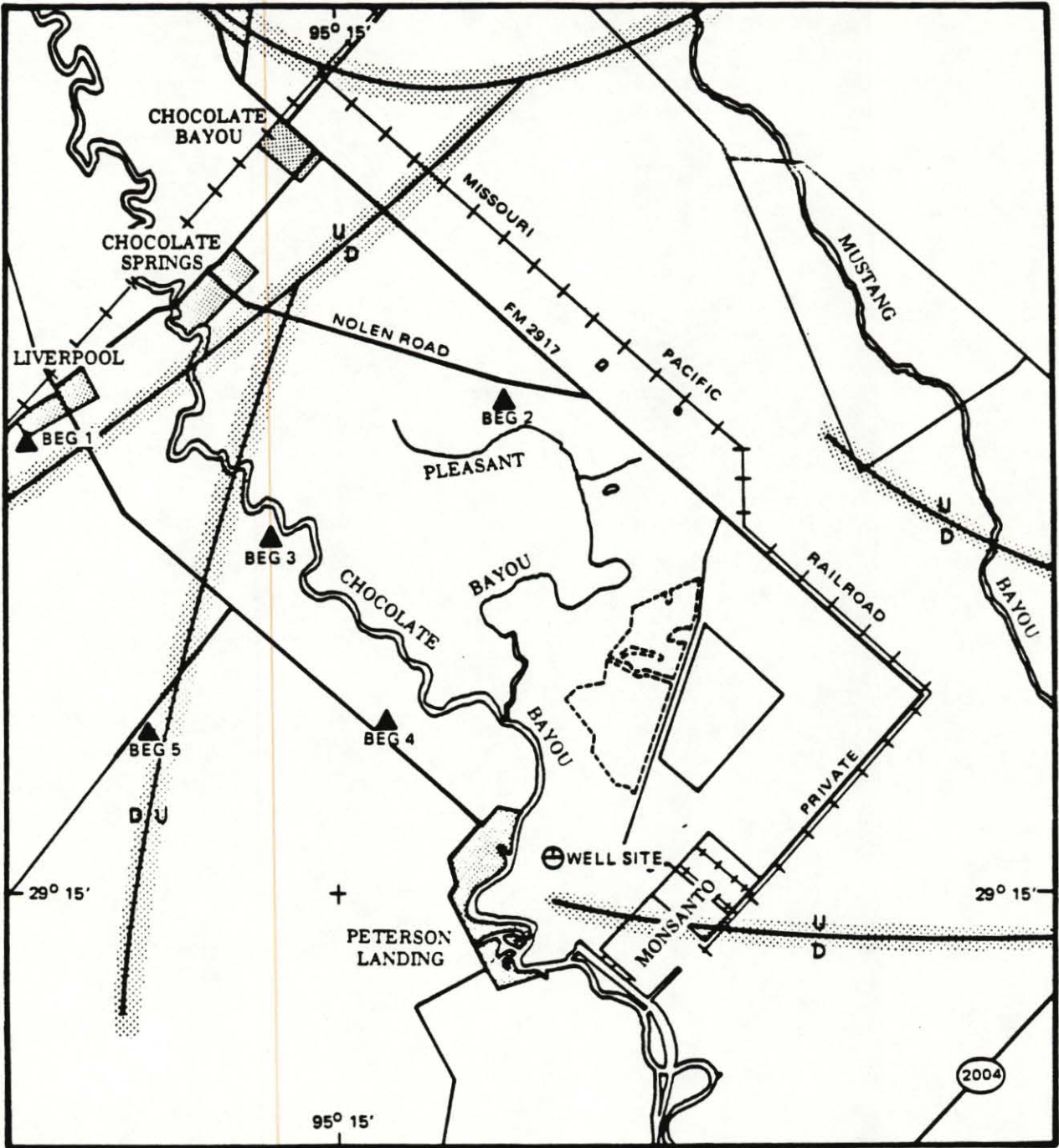
G 11908

FIGURE 7. BRAZORIA COUNTY TEXAS SEISMIC ARRAY

G 11907

-13-

three or more stations is significant. This distinction is quite important. Detection capability is analogous in probability set theory to the set union, whereas the location capability is analogous to set intersection. Both of these capabilities are spatially and temporally variable depending upon the ambient noise conditions and the relative amplitude of the signal. This is conveniently illustrated for Brazoria in figure 8, by assuming the detection threshold for a magnitude 1.0 earthquake during average background noise conditions is 3.0 kilometers as indicated in figure 5. On the one hand, the lightly shaded area demonstrates the detection capabilities; on the other hand, the darkly shaded area demonstrates the region of three or more station location capabilities. It is clear from figure 8 that location capabilities are strongly dependent upon station distribution and operational performance of the individual stations.

In summary, the design of the network can dramatically affect the capabilities to perform specific tasks with the data. Location capabilities in particular are profoundly affected by spatial distribution of the stations and individual stations operational performance. Operational performance tables for network stations are therefore one measure of the location capability of the network. It is for this reason that we include such tables in the monthly reports and reproduce them here as Appendix I.

Table 1. Brazoria County Texas Seismic Array

Site	Latitude(N) Deg	Min	Sec	Longitude(W) Deg	Min	Sec	Elevation Feet	Magnification X 1000 @ 5 Hz	VCO Hz
BEG1	29	17	28	95	16	53	-87	134	1360
BEG2	29	17	32	95	14	01	-87	138	2380
BEG3	29	16	54	95	15	22.5	-97	141	1020
BEG4	29	15	54	95	14	45.2	-90	98	2040
BEG5	29	15	53.4	95	16	10.3	-84	136	1700
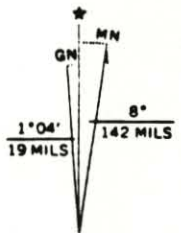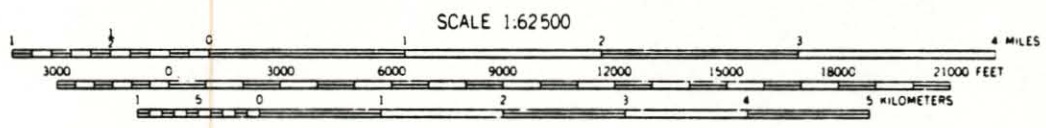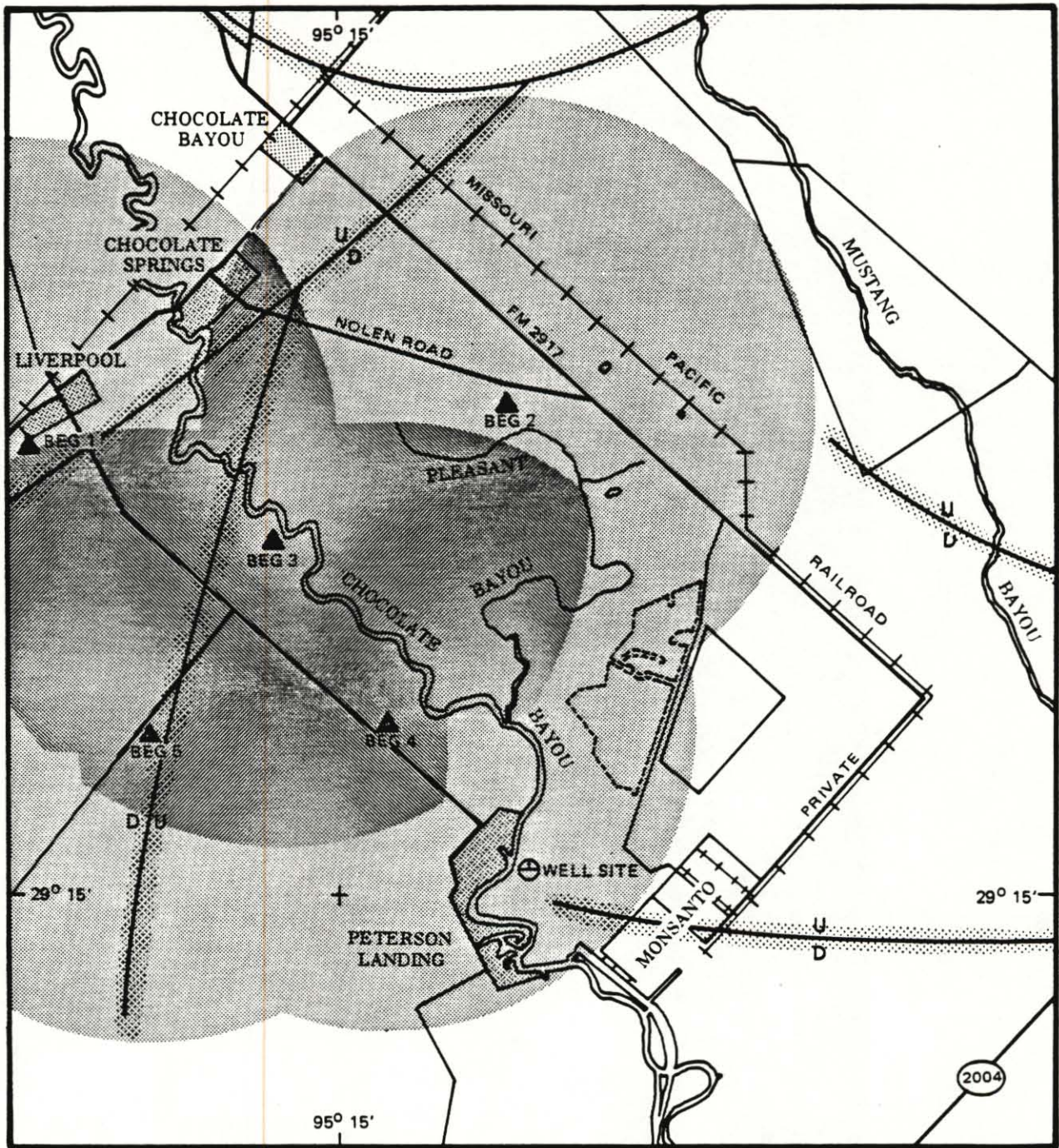
TR82-2

FIGURE 8. DETECTION AND LOCATION PROBABILITIES FOR A MAGNITUDE 1.0 EARTHQUAKE
DURING AVERAGE BACKGROUND NOISE CONDITIONS

G 11907J

-15/16-

TR 82-2

DATA ANALYSIS PROCEDURES

Data generated by monitoring systems are analyzed using standard microseismic data analysis techniques to yield basic information about the origin times, locations, and magnitudes of observed events. The standard analysis sequence used by Teledyne Geotech is illustrated in figure 9.

The 16 mm film seismograms are reviewed carefully to detect any microseismic events that may occur. When an event is detected, the analyst measures the amplitude, period, and arrival times of the P (compressional), S (shear), and L_R (surface) wave of the event. The desired accuracy of the arrival time estimates is +0.01 second for P waves and +0.05 second for S waves. If this degree of accuracy cannot be achieved utilizing the film records, the analyst may request a filtered version of the signal recorded on magnetic tape. Filter options include variable high pass, low pass, and band-pass operators. The amplitude, period and arrival time data are stored for subsequent input into a computer code (MEHYPO) which estimates the origin times, source coordinates and local magnitudes of the observed events. This code utilizes the arrival time data, the sensor location data and a plane layered seismic velocity model of the local subsurface structure to estimate the origin times and the source coordinates of the observed events. The estimation algorithm is similar to that described by Lee and Lahr (1972) in that it finds the origin time and set of source coordinates which minimizes the mean square difference between observed and predicted arrival times at the various sensor locations. The code also provides various location uncertainty estimates which are based upon the assumption that the arrival time errors are normally distributed and that the seismic velocity structure is known without error. The sensor frequency response data, the P-wave amplitude and period data are used to compute the local magnitudes of the observed events.

The P-wave velocity structure for the Gulf Coast used in the analysis of event location is illustrated in figure 10 and listed in Table 2. This velocity structure is a blend of data from Brazoria County, Texas and Parcperdue, Louisiana.

The S-wave velocity structure was derived from the P-wave velocity structure using the formulation:

$$V_S = V_P / \left(1 + \frac{1}{1-2\sigma}\right) 1/2$$

where: V_S = Shear wave velocity
         V_P = Compressional wave velocity
         σ = Poisson ratio

Water has a Poisson ratio of 0.5 and most competent rock has a Poisson ratio of 0.25. Lash (Geophysics, 1980, pp. 1373-1411) has determined the Poisson ratio for surficial Gulf Coast sediments to be greater than 0.45 with the ratio decreasing with increasing depth. For S-wave velocities in Table 3, we have assumed a Poisson ratio of 0.45 for layers 1 through 7, 0.40 for layers 8 through 19, and 0.30 for layers 20 through 22. To utilize S-waves for hypocenter location, we are using a fixed V_P/V_S ratio of 1.732 and treating them as pseudo P-wave arrivals.
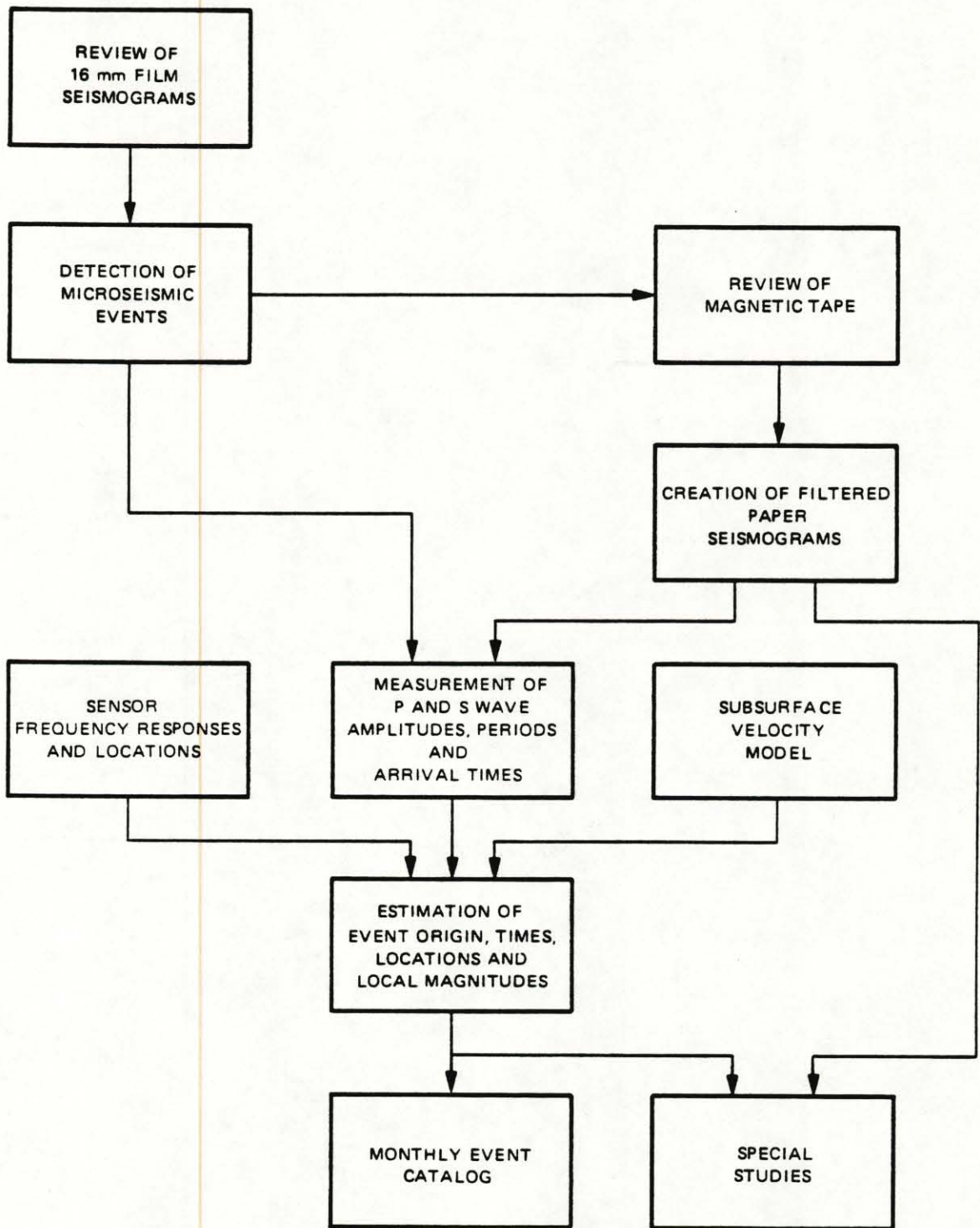
FIGURE 9. STANDARD ANALYSIS PROCEDURE BLOCK DIAGRAM

G 12360
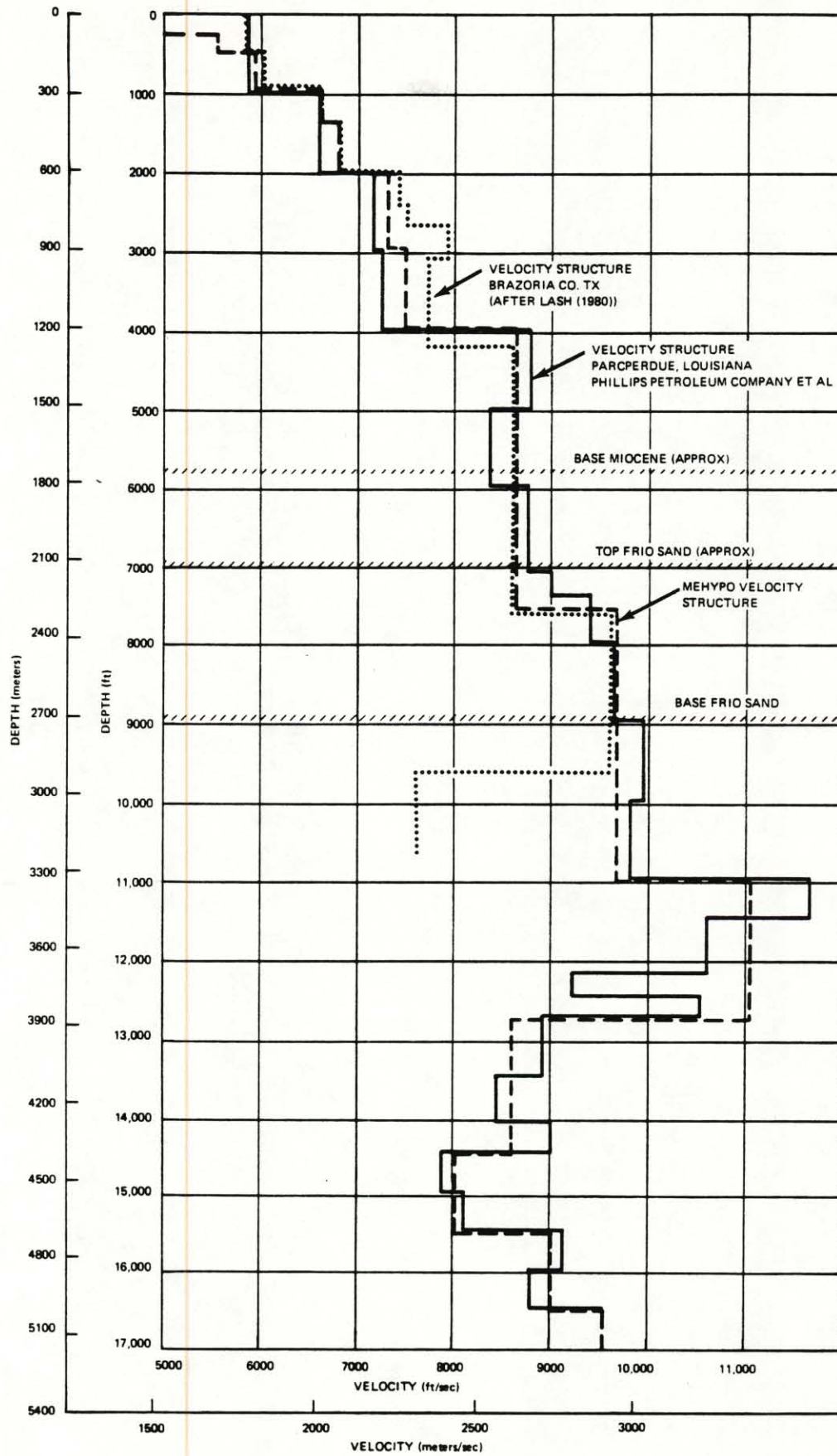
FIGURE 10. P-WAVE VELOCITY STRUCTURE

-19-

G 11746

TR82-2

Table 2

Layer Parameters	P—Wave Vel. (Km/sec)	S—Wave Vel. (Km/sec)	Thickness (Km)
1	0.6100	.352	0.0091
2	1.7070	.986	0.1000
3	1.7500	1.010	0.0400
4	1.8000	1.039	0.1500
5	2.0120	1.162	0.1220
6	2.0730	1.197	0.2140
7	2.2550	1.302	0.2900
8	2.2860	1.320	0.3100
9	2.6210	1.513	1.036
10	2.9260	1.689	1.0500
11	3.3530	1.936	0.5500
12	2.6210	1.513	0.5200
13	2.4380	1.403	0.3100
14	2.7430	1.584	0.3100
15	2.9260	1.689	0.3000
16	3.1700	1.830	0.3000
17	3.5000	2.021	0.3000
18	3.8000	2.194	1000.0000

Epicenters are computed only for events observed at three or more stations because of possible ambiguities of solutions based on data from fewer stations.

Some of the signals of interest consist primarily of surface waves. The velocities of the fundamental, first and second higher mode Rayleigh (surface) waves for this region are illustrated in figure 11 and listed in table 3. Because the average surface wave observed has a frequency less than two hertz, it is possible to get a general (not accurate) location of the sources of these signals using a fixed average acoustic velocity. Occasionally, these events will be listed in the monthly event catalog.

Local seismic magnitudes are based upon maximum surface wave amplitude and are calculated as:

$$M_L = \log_{10} (A/2) - 1.15 + 0.8 \log_{10} (X)^2$$

where M_L is the local magnitude

where   A is the peak to peak surface wave amplitude in nanometers (10^{-9} meters)

where $X = [(\text{epicentral distance})^2 + (\text{hypocentral depth})^2]^{1/2}$
          (in kilometers)   (in kilometers)

and $X \geq 1.0$

The constant −1.15 in the magnitude equation assumes a surface wave to P-wave amplitude ratio of 10. Thus, a magnitude 0 event at 1 km distance would generate surface waves with a peak to peak amplitude of 28.3 nm and p waves with an amplitude of about 2.8 nm.

Magnitudes may be calculated alternatively using duration as

$$M_D = -2.22 + 2.28 \log (D)$$

where D is duration in seconds from onset of P to return of code to ambient noise level.
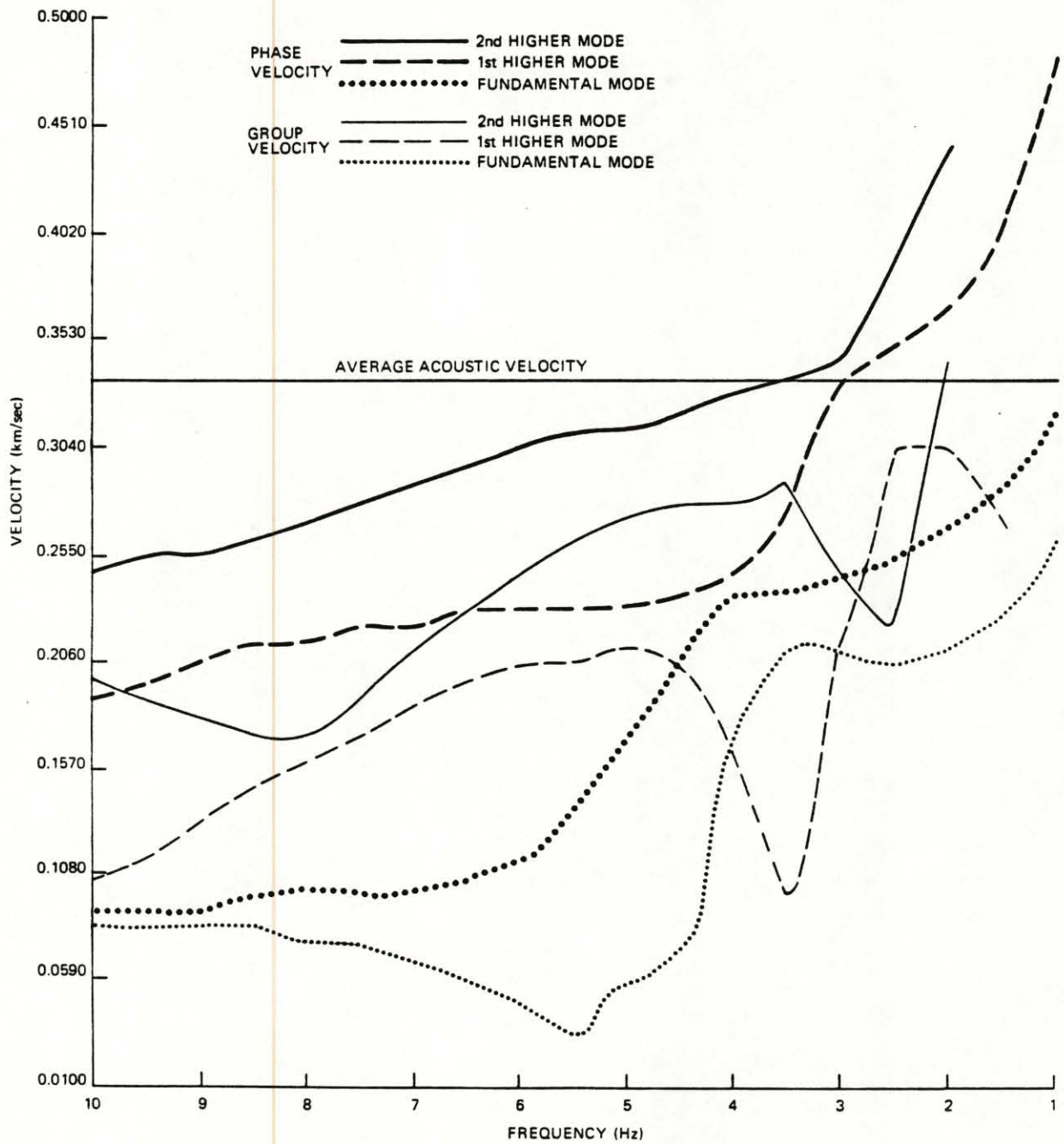
FIGURE 11. RAYLEIGH WAVE PHASE AND GROUP VELOCITIES FOR THE TEXAS AND LOUISIANA COAST

G 11793

-22-

Table 3

FUNDAMENTAL MODE RAYLEIGH WAVE

Frequency (Hertz)	Period (Sec)	Wave Number (Km^{-1})	Phase Velocity (Km/sec)	Group Velocity (Km/sec)
1.00000	1.00000	19.29860	0.32558	0.26618
1.50000	0.66667	31.90403	0.29541	0.23458
2.00000	0.50000	45.92595	0.27362	0.21669
2.50000	0.40000	60.59310	0.25924	0.21358
3.00000	0.33333	75.24859	0.25050	0.21464
3.50000	0.28571	89.75047	0.24503	0.22083
4.00000	0.25000	104.85898	0.23968	0.17546
4.50000	0.22222	133.38976	0.21197	0.07772
5.00000	0.20000	176.47058	0.17802	0.06247
5.50000	0.18182	242.44373	0.14254	0.04259
6.00000	0.16667	308.23688	0.12231	0.05330
6.50000	0.15385	362.21878	0.11275	0.06311
7.00000	0.14286	409.04129	0.10753	0.07079
7.50000	0.13333	451.68350	0.10433	0.07635
8.00000	0.12500	491.70151	0.10223	0.08049
8.50000	0.11765	529.96375	0.10077	0.08362
9.00000	0.11111	566.97290	0.09974	0.08607
9.50000	0.10526	603.06219	0.09898	0.08795
10.00000	0.10000	638.48730	0.09841	0.08933

1ST HIGHER MODE RAYLEIGH WAVE

Frequency (Hertz)	Period (sec)	Wave Number (Km^{-1})	Phase Velocity (Km/sec)	Group Velocity (Km/sec)
1.50000	0.66667	22.80624	0.41325	0.27451
2.00000	0.50000	33.51661	0.37493	0.30512
2.50000	0.40000	43.77451	0.35884	0.30399
3.00000	0.33333	55.12251	0.34196	0.22885
3.50000	0.28571	77.18942	0.28490	0.10324
4.00000	0.25000	101.83848	0.24679	0.16670
4.50000	0.22222	118.03994	0.23953	0.21264
5.00000	0.20000	132.47482	0.23715	0.21849
5.50000	0.18182	147.03320	0.23503	0.21372
6.00000	0.16667	161.87672	0.23289	0.20898
6.50000	0.15385	177.17639	0.23051	0.20141
7.00000	0.14286	193.15668	0.22770	0.19137
7.50000	0.13333	210.12578	0.22427	0.17864
8.00000	0.12500	228.45786	0.22002	0.16413
8.50000	0.11765	248.51895	0.21490	0.14944
9.00000	0.11111	270.57816	0.20899	0.13583
9.50000	0.10526	294.85092	0.20244	0.12338
10.00000	0.10000	321.57187	0.19539	0.11223

Table 3 (continued)

2ND HIGHER MODE RAYLEIGH WAVE DISPERSION FUNCTION

Frequency (Hertz)	Period (sec)	Wave Number (Km^{-1})	Phase Velocity (Km/sec)	Group Velocity (Km/sec)
2.00000	0.50000	27.89075	0.45056	0.35147
2.50000	0.40000	39.13124	0.40142	0.22453
3.00000	0.33333	53.70377	0.35099	0.24685
3.50000	0.28571	64.90845	0.33880	0.29249
4.00000	0.25000	75.87106	0.33126	0.28384
4.50000	0.22222	86.96890	0.32511	0.28110
5.00000	0.20000	98.28802	0.31963	0.27371
5.50000	0.18182	109.97196	0.31424	0.26349
6.00000	0.16667	122.19407	0.30852	0.25039
6.50000	0.15385	135.11926	0.30226	0.23564
7.00000	0.14286	148.96704	0.29525	0.21737
7.50000	0.13333	164.21091	0.28697	0.19476
8.00000	0.12500	181.19171	0.27742	0.17817
8.50000	0.11765	199.00099	0.26838	0.17696
9.00000	0.11111	216.40881	0.26130	0.18465
9.50000	0.10526	233.01805	0.25616	0.19351
10.00000	0.10000	248.91968	0.25242	0.20164

DATA ANALYSIS LIMITATIONS

The data analysis procedures described in the previous section and the assumptions made for routine hypocenter location impose additional constraints on the conclusions which can be drawn from the data. In this section, we will address the limitations imposed by the analysis procedures.

The precision of locating explosions or earthquakes using seismic array data is dependent upon three dominant factors; (1) the quantity and quality of the seismic arrival time data, (2) the accuracy of the earth model, i.e., the velocity structure, and (3) the type of inversion procedure being used.

The location procedure used is a least squares error analysis in which a trial location and origin time are specified with a given velocity structure, and arrival times for given station locations are computed and compared with observed arrival times. The iterative process then moves the trial location and origin time to best fit the observed values of the given arrival times. The accuracy of the final location is, therefore, dependent on the certainty of the velocity structure and arrival time readings. It is important to note here the distinction between accuracy and precision of location. The accuracy of location is a measure of how likely the computed location is the real location. The precision of location is a measure of the finiteness of the solution, i.e., the confidence of the solution. Depending on the reality of the assumptions made, the solutions derived from least squares inversion of the arrival time data could be very precise but not accurate. Measures of precision, i.e., 90% confidence in the location determined, can be generated based on the earth model used and the data quality. Accuracy, on the other hand, requires additional information such as calibration events from which absolute travel time errors can be known. For this reason, most event loca- tion schemes state precision parameters such as error ellipse dimensions, and the accuracy of the location is usually not know.

The lack of fidelity of computed hypocenters to actual hypocenters is most often related to the inappropriateness of the assumed velocity structure. The earth models used assume isotropic flat layers generally with a fixed P- wave to S-wave velocity ratio. Any departure of the real earth model from this assumed model results in systematic mislocation errors which may or may not result in significantly inaccurate locations. We are confident that the structure is sufficiently complex in comparison to a simple flat earth model that systematic mislocations are highly likely. At this time, without speci- fic calibration events for accuracy, we cannot specify any accuracy constraints on the solutions reported for the Brazoria array. We can only assume that systematic inaccuracies are small and that the imprecision prob- ably embodies the real event location.

Unlike the accuracy, however, the precision of the hypocenters is given for each solution set. The precision parameters are embodied in 90% confidence error ellipse parameters which include the semimajor and semiminor axis lengths and the orientation of the error ellipse semimajor axis with respect

to north. The precision parameters embody the sum of all possible errors such as timing errors for individual arrivals, inaccuracies in the velocity model, station mislocations, etc. If the stations had no mislocations, were equally spaced azimuthally around the epicenter and the earth model were perfectly known, then, the precision parameter would reflect only the confidence of individual arrival time picks. The sources of error are hopelessly intertwined, however, so the confidence ellipse is a composite picture of all errors. Thus, the precision parameters state that given all sources of error, the computed location of the event can be anywhere within the error ellipse given 90% confidence in all input parameters. Finally, it is important to realize that given an epicenter location, there is a direct trade-off between the origin time and depth in solution space. What this means is that without additional information such as a depth phase arrival time, the depth error and origin time error are not clearly separable. Thus, the hypocenter depth will usually be very poorly constrained in the least squares error procedure even in the best of cases. For this reason, hypocenter depth errors are not stated in our reports.

If solutions are based on surface wave arrival times, as stated in the previous section, only epicenter location and origin time can be determined.

In summary, the locations of events recorded by the Brazoria array have stated precision parameters in terms of a 90% confidence ellipse. It is likely that there are systematic errors due to complex velocity structure which lead to uncertain inaccuracies of reported locations. Because of the trade-off between depth and origin time determination in the least squares procedure, depth determinations may be neither precise nor accurate.

-26-

THE MONTHLY EVENT CATALOG

Each month an event catalog is produced and event locations computed using
the MEHYPO algorithm. Data utilized to produce the event catalog are
identified. Three types of events may be included in the catalogs:
explosions, natural events which have identifiable compressional and/or shear
waves, and surface/acoustic wave events, the origin of which are unknown but
suspected to be natural. Acoustic signals related to atmospheric events such
as thunder are not included.

Explosions such as exploration shots are entered as follows: the best
recorded shot of the sequence is timed and located using MEHYPO. No magni-
tudes are calculated, and the remainder of the shot sequence is identified by
time of occurrence only. The one identified shot location can be taken as a
general location for the sequence. Explosions more than ten kilometers out-
side the array cannot be located accurately and are identified only by direc-
tion of approach.

Natural events for which P and/or S phases are identified are thoroughly
analyzed. The arrival times and amplitudes of significant phases are cata-
loged and the hypocenter parameters determined. If the events are prominent,
photo duplicates of the records are included. Magnitudes are computed.

Surface/acoustic wave signals will be identified by origin time duration and
sustained amplitude if they are suspected to be natural geodynamical events.
If locations are able to be determined, they will be included.

A composite map illustrating located events is given if relevant. The map
base used is a 1:62,500 direct overlay of the 15' U.S. topographic maps of
the area.

A catalog of events for November, 1981, is included in this annual report.
The data for November are given in Table 4 and the results in Table 5. Event
locations for November are illustrated on figure 12.

DISCUSSION OF NOVEMBER, 1981, ACTIVITY

During the month of November, 1981, seventeen events of interest were
recorded by the Brazoria seismic array. The data for these events are given
in Table 4. Three of the events (1, 2, 4) were occurrences of rumble-type
noise described in previous technical reports. One earthquake (16) was a
teleseism. Nine of the events (5, 7, 8, 9, 10, 11, 12, 14, 17) were explora-
tion shot series either within or outside the array. Events 3, 6, 13, and 15
may have been earthquakes or single explosions. Events 13 and 15 did not
have convergent solutions given the arrival times read. Event 6 was located
using Rayleigh waves and occurred at a likely time for an explosion; we have
therefore classified this event as an explosion. Only event 3 meets all of
the criteria to be an earthquake. A copy of the seismogram for this event is
illustrated as figure 13. The computed locations of the November activity
are given in Table 5 and illustrated in figure 12.

Entries for the table 4 data log utilize the following notation conventions:

Station Identification

BEG1, BEG2, BEG3, BEG4, BEG5

Phase Identification

P - compressional wave

S - shear wave

LR - Rayleigh surface wave

i - impulsive first motion

e - emergent first motion

c - compressional first motion

d - dilatational first motion

? - ambiguity of designation

pP - P-wave reflected at the crust near the epicenter

sS - S-wave converted to P-wave at reflection like pP

Airy - Airy phase (minimum group velocity) of Rayleigh wave.

Phase Timing

Times are designated in Universal Coordinated Time (UTC) which is equivalent to Central Standard Time + six hours. Explosions in a sequence may be designated by hour and minute only.

Phase Amplitude and Period

A_m = maximum 0-peak amplitude of the phase in mm observed on develocorder review (20 x magnification)

A = sustained 0-P amplitude in mm observed on develocorder review (20 x magnification) of a train of waves.

T = period of the wave in seconds.

D = duration of signal in seconds from onset of P to code = ambient noise.

C = number of cycles in a wave train.

Table 4. Brazoria Data Log for November, 1981

1. 81-11-3
    19:08:20
    Rumble

    Duration 50 seconds maximum amplitude on BEG5 peak to peak is 20 mm.,
    sustained amplitude peak to peak is 11 mm. Order of arrival is stations
    5, 1, 3, 4, 2.

2. 81-11-3
    20:29:00
    Rumble

    Duration 45 seconds, sustained amplitude on BEG 5 is approximately 10 mm.

3. 81-11-5
    09:46:58.0
    Earthquake

    | BEG1 | eP | 09:47:01.5; |
    | BEG2 | iP | 09:46:59.1; |
    | BEG3 | iP | 09:46:59.95; |
    | BEG4 | iP | 09:46:59.95; |
    | BEG5 | eP | 09:47:00.4 |

4. 81-11-6
    19:32:00
    Rumble

    Duration 12 seconds.

5. 81-11-6
    21:39:47.8
    Explosion Series

    | BEG1 | eP? | 21:39:51.5; |
    | | iS | 21:39:53.5; |
    | | LR | 21:39:56.3; |
    | BEG3 | S | 21:39:53.45, |
    | | LR | 21:39:56.4; |
    | BEG4 | iP | 21:39:51.75, |
    | | LR | 21:39:56.1; |
    | BEG5 | iP | 21:39:51.6, |
    | | LR | 21:39:56.2, |

    Additional shots: 21:43:03, 21:44:30, 22:42:50, 22:47:08, 22:49:27,
    22:54:20, 22:58:14, 23:05:09, 23:08:08.

6. 81-11-9
    19:19:49.7
    Explosion or Earthquake ?

BEG1	LR	19:19:54.7;
BEG2	LR?	19:19:57.7,
	LR	19:20:06.0;
BEG3	P?	19:19:54.5,
	LR	19:20:01.5;
BEG4	LR	19:20:04.5;
BEG5	LR	19:19:59.15

7. 81-11-11
    18:09:47.7
    Explosion Series

BEG1	P	18:09:51.15;
BEG2	iPd	18:09:49.65,
	iS	18:09:50.2,
	iLR	18:09:51.15;
BEG3	iPd	18:09:49.3,
	iS	18:09:50.25,
	iLR	18:09:50.9;
BEG4	iPc	18:09:48.85,
	iS	18:09:49.55,
	LR	18:09:50.1, D = 8.5;
BEG5	iPc	18:09:49.25,
	eS	18:09:50.1

    Additionnal shots: 18:26:02, 18:32:00, 18:37:25, 18:49:50, 18:55:20,
    20:09:00, 20:13:46, 21:14:56, 21:23:37, 21:31:04, 21:37:06, 21:43:38,
    21:52:43, 21:57:55, 22:02:07, 22:09:15, 22:27:36, 22:33:29, 22:40:08,
    22:48:14

8. 81-11-12
    16:55:02.0
    Explosion Series

BEG1	iP	16:55:04.15;
BEG2	iP	16:55:03.45,
	S	16:55:05.1;
BEG3	iP	16:55:03.5,
	S	16:55:04.0;
BEG4	iP	16:55:03.5,
	iS	16:55:04.1;
BEG5	iP	16:55:03.6,
	S	16:55:04.35

    Additional shots: 16:15:10, 16:36:50, 16:43:30, 16:48:22, 17:18:19,
    17:23:53, 17:29:10, 17:52:30, 18:00:09, 18:08:13, 18:27:26, 18:33:11,
    18:39:48, 18:45:38, 18:51:18, 18:57:47, 19:18:37, 19:24:42

-32-

9. 81-11-22
    14:41:44.8
    Explosion Series

    BEG1   P   14:41:48.75,
                ?   14:41:49.1;
    BEG2   eP   14:41:47.9;
    BEG3   P   14:41:47.9,
                ?   14:41:48.7;
    BEG4   eP   14:41:47.5;
    BEG5   P   14:41:47.7

    Additional shots: 14:45:27, 14:49:45, 14:53:30, 14:57:06, 16:25:08,
    16:31:57, 16:41:07, 16:58:33, 17:10:32, 17:15:14, 17:22:46, 17:29:55,
    17:37:22, 17:45:29, 17:52:34, 18:05:40, 18:45:48, 18:50:14, 18:54:43,
    18:59:14, 19:03:51, 19:08:58, 19:13:24, 19:24:06, 19:43:50, 19:48:20,
    20:02:22, 21:00:42, 21:10:45, 21:29:46, 21:38:53, 21:44:33, 21:54:42

10. 81-11-23
    19:46:49.3
    Explosion Series

    BEG1   iP   19:46:51.4;
    BEG2   eP   19:46:51.25,
                iS   19:46:52.05;
    BEG3   iP   19:46:51.0;
    BEG4   iP   19:46:50.25;
    BEG5   iP   19:46:50.35

    Additional shots: 14:25:37, 18:44:47, 19:07:59, 19:14:39, 19:53:08,
    19:58:01, 20:02:44, 20:37:36, 20:42:53, 20:50:43, 21:00:56, 21:27:47,
    21:32:21, 21:37:02, 21:41:27, 21:45:30, 22:02:10, 22:06:59, 22:15:18*,
    22:20:45, 22:24:55, 22:29:20, 22:49:02, 22:50:31, 23:30:00

    * P to LR separation is approximately 22 seconds.

11. 81-11-24
    17:17:55.8
    Explosion Series

    BEG1   iP   17:17:57.85;
    BEG2   iP   17:17:58.35;
    BEG3   iP   17:17:57.7;
    BEG4   iP   17:17:57.2;
    BEG5   iP   17:17:56.8

    17:10:41, 17:23:41, 17:46:23, 17:50:06, 18:10:39, 18:13:30, 18:18:33,
    18:23:44 18:29:51, 18:35:17, 18:41:15, 18:46:00

-33-

```
12.  81-11-24
     22:53:27.5
     Explosion Series

     BEG1       iP       22:53:30.5,
                iS?      22:53:31.45;
     BEG2       iP       22:53:29.7;
     BEG3       iP       22:53:28.9;
     BEG4       iP       22:53:28.35,
                iS?      22:53:29.1;
     BEG5       iP       22:53:28.75

     Additional shots:   21:12:26, 21:21:15, 21:25:20, 21:29:46, 21:33:55,
     21:38:10, 21:42:10, 21:47:00, 21:52:11, 21:56:14, 22:21:10, 22:26:54,
     22:44:10, 22:48:42, 23:09:20, 23:13:42, 23:17:54, 23:22:14/ 81-11-25:
     17:15:27, 17:39:18, 17:49:07, 18:08:15, 18:16:55, 18:46:31, 18:51:36,
     19:54:08, 20:00:12, 20:06:38, 20:13:58, 20:46:03, 21:00:27, 21:11:12,
     21:17:55, 21:23:32


13.  81-11-27
     18:50:10
     Explosion ?

     BEG1       iP       18:50:20.1;
     BEG2       eP       18:50:22.4;
     BEG3       eP       18:50:21.55;
     BEG4       eP       18:50:23.0;
     BEG5       iP       18:50:21.75


14.  18-11-28
     22:39:38.3
     Explosion Series

     BEG1       iP       22:39:42.0;
     BEG2       iP       22:39:41.55;
     BEG3       iP       22:39:41.4;
     BEG4       iP       22:39:40.55;
     BEG5       iP       22:39:41.05

     Additional shots:   20:25:09, 20:45:12, 20:55:25, 21:00:24, 21:13:01,
     21:22:58, 21:27:47, 22:52:14, 23:01:32, 23:11:25


15.  81-11-29
     04:20:30
     Acoustic Signal

     BEG1                04:20:54.05;
     BEG3                04:20:45.1;
     BEG4                04:20:48.5;
     BEG5                04:20:54.4
```

TR82-2

16. 81-11-30
    15:51:27.7
    Teleseism

    BEG1   eLR?   15:51:27.45, Am = 10.0;
    BEG3   eLR?   15:51:27.45, Am = 3.5;
    BEG4   LR?   15:51:27.45, Am = 4.5;
    BEG5   iLR?   15:51:27.45, Am = 6.0, T = 0.5

    Probable sequence of arrival from Am phases is SE

17. 81-11-30
    19:42:15.2
    Explosion Series

    BEG1   iP   19:42:17.7;
    BEG2   iP   19:42:17.3,
                 iS?   19:42:17.85;
    BEG3   iP   19:42:17.05;
    BEG4   iP   19:42:16.3;
    BEG5   iP   19:42:16.8

    Additional shots: 16:47:02, 16:53:21, 17:40:08, 19:52:17, 19:56:40,
    20:17:05, 20:33:37, 20:43:24, 20:50:57, 21:03:42, 21:09:23, 21:26:46,
    21:38:22, 21:48:57, 21:54:16, 22:13:22, 22:20:03, 22:24:10, 22:28:23,
    22:34:11, 22:39:02

-35-

Table 5. BEG array event log for November, 1981

No.	Day	Origin Time (UCT)			Latitude (N)			Longitude (W)			Depth (km)	Magnitude		90% Confidence Ellipse		Comments
		Hr	Min	Sec	o	'	"	o	'	"		M_L	M_D	Sem. Major Axes	AZ1	
3.	5	09	46	58.1	29	17	03.2	95	14	18.8	-	-	-	7.8 km x 1.5 km	90	Earthquake
5.	6	21	39	47.8	29	20	31.2	95	14	31.1	0.0	-	-	5.6 km x 2.6 km	135	Explosion Series
6.*	9	19	19	49.7	29	17	02.0	95	16	20.2	0.0	-	-	2.9 km x 1.9 km	45	Explosion or Earthquake?
7.	11	18	09	47.7	29	16	25.0	95	14	27.8	0.0	-	-	1.9 km x 0.7 km	115	Explosion Series
8.	12	16	55	02.0	29	16	35.6	95	14	52.8	0.0	-	-	0.9 km x 0.5 km	72	Explosion Series
9.	22	14	41	44.8	29	14	20.1	95	13	39.7	0.0	-	-	10.3 km x 4.7 km	151	Explosion Series
10.	23	19	46	49.3	Outside array											Explosion Series
11.	24	17	17	55.8	29	15	52.1	95	15	06.8	0.0	-	-	2.9 km x 1.0 km	180	Explosion Series
12.	24	22	53	27.5	29	15	53.5	95	15	17.0	0.0	-	-	2.2 km x 0.7 km	6	Explosion Series
13.	27	18	37	29.3	-	-	-	-	-	-	-	-	-	-	-	-	Explosion?
14.	28	22	39	38.3	29	14	07.3	95	14	06.4	0.0	-	-	2.0 km x 1.2 km	143	Explosion Series
15.*	29	04	20	--	-	-	-	-	-	-	-	-	-	-	-	-	Acoustic Signal
17.	30	19	42	15.2	29	16	23.9	95	14	38.9	0.0	-	-	2.6 km x 1.1 km	116	Explosion Series

* Located using Rayleigh waves
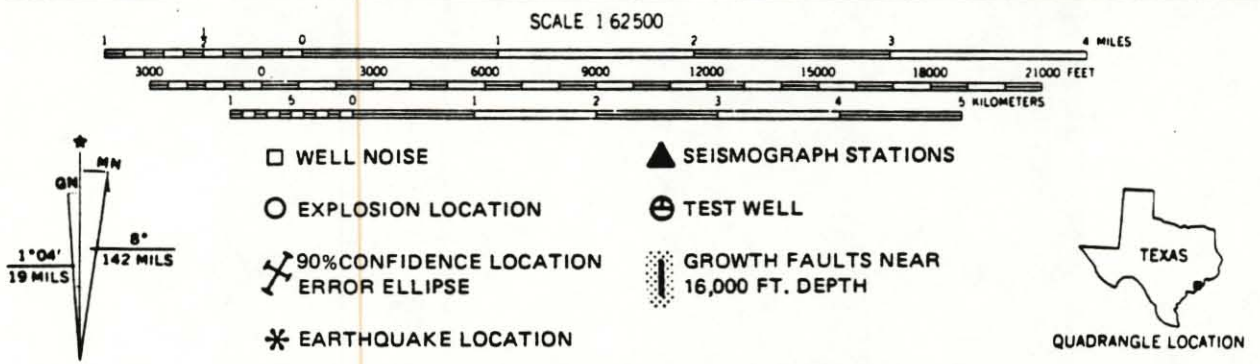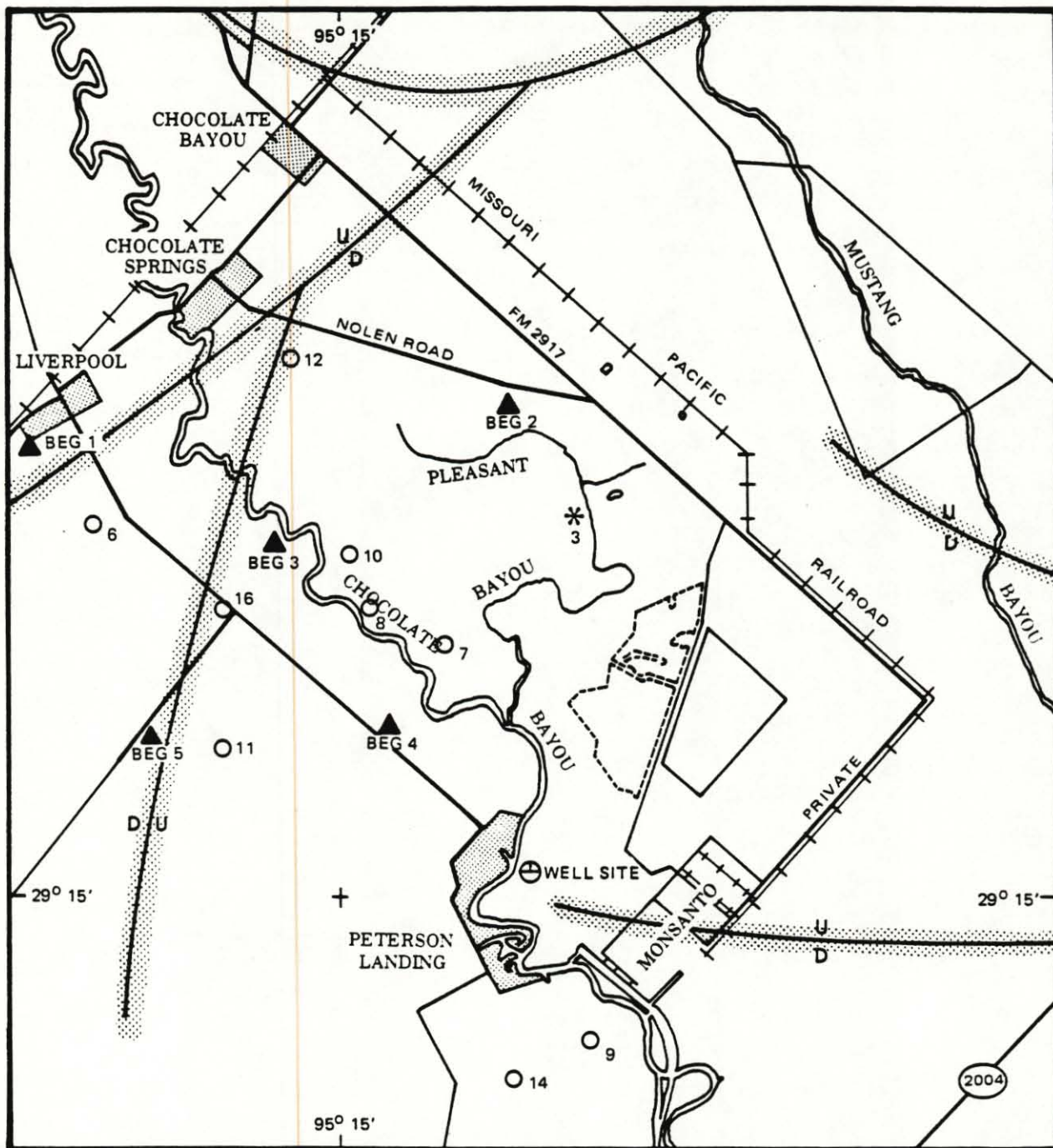
FIGURE 12. EVENT LOCATIONS FOR NOVEMBER, 1981

Legend:

□ WELL NOISE

○ EXPLOSION LOCATION

✖ 90% CONFIDENCE LOCATION ERROR ELLIPSE

✳ EARTHQUAKE LOCATION

▲ SEISMOGRAPH STATIONS

⊕ TEST WELL

░ GROWTH FAULTS NEAR 16,000 FT. DEPTH

SCALE 1 62500

TEXAS

QUADRANGLE LOCATION

G 11907H

-37-
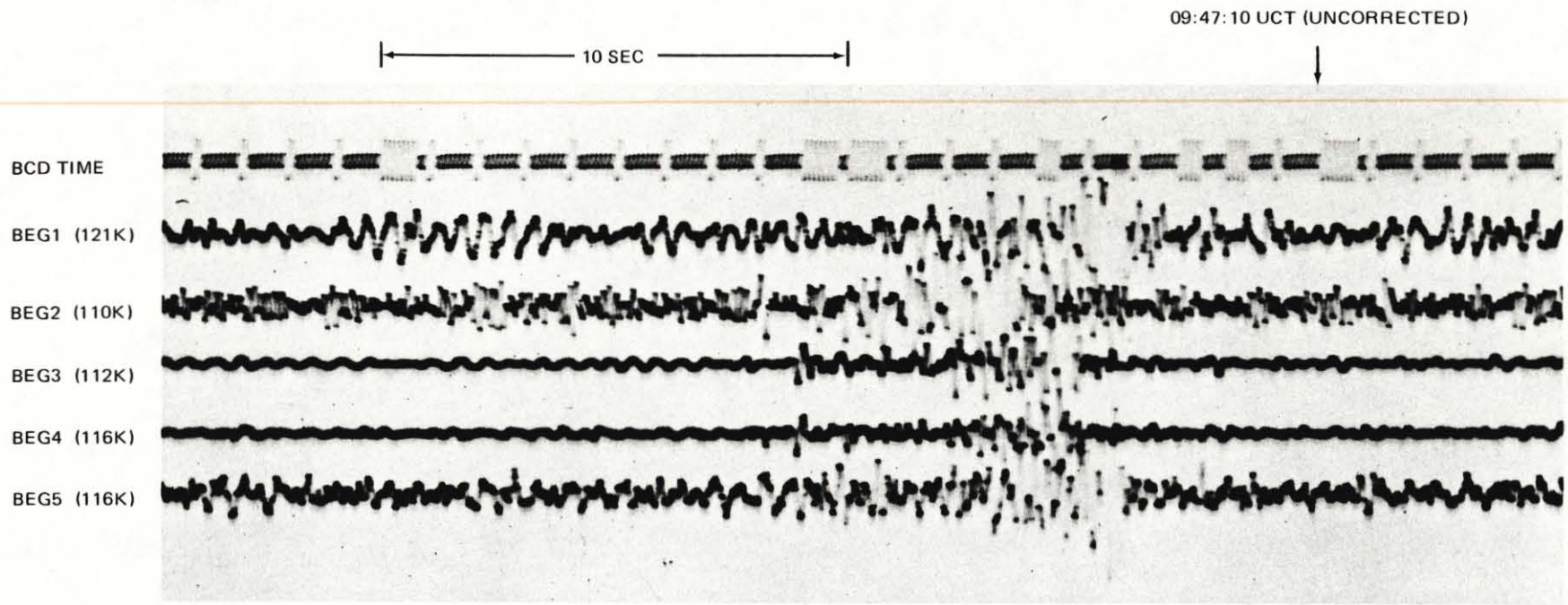
FIGURE 13. EARTHQUAKE 5 NOVEMBER 1981, 09:46:58.1 (EVENT 3 OF TABLES 4 AND 5)

G 124 18

DISCUSSION OF 1981 EVENTS LOCATED USING SURFACE WAVES

During 1981, nineteen events tentatively classified as earthquakes or single explosions were recorded by the Brazoria seismograph array for which no body waves were identifiable. Epicenters for these events were computed assuming that recorded phases were surface waves which have distance-invariant velocities. Because of the slowness with which the wave fronts traversed the array, it was thought initially that these arrivals were acoustic coupled Rayleigh waves which should have velocities of approximately 330 meters/second. Subsequent analyses, however, cast some doubt on the singularity of this assumed velocity. We decided, therefore, to reexamine these nineteen events and relocate them based on the best solution obtained, i.e., on the solution having the smallest error ellipse.

For each of the nineteen events, epicenters and 90% confidence ellipses were generated given their respective arrival times and fixed half-space velocities. Solutions were generated given velocities from 150 m/sec to 550 m/sec in 25 m/sec increments. It was assumed that the area of the 90% error ellipse would pass through a minimum value when the appropriate velocity was used in the solution. The results of these analyses strongly suggested that there was more than one characteristic velocity of surface waves important for epicenter computations at the Brazoria array.

Because of the small sample size and variability of data quality, it was necessary to devise a methodology to examine the distribution of observed surface wave velocities which might represent more accurately the results expected for a larger data set. The methodology we selected was to create individually normalized modified probability density functions (mpdf) for each of the nineteen events from plots of velocity versus area of 90% confidence ellipses. These individual mpdf constitute the best estimates of the surface wave velocities necessary to obtain the most likely locations for the epicenters. The individual mpdf were then integrated to yield a composite IPdf (Integrated probability density function) for the nineteen events. Maxima for the IPdf are the most likely surface wave velocities represented in the data set.

Figure 14 a and b illustrate two typical probability density functions for an event 26 June and 3 September respectively. The event 26 June (figure 14a) is an example of a solution which converges to a very sharply defined minimum in error ellipse dimensions at a velocity of 350 m/sec. On the other hand, the event 3 September (figure 14b) converges to a minimum in error ellipse dimensions over a much broader range of velocities. The absolute ellipse area errors for the two events are also significantly different. These differences are related to the quality of the arrival time data used in the solutions. To ensure the probability density functions from each event contributed equally to an integrated probability density function, we normalized each pdf and truncated the pdf at 10% of the modal minimum value in area. We define these new functions as normalized modified probability density functions (mpdf). The mpdf for the events on figure 14 a and b are illustrated by the shaded regions of each diagram. The mpdf then are normalized to span the range of values from 0 to 1 (1 being the value of the modal minimum). The selection of the 10% increase in ellipse area as the

-39-
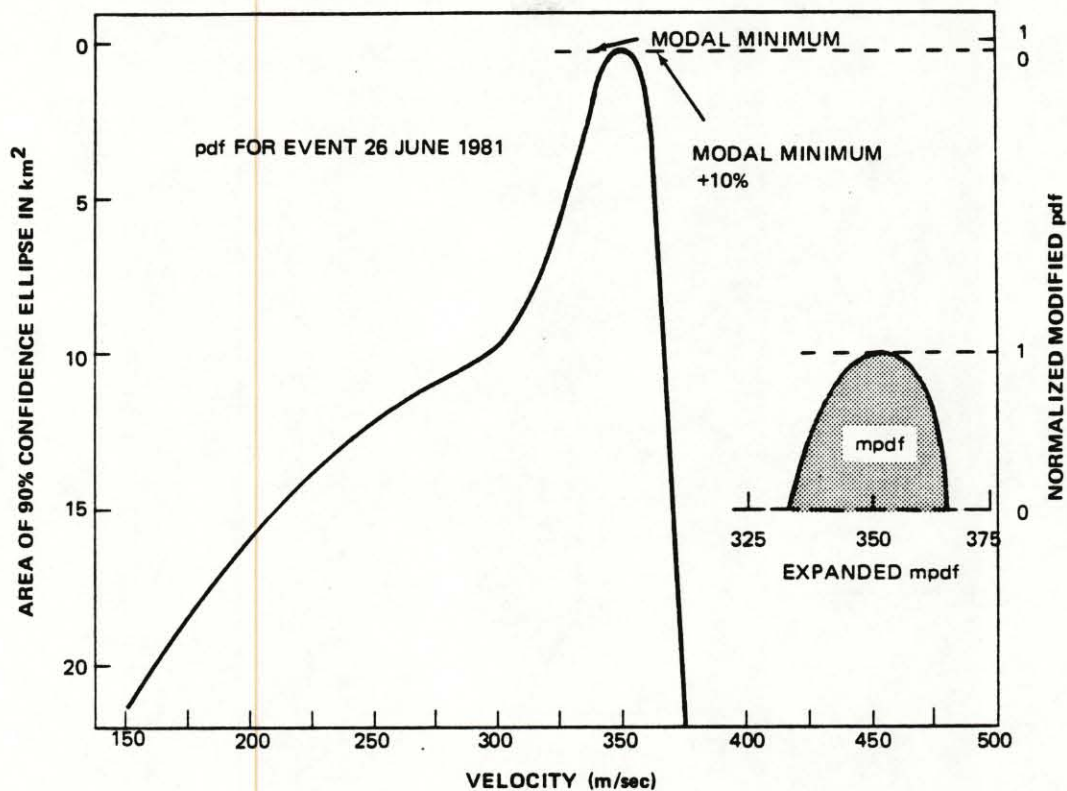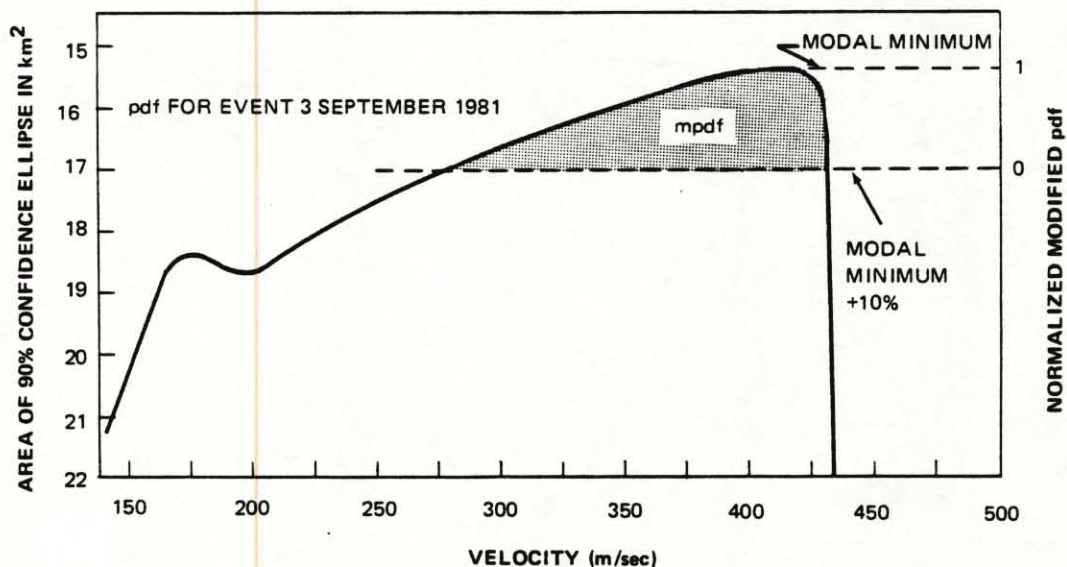
FIGURE 14. a. PROBABILITY DENSITY FUNCTION (pdf) FOR EVENT 26 JUNE 1981. b. pdf
FOR EVENT 3 SEPTEMBER 1981. MODIFIED NORMALIZED pdf's (SHADED
AREAS) ARE DEFINED BY MODAL MINIMUM VALUE +10%. SEE TEXT FOR
ADDITIONAL DETAILS.

G 12419

-40-

cut off points for the truncated mpdf is arbitrary and could have been any other percentage. We chose this percentage increase in error to reflect what we consider to be a reasonable estimation of our confidence in the data. Three of the nineteen events did not generate pdf's which had solution minima. These three were discarded from the integrated probability density function.

The normalized mpdf's for the remaining sixteen events were integrated to form the IPdf (integrated probability density function). The IPdf as a function of velocity is illustrated as figure 15. No units are specified on this function because it has not been normalized to range from 0 to 1. The horizontal dashed line on figure 15 illustrates the level of the IPdf if the area under the curve were uniformly distributed across the velocity band 150 m/sec to 500 m/sec.

The IPdf of figure 15 clearly indicates there are two preferred surface wave velocities which yield epicenter solutions with minimal errors. These are a band from 225 to 250 m/sec and a second at 350 m/sec. This does not mean that, given an arrival time data set, either velocity will yield a solution with an equivalent minimal error. It does mean that two types of events are being recorded by the Brazoria array which have no identifiable body waves. One propagates energy as surface waves with a velocity of approximately 240 m/sec, the other with a velocity of approximately 350 m/sec.

Table 6 lists the events of 1981 which were located using surface waves. The recomputed epicenters based on the best estimates of the surface wave velocity are listed in Table 6, and the locations are illustrated in figure 16.

Why the velocities are bimodally distributed is not clearly understood. There is no obvious geographic distinction between events which have preferred solutions at 240 m/sec versus 350 m/sec. In addition, there is no apparent similarity or difference in the characteristic appearance of the events with the same preferred or different solution velocities. This will be an area requiring further investigation.

Whether or not these events are earthquakes or single explosions is unresolved. It can only be speculated at this time that the events with unusual times of occurrence are earthquakes.
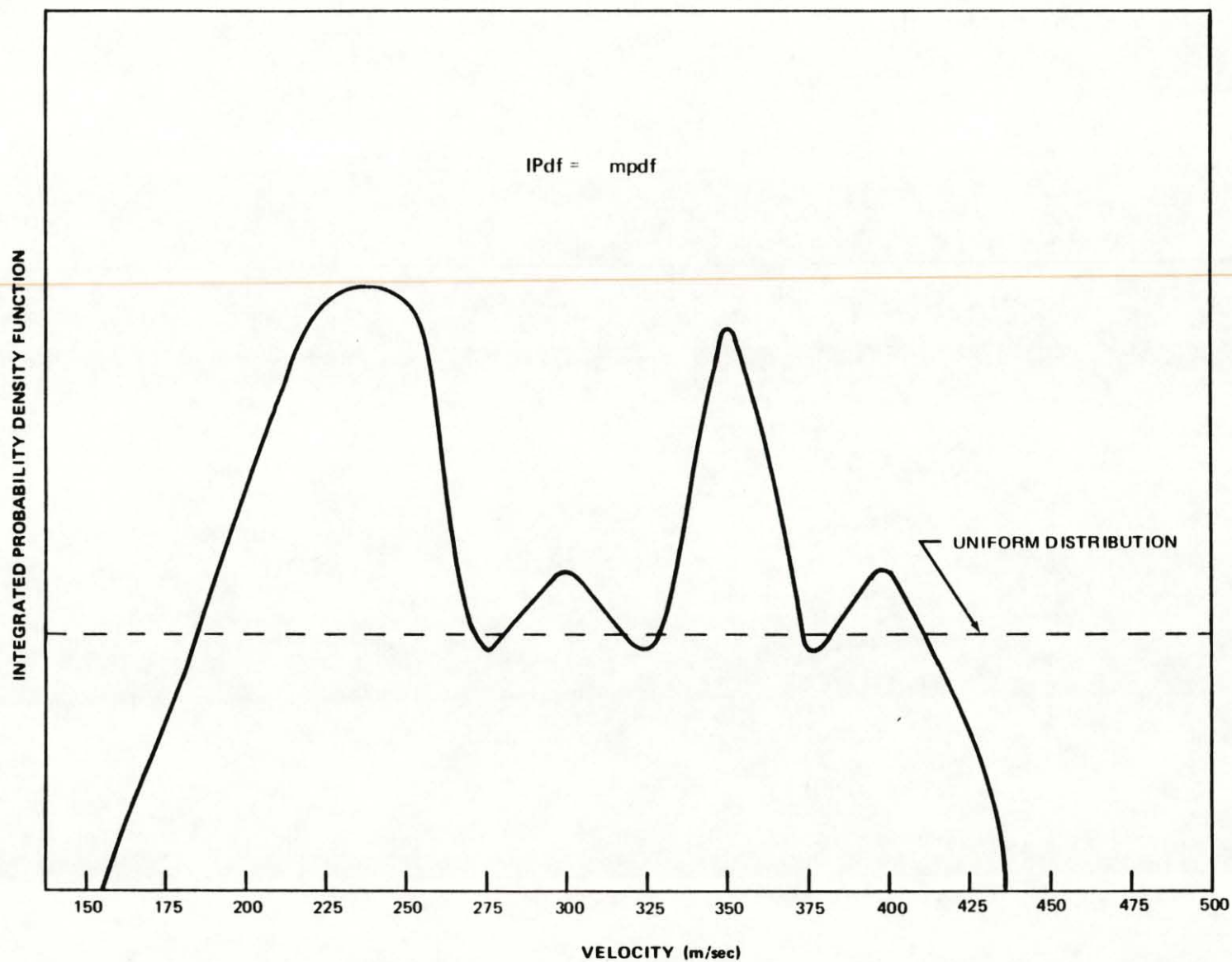
FIGURE 15. MAXIMUM LIKELIHOOD DISTRIBUTION OF SURFACE WAVE VELOCITIES AT THE BRAZORIA, TEXAS SEISMIC ARRAY

G 12420

FIGURE 16. 1981 EVENTS RELOCATED USING SURFACE WAVES

G 11907K

-43-

Table 6. 1981 Events Relocated Using Surface Waves

No.	Mo	Day	Origin Time (UCT) Hr	Min	Sec	Latitude (N) o	'	"	Longitude (W) o	'	"	Depth (km)	Magnitude M_L M_D	90% Confidence Ellipse Sem. Major Axes	AZ1	Velocity (m/sec)
1	5	3	14	30	32.0	29	18	13.4	95	15	21.4			1.0 km x .2 km	1	325
2	5	3	18	26	26.8	29	17	43.7	95	15	20.0			.6 km x .4 km	174	400
3	5	4	01	25	38.5	29	16	27.1	95	15	19.0			3.5 km x .4 km	108	200
4	5	10	00	27	13.2	29	16	31.9	95	16	10.6			.1 km x .1 km	63	350
5	6	5	07	06	42.3	29	16	27.5	95	15	27.9			3.3 km x 1.8 km	64	225
6	6	25	07	52	19.8	29	15	35.6	95	13	11.9			.4 km x .1 km	126	350
7	6	27	10	16	40.2	29	14	04.6	95	10	46.7			14.5 km x 1.1 km	123	350
8	7	7	08	59	17.0	29.10		31.0	95	11	44.9			24.8 km x 1.4 km	28	375
9	7	7	09	42	21.3	29	16	00.9	95	15	22.2			3.1 km x 2.0 km	1	250
10	8	20	06	54	01.8	29	16	49.3	95	15	19.6			5.3 km x 4.3 km	143	250
11	8	29	07	33	07.8	28	54	57.1	95	16	36.0			241.0 km x 5.9 km	31	350
12	8	29	08	35	13.2	29	16	10.3	95	15	19.9			.6 km x .2 km	65	300
13	9	3	12	33	39.8	29	15	59.6	95	15	25.9			2.5 km x 1.9 km	138	425
14	9	15	14	57	22.1	29	16	16.0	95	15	19.7			2.9 km x 2.1 km	93	250
15	10	14	01	51	30.1	29	16	07.4	95	15	24.9			2.3 km x 1.5 km	144	300
16	10	27	17	43	05.5	29	15	58.3	95	15	22.9			2.8 km x 1.7 km	4	225

DISCUSSION OF 1981 MICROEARTHQUAKES LOCATED USING BODY WAVES

Fifteen possible microearthquakes for which body phases were recorded in 1981 were reexamined to determine if, in retrospection, they could be discriminated positively as microearthquakes and not explosions and to relocate the events given revised earth models and phase arrival times. Five of the original fifteen events were determined to be either explosions or to have insufficient data for discrimination or relocation. Phase arrivals for the remaining ten events were retimed and hypocenters recomputed. Because the correct Poisson ratio (a measure of relative elastic parameters) for the Gulf Coast is in question, we recomputed hypocenters assuming a Poisson ratio of 0.25 (a typical value for most rock) and 0.45 (a value suggested by Lash for Gulf Coast sediments based on surface wave studies. This Poisson ratio is typical of water-saturated but relatively unconsolidated sediments.). The purpose of this exercise is to determine the best possible hypocentral solution. Since S-wave arrivals are treated as pseudo P-wave arivals in the MEHYPO algorithm, it is important to have the most representative P-wave to S-wave velocity ratio, particularly for locating events which have significant numbers of S-wave observations relative to P-wave observations. In all cases, we found that hypocenter solutions computed using a Poisson ratio of 0.25 ($Vp/Vs = 1.732$) had smaller asociated errors than those computed using a Poisson ratio of 0.45 ($Vp/Vs = 2.445$). All hypocenters reported here are smallest error solutions. The ten relocated earthquakes and their identified phase arrivals are listed in Table 7. The locations of these events are illustrated in figure 17. All hypocentral depths are constrained to less than ± 250 meters. Most of these events have small 90% confidence error ellipses, but it is important to realize this statistical uncertainty parameter is very conservative, and the computed and exact locations are likely within a few hundred meters of each other in the worst case. Seismograms of all events listed in Table 7 (except for event 6) are included in this report. These seismograms have been included to illustrate the quality of the data used in each solution. The earthquakes appear to be distributed from the surface to a depth of 6.0 kilometers. All events are apparently related to movements along the north-south trending growth fault which passes between BEG3 and BEG5 on the location maps.

-45-

Table 7. Earthquakes Located Using Body Phases During 1981

1. 81-01-01/G11700A
   03:32:29.3 +0.04
   29°15'26"N
   95°15'36.3"W
   H = 6.0, M_D =
   90% confidence error ellipse Az = 17°, a = 0.5 km, b = 0.3 km

BEG1	ePd	03:32:31.80 +0.03,
	S	03:32:33.35,
	LR	03:32:34.82;
BEG2	ePc	03:32:31.95 +0.05,
	eS	03:32:33.61,
	LR	03:32:34.87;
BEG3	ePc	03:32:31.61 +0.02,
	LR	03:32:34.57;
BEG4	eP	03:32:31.44 +0.02,
	iS	03:32:32.79 +0.02,
	LR	03:32:34.46;
BEG5	ePd	03:32:31.38 +0.02,
	iS	03:32:32.77 +0.02,
	LR	03:32:34.46

2. 81-05-12/G12421
   21:03:42.9 +0.02
   29°15'38.2"N
   95°16'04.5"W
   H = 5.0, M_D =
   90% confidence error ellipse Az = 138°, a = 3.4 km, b = 3.2 km

BEG3	iPd	21:03:44.95;
BEG4	P	21:03:44.9;
BEG5	P	21:03:44.7;
	S	21:03:45.9;
	?	21:03:46.45;
	LR	Am = 19

3. 81-05-13/G12422
   16:14:12,8 +0.19
   29°15'12.6"N
   95°16'12.0"W
   H = 1.0, M_D =
   90% confidence error ellipse Az = 26°, a = 0.9 km, b = 0.5 km

BEG3	P	16:14:14.7;
BEG4	P	16:14:14.5;
	S	16:14:15.55;
BEG5	P	16:14:14.0;
	LR	Am = 12

Table 7.   Earthquakes Located Using Body Phases During 1981 (continued)

4.   81-05-13/G12423
     16:23:33.05 +0.44
     29°14'20.5"N
     95°16'21.6"W
     H = 0 km, M_D =
     90% confidence error ellipse Az = 133°, a = 1.8 km, b = 1.5 km

     BEG3   eP   16:23:36.1,
                   S   16:23:37.95;
     BEG4   P   16:23:35.55;
                   S   16:23:37.35;
     BEG5   iP   16:23:35.3
                   S   16:23:36.65

5.   81-05-28/G12424
     13:39:02.5 +0.13
     29°17'09.7"N
     95°14'56.0"W
     H = 0 km, M_D =
     90% confidence error ellipse Az = 148°, a = 0.6 km, b = 0.3 km

     BEG2   iPc   13:39:03.95;
     BEG3   iPc   13:39:03.6,
                   S   13:39:04.5;
     BEG4   iP   13:39:04.4,
                   S   13:39:05.45;
                   D   4.5
     BEG5   iP   13:39:04.75
                   S   13:39:06.0

6.   81-06-20
     20:57:20.2 +0.47
     29°16'59.8"N
     95°16'16.5"W
     H = 0.0 km, M_D =
     90% confidence error ellipse Az = 37°, a = 2.7 km, b = .7 km

     BEG1   P   20:57:21.07,
                   S   20:57:21.55;
     BEG2   P?   20:57:23.15;
     BEG3   P   20:57:22.1,
                   S   20:57:22.5;
     BEG4   LR   20:57:23.5;
     BEG5   P?   20:57:21.75

Table 7. Earthquakes Located Using Body Phases During 1981 (continued)

7. 81-06-21/G12425
    16:23:02.7
    29°17'42.8"N
    95°15'03.4"W
    H = 0.0, M_D =
    90% confidence error ellipse Ax = 155°, a = 3.7 km, b = 1.5 km

BEG1	iP	16:23:04.9;
BEG2	iP	16:23:03.95;
BEG3	iP	16:23:03.95;
BEG4	iP	16:23:05.28;
BEG5	iP	16:23:05.3

8. 81-10-02/G12426
    07:27:32.9 +0.28
    29°16'03.7"N
    95°15'26.2"W
    H = 0.0 km, M_D =
    90% confidence error ellipse Az = 0°, a = 1.3 km, b = 0.5 km

BEG1	iP	07:27:35.7,
	iS	07:27:36.4,
	LR	07:27:37.9;
BEG3	eS?	07:27:35.4,
	LR	07:27:37.35;
BEG4	eP	07:27:34.0,
	iS	07:27:34.7,
	LR	07:27:36.2;
BEG5	iP	07:27:33.95,
	iS	07:27:34.8,
	LR	07:27:36.15, Am = 4.5

9. 81-10-02/G12426
    07:27:43.9
    29°15'22.4"N
    95°15'26.6"W
    H = 0.0L, M_D =
    90% confidence error ellipse Az = 179°, a = 3.0 km, b = 0.5 km

BEG1	eP	07:27:46.7,
	S	07:27:47.6,
	LR	07:27:48.9;
BEG2	iP	07:27:46.85;
BEG3	iP	07:27:46.4,
	LR	07:27:48.5;
BEG4	iP	07:27:45.4,
	iS	07:27:45.9,
	LR	07:27:47.55;
BEG5	iP	07:27:45.1,
	iS	07:27:46.1
	LR	07:27:47.4, Am = 4.5

-48-

Table 7. Earthquakes Located Using Body Phases During 1981 (continued)

10. 81-11-05
     09:46:58.1 +1.81
     29°17'03.2"$\overline{\text{N}}$
     95°14'18.8"W
     H = 0.0, M_D =
     90% confidence error ellipse Az = 92°, a = 7.8 km, b = 1.5 km

     BEG1   eP   09:47:01.5;
     BEG2   iP   09:46:59.1;
     BEG3   iP   09:46:59.95;
     BEG4   iP   09:46:59.95;
     BEG5   eP   09:47:00.4

95° 15'

CHOCOLATE
BAYOU

CHOCOLATE
SPRINGS

LIVERPOOL

BEG 1

MISSOURI

FM 2917

NOLEN ROAD

U
D

D

PACIFIC

MUSTANG

7

BEG 2

PLEASANT

5

*10

6

BEG 3

BAYOU

RAILROAD

U
D

BAYOU

CHOCOLATE

BAYOU

BEG 5

8

BEG 4

PRIVATE

2

D U

WELL SITE

1

9

MONSANTO

29° 15'

29° 15'

3

+

PETERSON
LANDING

U
D

(2004)

4

95° 15'

SCALE 1 62500

1   ½   0   1   2   3   4 MILES

3000   0   3000   6000   9000   12000   15000   18000   21000 FEET

1   .5   0   1   2   3   4   5 KILOMETERS

GN MN

1°04'   8°
19 MILS   142 MILS

90% CONFIDENCE LOCATION
ERROR ELLIPSE

* EARTHQUAKE LOCATION

▲ SEISMOGRAPH STATIONS

⊕ TEST WELL

GROWTH FAULTS NEAR
16,000 FT. DEPTH

TEXAS

QUADRANGLE LOCATION

FIGURE 17. RELOCATED EARTHQUAKES FOR 1981 (USING BODY WAVES)

G 11907 L

-50-
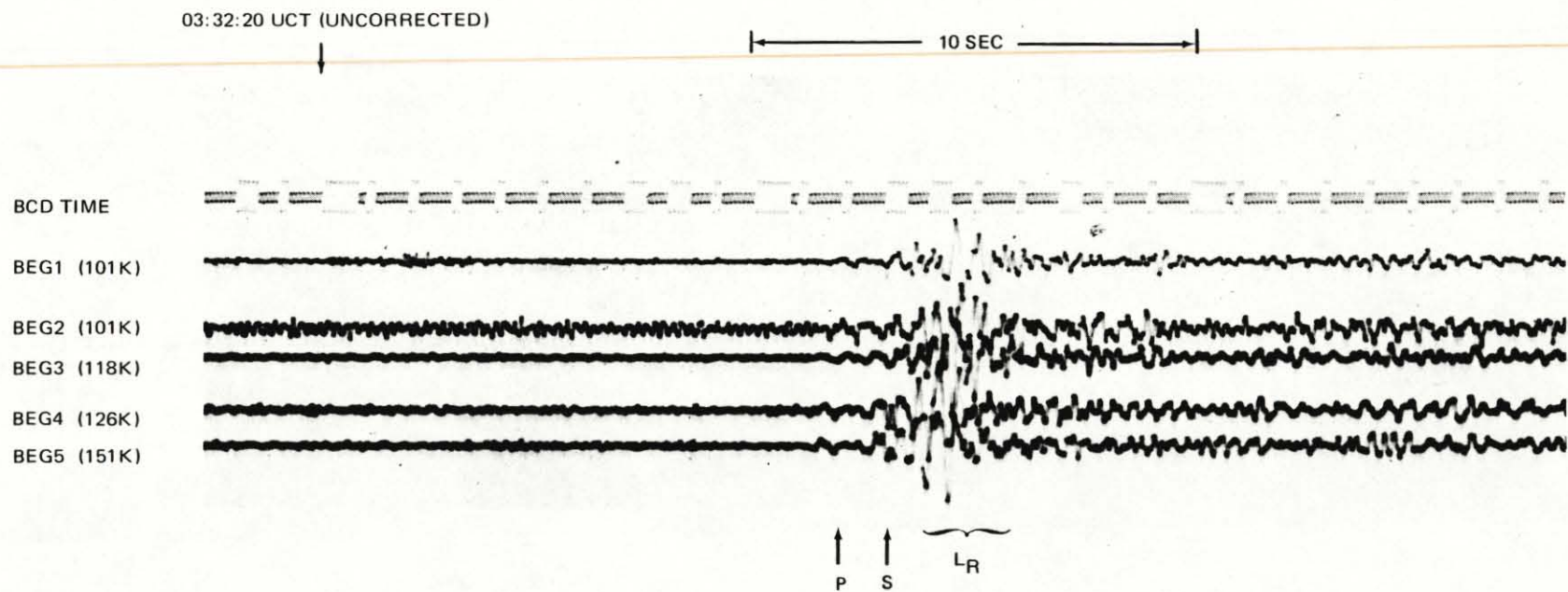
FIGURE 18. EARTHQUAKE 1 JANUARY 1981, 03:32:29.3 UCT (EVENT 1 OF TABLE 7)

G11700A
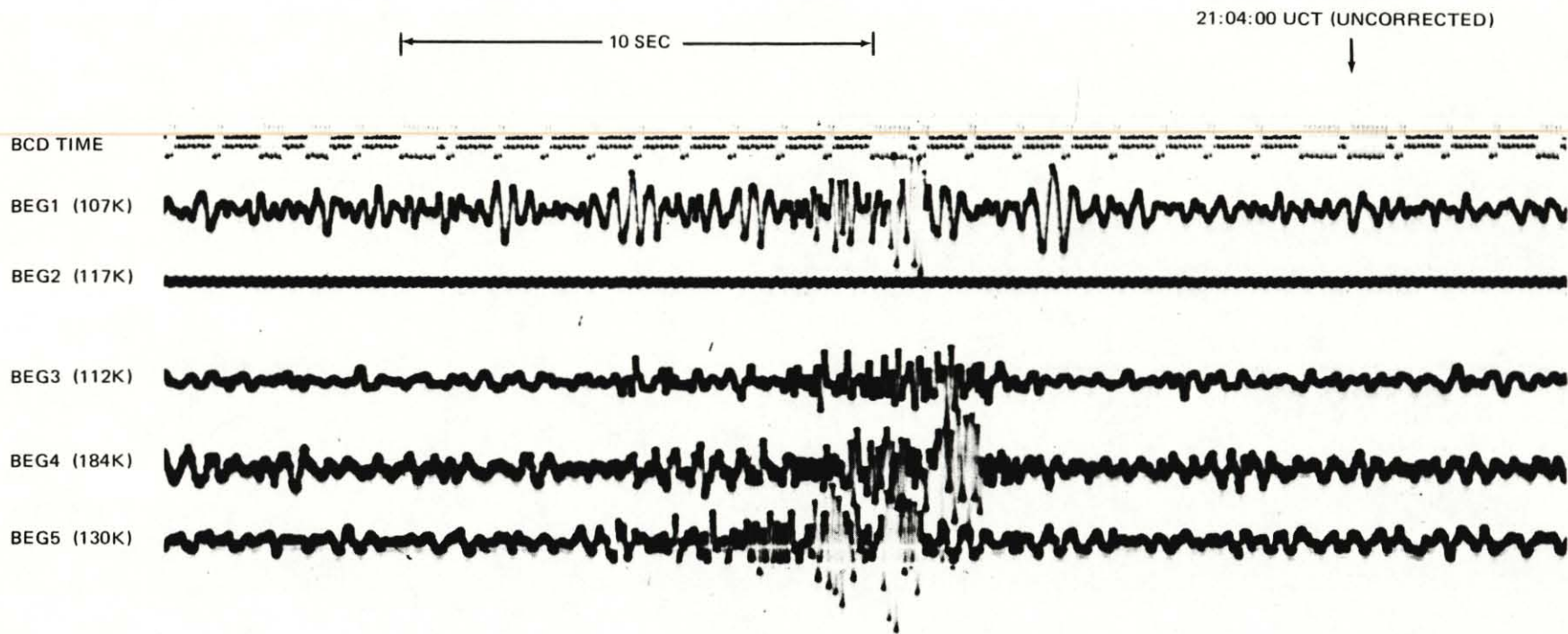
FIGURE 19. EARTHQUAKE 12 MAY 1981, 21:03:42.9 UCT, DEPTH 5 km

G 12421

FIGURE 20. EARTHQUAKE 13 MAY 1981, 16:14:12.8 UCT, DEPTH 1.0 km (EVENT 3 OF TABLE 7)
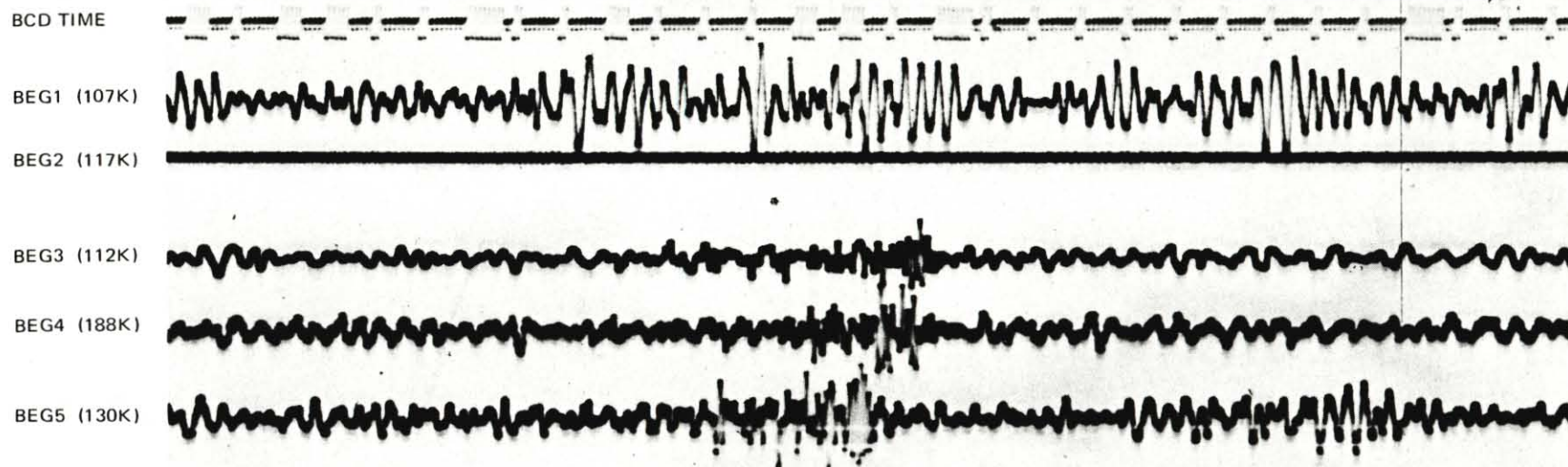
FIGURE 21. EARTHQUAKE 13 MAY 1981, 16:23:33.05 UCT, DEPTH 0.0 km (EVENT 4 OF TABLE 7)

G 12423

13: 39: 10 UCT (UNCORRECTED)

|← 10 SEC →|

BCD TIME

BEG1 (107K)

BEG2 (117K)

BEG3 (112K)

BEG4 (184K)
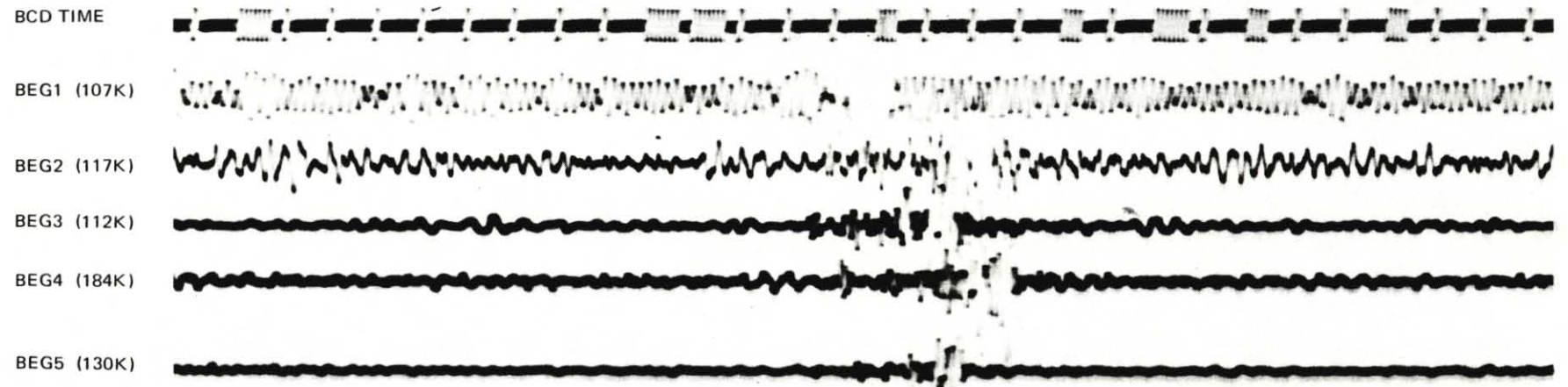
BEG5 (130K)

-55-

FIGURE 22. EARTHQUAKE 28 MAY 1981, 13:39:02.5 UCT, DEPTH 5 km (EVENT 5 OF TABLE 7)

G 12424

16:23:20 UCT (UNCORRECTED)

10 SEC

BCD TIME

BEG1 (116K)

BEG2 (136K)

BEG3 (130K)

BEG4 (128K)

BEG5 (136K)

-56-
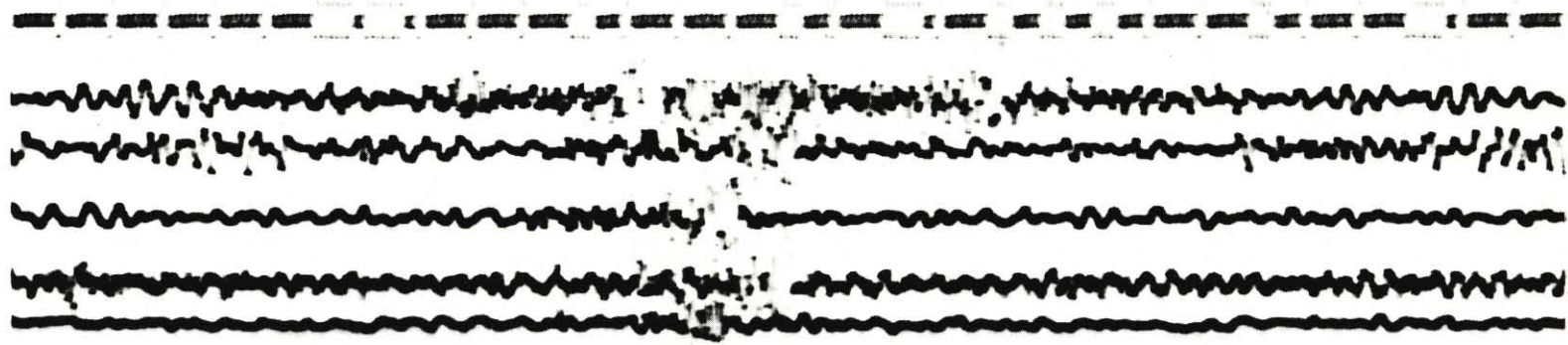
FIGURE 23. EARTHQUAKE 21 JUNE 1981, 16:23:02.7 UCT, DEPTH 5 km (EVENT 7 OF TABLE 7)

G 12425

07:27:30 UCT (UNCORRECTED)

|◄──────── 10 SEC ────────►|

BCD TIME

BEG1 (121K)

BEG2 (110K)

BEG3 (112K)

BEG4 (116K)

BEG5 (116K)
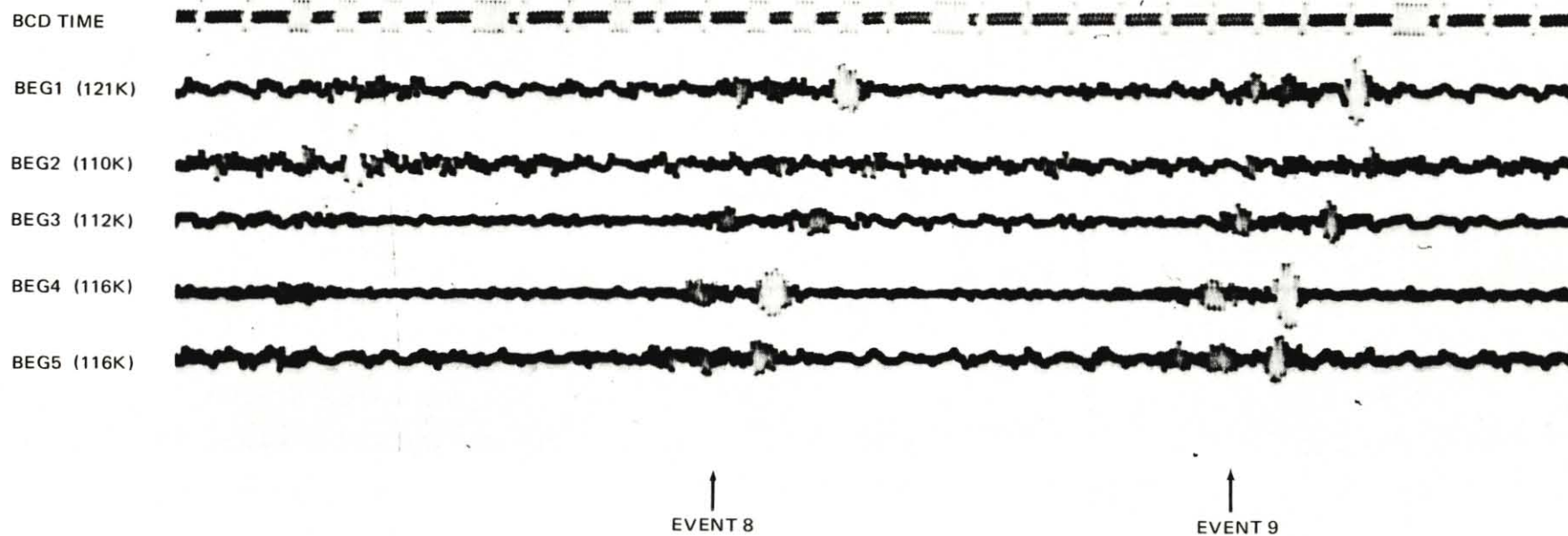
EVENT 8

EVENT 9

FIGURE 24. EARTHQUAKES 2 OCTOBER 1981 (EVENTS 8 AND 9 OF TABLE 7)

G 12426

DISCUSSION OF RUMBLE AND HARMONIC TREMOR ACTIVITY

During 1981, we began to document other types of recorded seismic activity in addition to more typical microearthquakes. The sources of these signals may be very different than those which generate more typical microearthquakes. Only more analyses of these events will yield any insight into their origin.

One type of signal recorded by the Brazoria array which is atypical of conventional microseismic events is illustrated in figures 25 and 26. We have referred to this event type as rumble. It characteristically has an emergent onset precluding normal hypocenter calculations, a duration which is variable but ranges from ten to eighty seconds, and incoherent phases across the array, although all stations will be affected by it. This type of signal has been observed throughout the recording history of the network, but it was thought initially to be some telemetry noise of unknown origin. Table 8 lists the occurrences which have been documented since May 1981. It is important to realize that this listing is complete only from August to the present. There is no a priori reason to believe that the activity was less frequent early in the network operation.

We can only speculate as to the origin of these signals. We believe that the phase incoherence across the array is an indication that these signals are generated by the coalescence of the phase arrivals from a large number of small microearthquakes which are distributed over some finite area. Thus, this type of signal may be what one should expect from a "noisy" creep as illustrated in the displacement history of figure 1. These may be typical signals generated during an episode of subsidence. An interesting experiment would be to see if the occurrences of these events correspond with long-period tilt and/or strain steps locally. During the next year, we hope to document enough of these events to proceed with further processing. At this time, the origin of these signals is unknown.

10 SEC.

093650

09 36

BEG 1 (116K)
BEG 2 (103K)
BEG 3 (130K)
BEG 4 (102K)
BEG 5 (108K)

a.

093650

09 37

BEG 1 (116K)
BEG 2 (103K)
BEG 3 (130K)
BEG 4 (102K)
BEG 5 (108K)
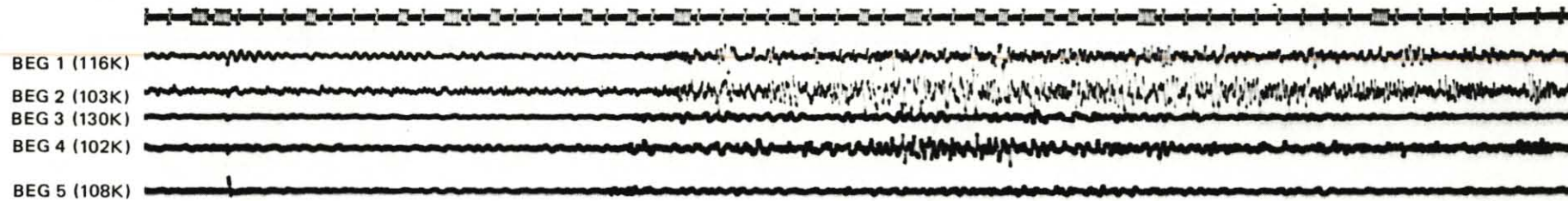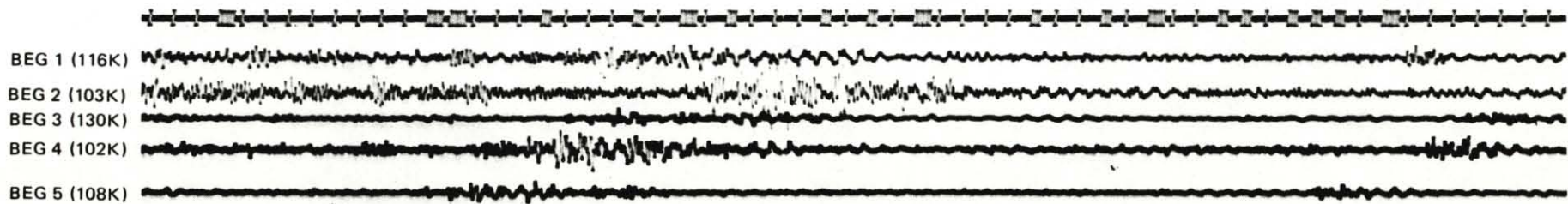
b.

FIGURE 25. EVENT 25 MAY 1981. THIS TYPE OF SIGNAL OCCURS PERIODICALLY. THERE ARE NO CLEAR ARRIVAL
ONSETS, AND, FREQUENTLY, THESE EVENTS WILL BE FOLLOWED WITH TRAINS OF ONE HERTZ WAVES
LASTING MANY HOURS. THE ORIGIN OF THESE SIGNALS IS UNKNOWN. PART B IS A CONTINUATION
OF A. WITH AN ELEVEN-SECOND OVERLAP.

G 11991
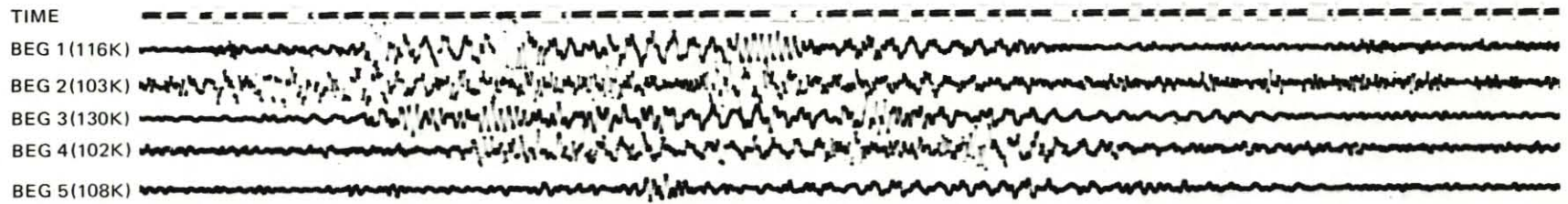
FIGURE 26. RUMBLE EVENT NUMBER 5, 15 AUGUST 1981. DURATION 50 SECONDS.

G 12175

Table 8. Occurrences of 1981 Events Identified as Rumble.

Mo	Day	Hr	Min	Duration	Amplitude
		(UCT)		(Sec)	(mm)*
5	25	09	36	60	
8	6	02	57	64	
8	15	14	26	50	
8	15	15	21	30	
8	15	15	22	45	
8	22	11	09	75	
8	31	08	19	40	
8	31	08	52	-	
8	31	08	56	-	
8	31	15	02	34	
9	8	02	08	40	15
9	8	02	10	25	
9	8	02	14	35	
10	6	08	51	20	8
10	18	11	30	25	22
10	18	11	51	15	
10	18	19	51		

* Amplitude measured P-P on develocorder film viewer (X20)

TR82-2

A second type of signal which has only been observed eight times (all sub-sequent to the phase II testing of the Pleasant Bayou No. 2 well) we have referred to as harmonic tremor. The reason for this nomenclature comes from studies of volcanoes where harmonic tremor is commonly observed prior to eruption. The characteristic of harmonic tremor which is easily identified is a nearly purely monotonic vibration which is regionally pervasive. The source of these signals at volcanoes is still debated, but it is strongly argued that these signals are generated by fluid transport through a complex conduit system. Table 9 lists the times when harmonic tremor has been observed by the Brazoria array.

Table 9. 1981 Occurrences of Harmonic Tremor

Month	Day	Approximate Onset Time (UCT)	Approximate Termination (UCT)
8	4	12:19	13:49
8	17	15:13	15:47
8	22	15:59	16:01
8	23	05:14	05:26
8	31	04:43	10:32
9	7	15:08	15:11
10	2	00:30	07:39
10	18	08:40	12:14

Two examples of this phenomenon are illustrated as figure 27 and figure 28. Although the signal level of figure 28 is significantly smaller than that of figure 27, the period of the harmonic wave is identical, 0.8 ± 0.05 seconds.

Preliminary analysis of the main eposide of harmonic tremor on 4 August 1981 from 12:19:24.7 UCT until 13:49:20 UCT has been performed using analog tape playback through a Hewlett Packard spectrum analyzer. Although the harmonic tremor appeared on all Brazoria array stations, channel 4 of the tape system malfunctioned, so analysis of the signal on BEG4 was not possible.

The spectrum analysis procedure consisted of playing the various data channels through the spectrum analyzer which digitized the analog data in eight-second blocks, bandpass filtered (Hanning or Boxcar windows) the results and displayed the RMS (root mean squared) amplitudes as a function of frequency. The spectra presented in this report are the result of integrating the amplitude data for several blocks (either linearly or exponential decay weighted).

Characteristic ambient spectra at the Brazoria array for 8 August 1981 are illustrated in figure 29a. Fourteen-minute time segments which were free from cultural and/or natural events were selected for analyses. The data for stations BEG1, BEG2, BEG3, and BEG5 were analyzed using a Hanning filter window with linear summation of the eight-second block spectra for 105 blocks. The RMS amplitude spectra for the frequency range 0 through 3 seconds are illustrated in figure 29a. All of the channels except BEG2 display RMS

├─────────── 1 MINUTE ───────────┤

BEG1 (116K)
BEG2 (103K)
BEG3 (100K)
BEG4 (102K)
BEG5 (108K)
LSU1 (51K)
LSU2 (49K)
LSU3 (51K)
LSU4 (53K)
LSU5 (53K)
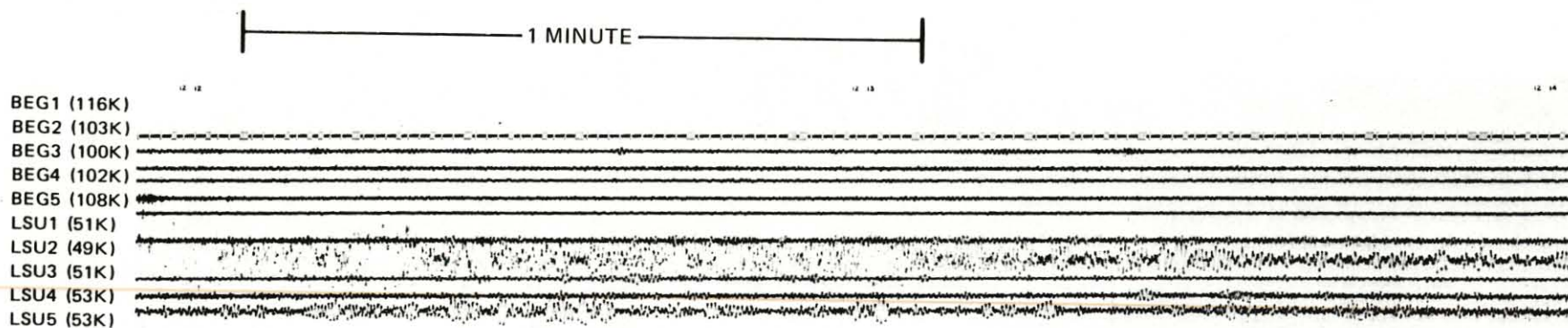
FIGURE 27a. NORMAL BACKGROUND AT THE BRAZORIA ARRAY. HIGH LEVEL NOISE AT THE
PARCPERDUE ARRAY TYPICAL WITH GULF STORMS.

├─────────── 1 MINUTE ───────────┤

BEG1 (116K)
BEG2 (103K)
BEG3 (100K)
BEG4 (102K)
BEG5 (108K)
LSU1 (51K)
LSU2 (49K)
LSU3 (51K)
LSU4 (53K)
LSU5 (53K)
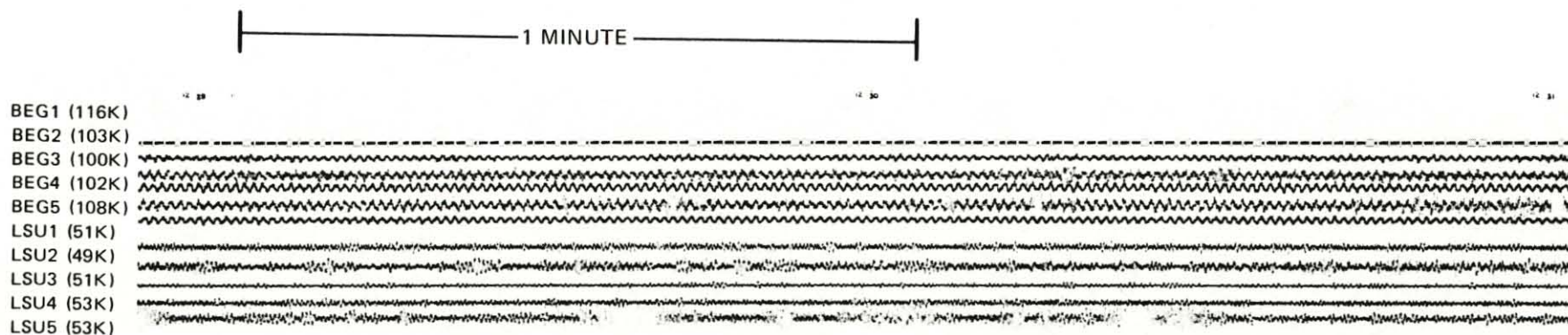
FIGURE 27b. HARMONIC TREMOR AT THE BRAZORIA ARRAY, AUGUST 4, 1981.
DURATION NINETY MINUTES FROM 12:19:24 UCT. MAXIMUM
GROUND DISPLACEMENT 6.5 NANOMETERS AT A PERIOD OF
0.8 ±0.05 SECOND.

G12176

FIGURE 28. HARMONIC TREMOR WITH THREE MICROEARTHQUAKES 2 OCTOBER 1981, 0726 – 0730 UCT

G 12290

-69-
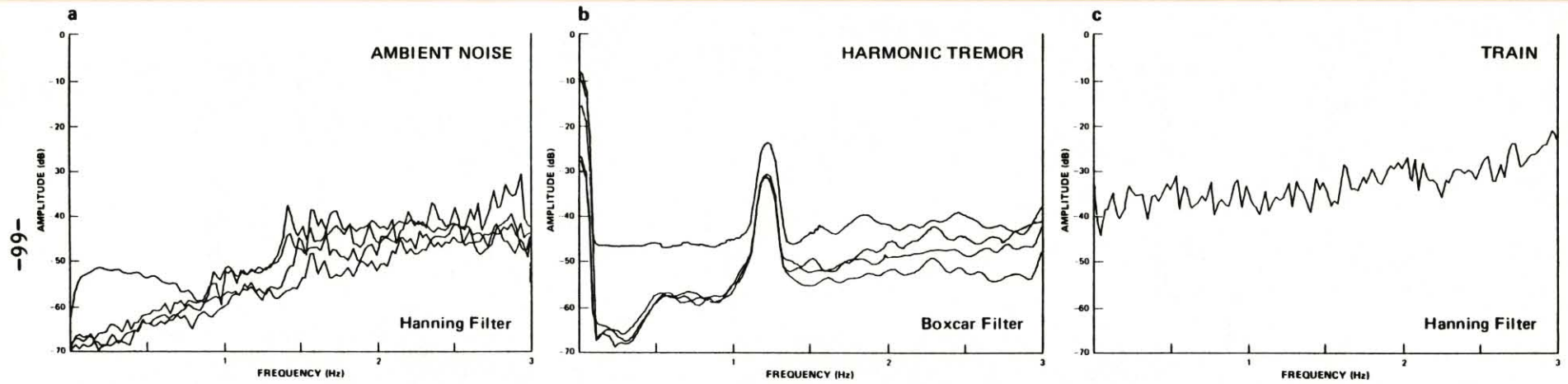
FIGURE 29. a. AMBIENT AMPLITUDE SPECTRA FOR BEG1, BEG2, BEG3, AND BEG5 FOR 8 AUGUST 1981. b. AMPLITUDE SPECTRA FOR
BEG1, BEG2, BEG3, AND BEG5 FOR 8 AUGUST 1981 FROM 12:19 THROUGH 12:35 UCT DURING THE OCCURRENCE OF THE
HARMONIC TREMOR   c. AMPLITUDE SPECTRUM FOR BEG1 DURING THE PASSAGE OF A TRAIN ON 8 AUGUST 1981. SEE
DISCUSSION FOR ADDITIONAL DETAILS.

G 12172

amplitude spectra in this frequency range which are approximately of -50 db. The general amplitude decrease with decreasing frequency is a characteristic of the instrumental frequency response. The higher amplitude lobe of energy on BEG2 at frequencies less than one hertz is caused by local drilling operations near that station. In comparison, the spectra displayed in figure 29b were obtained for a fourteen-minute analysis period beginning at 12:19 UCT on 8 August during the time of the harmonic tremor. A boxcar filter window was used rather than a Hanning filter window to improve the amplitude accuracy. This sacrificed the spectral resolution slightly which explains the more rounded appearance of spectra in figure 29b compared with those of 29a. Note that the RMS amplitude of the harmonic tremor is 20 db (10 times) above the ambient noise. The dominant frequency is 1.24 hertz, and the bandwidth is extremely narrow (indicating high selectivity of resonance or high Q, attenuation, away from the dominant resonant frequency). The offset of the spectra from BEG5 is due to higher magnification of this tape recorded channel and does not have any natural significance. This high-amplitude, narrow frequency band spectrum is also characteristic of harmonic tremor observed at volcanoes.

During the duration of the main episode of harmonic tremor on 4 August 1981, two trains passed the array. The station nearest to the tracks is BEG1. Figure 29c illustrates the spectrum of the train passage at BEG1 for comparison with both 29a and 29b. Note that the passage of a train generally increases the amplitudes throughout the frequency band from 0 to 3 hertz without producing a pronounced spectral peak at 1.24 hertz. We believe that this is additional evidence that the harmonic tremor is naturally and not culturally produced. Similarly, no teleseismic events nor Gulf of Mexico turbulence has been reported which might account for these signals; thus we conclude that these harmonic tremors which appear on all Brazoria stations are of local, natural origin.

Because the amplitude spectra illustrated in figure 29 are summed for 105 consecutive eight-second data blocks, it is not possible to resolve any temporal character of the harmonic tremor. To examine the temporal aspects of the harmonic tremor onset, the spectral analysis method was changed. The RMS amplitude at 1.24 hertz for each eight-second block weighted exponentially with the amplitudes of previous blocks was recorded for each data channel for the time period from 12:20 UCT through 12:33 UCT. The results of these analyses are graphed as amplitude versus time of the 1.24 hertz signals on figure 30. The analysis of channel 5 begins at 12:18 rather than 12:20 to illustrate onset of the first tremor episode.

The temporal variation of the recorded harmonic tremor amplitude is quite interesting. The initiation of the sustained event illustrated in figure 27 occurred in five stages. The first period of tremor began at approximately 18:30 UCT and had a duration of approximately thirty-two seconds. The cessation of the tremor was relatively abrupt even though the onset was emergent. The second period of tremor had a more abrupt onset at approximately 12:20, reaching a maximum amplitude at 12:20:20 UCT and decreasing in amplitude until it was not observable at approximately 12:20:52. The third period of tremor had an abrupt onset, (12:21 UCT), higher amplitude than either the first or second, a larger duration (80 seconds) and more gradual decay in amplitude than either of the first two periods. The fourth period of tremor

-67-
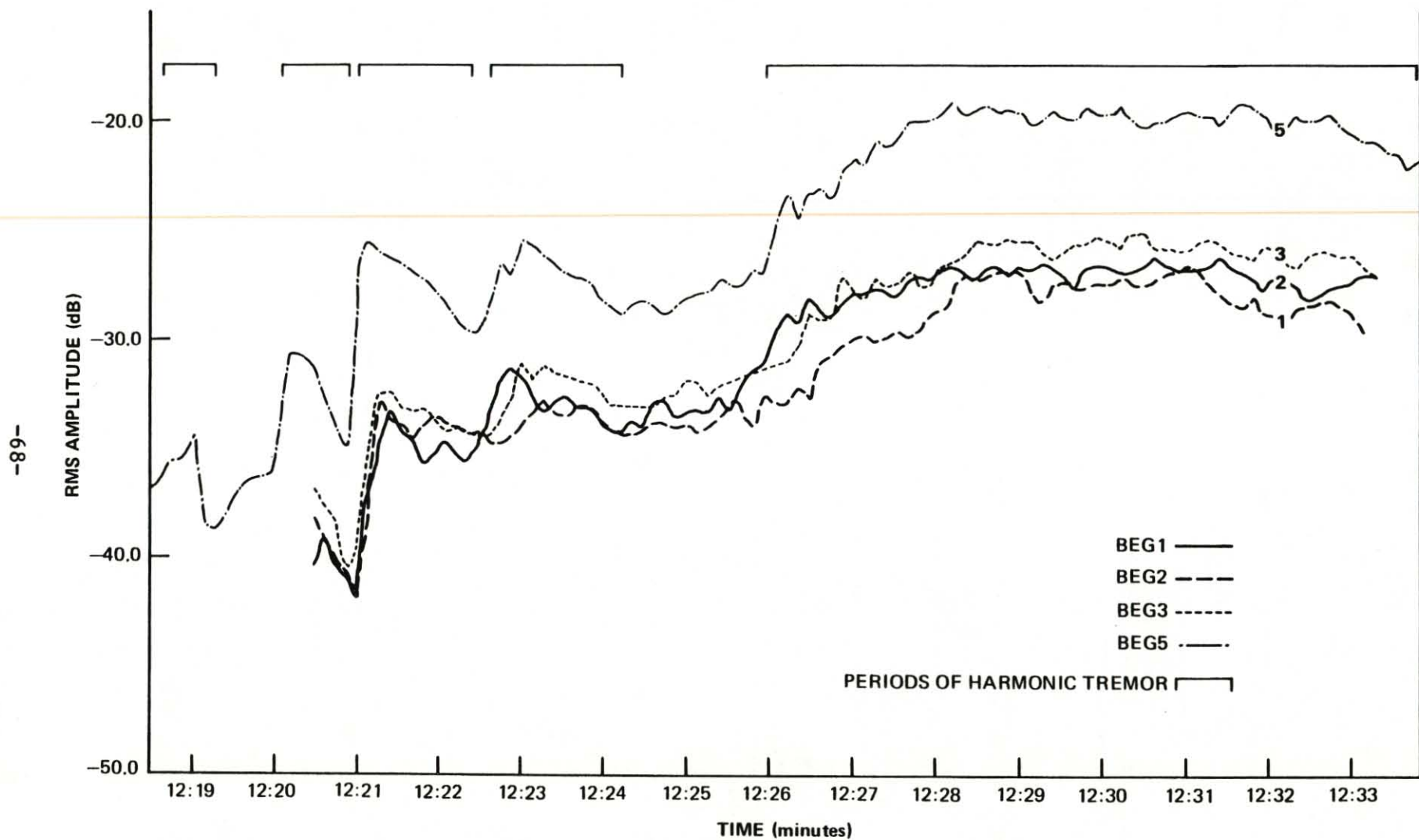
FIGURE 30. RMS AMPLITUDES GENERATED USING 8-SECOND DATA WINDOWS, HANNING FILTERED WITH EXPONENTIALLY WEIGHTED REGRESSIVE WINDOW SUMMATION

G 12173

was slightly longer in duration than the third (96 seconds), approximately the same amplitude as the third and was not separated by total quiescence from the third event as were the previous periods of tremor. Low level tremor continues from the end of the fourth period at approximately 12:24:20 until 12:25:50 when the main episode of large amplitude tremor begins. The amplitude of the main tremor period gradually increases from 12:26 UCT until 12:28 UCT where it reaches the maximum peak amplitude. The amplitude of the main episode of tremor is sustained at a high level until 12:33 when this analysis was terminated. A complete temporal analysis through 13:50 UCT will be presented in the annual technical report. The purpose of this analysis was to detail the initiation process. The results of this analysis indicate that the harmonic tremor of 8 August was begun in five separate periods. Each subsequent period was characterized by larger amplitudes and longer duration than the previous one. Thus, whatever is the source of these tremors, it is an episodic phenomenon which required at least four separate starts before the main event. This initiation behavior also strongly suggests a natural geological process. Complete analysis of this and subsequent smaller harmonic tremor episodes may improve significantly our understanding of the process which manifests itself as the harmonic tremor.

As a final preliminary analysis, cross covariance (coherency) analyses were computed for six station pairs. The analysis procedure was to linearly average the RMS amplitudes computed in the 105 eight-second time windows and then examine the coherence between the channels. Hanning windows were used to enhance spectral resolution, somewhat sacrificing amplitude accuracy. The results of these coherency estimates for the period of harmonic tremor are illustrated in figure 31. The six separate coherency estimates clearly indicate the importance of this signal across the array.

The period of harmonic tremor on 2 October may have provided a key observation to understanding the origin of the harmonic tremor. Three microearthquakes are identified on figure 28 and discussed in the previous section of this report. Shortly following these three locatable microearthquakes, the harmonic tremor episode ceased. Although this may be purely coincidental, we believe that the two phenomena are related. The occurrence of these three events evidently changed subsurface conditions which caused the source of the harmonic tremor to stop emitting energy.

A fluid-driven crack hypothesis to explain the source of harmonic tremor at volcanoes has been given by Aki, Fehler and Das (Journal of Volcanology and Geothermal Research, vol. 2, 1977, p.p 259-287) and subsequently supported by a theoretical study of Chouet (Journal of Geophysical Research, vol. 86, 1981, p.p. 5985-6016). We believe this explanation for harmonic tremor at the Brazoria array is equally applicable.
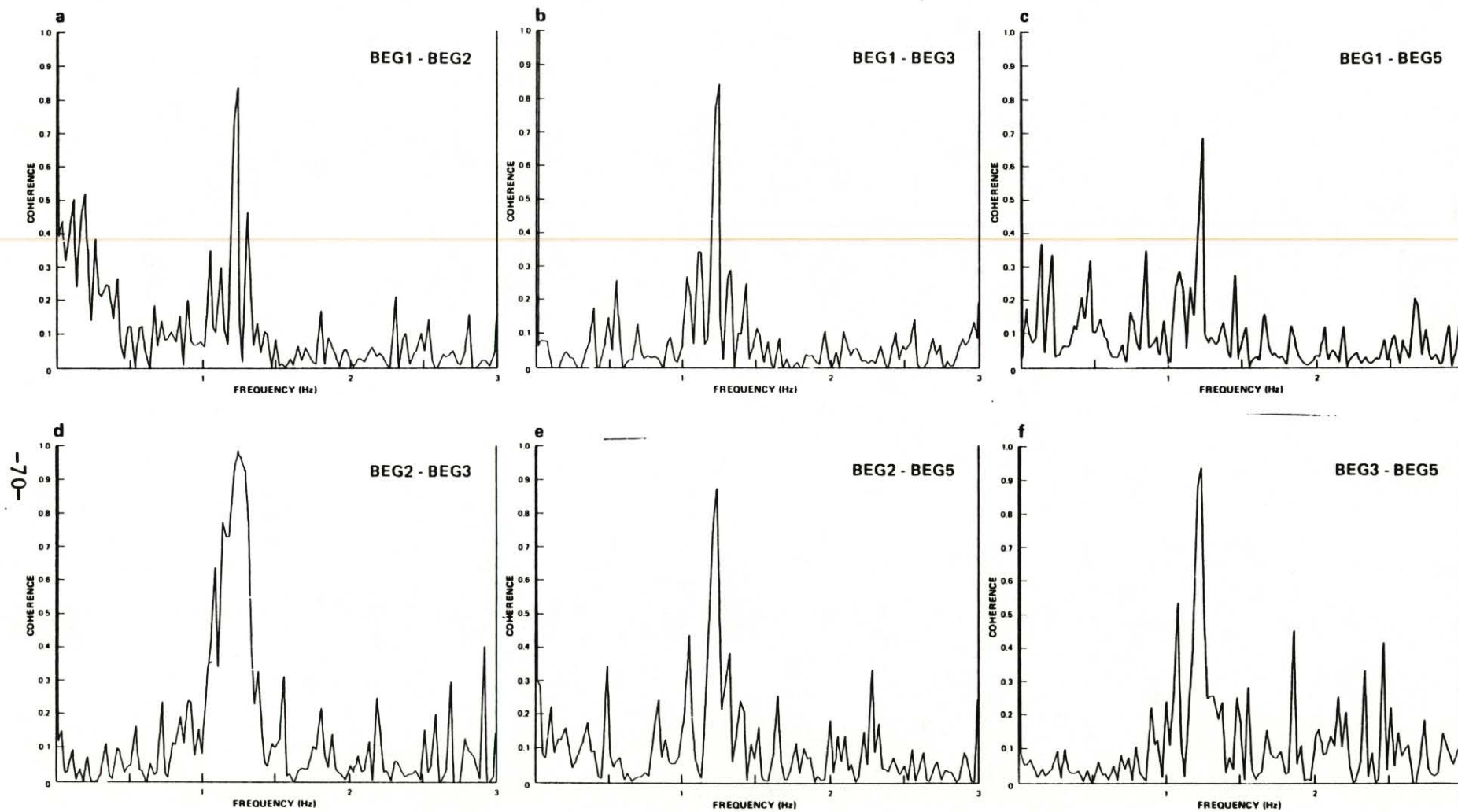
FIGURE 31. CROSS COVARIANCE SPECTRA FOR SIX STATION PAIRS AT THE BRAZORIA ARRAY DURING THE OCCURRENCE OF THE HARMONIC TREMOR 8 AUGUST 1981. a. BEG1 AND BEG2, b. BEG1 AND BEG3, c. BEG1 AND BEG5, d. BEG2 AND BEG3, e. BEG2 AND BEG5, f. BEG3 AND BEG5. SEE DISCUSSION SECTION FOR ADDITIONAL DETAILS.

G 12174

Figure 32 illustrates in block diagrams what may occur to cause the harmonic tremor. Figure 32a illustrates a faulted reservoir. For simplicity, it is assumed that the permeability of the displaced sections is the same and that the fault acts as a permeability barrier to flow between the two sections under normal conditions. Because there is a depth differential between sections 1 and 2, the hydrostatic loads of the two halves, P1 and P2, will not be equivalent. Under normal circumstances, the pressure differential (P2-P1) would be insufficient to permit dilatant opening of the fault as illustrated in figure 32.

Until recently, the majority of investigations into the role of pore fluids on fault behavior have tended to emphasize the influence of fluids in shear failure such as illustrated in figure 1b. Recent studies, however, such as those of Bowden, Curran and Roegiers (Int Jour Rock Mech and Mining Sci, vol. 17, 1980, p.p. 265-279) and Gowd and Rummel (Int Jour Rock Mechan and Mining Sci, vol. 17, 1980, p.p. 225-229) which used porous rather than relatively unporous rocks, have shown that there is a complex relationship between fault behavior in porous media and both shear and hydrostatic stresses. Depending on the conditions, faults can act as permeability barriers or permeability conduits to fluid migration (dilatant behavior) without suffering shear displacements. Alternatively, the influence of the fluids may be such that they increase or retard the likelihood of shear failure (shear behavior). Aki et. al., (1977) have shown that at volcanoes, because of stress concentrations at crack tips, the amount of stress normal to fault surfaces required to cause significant dilatant opening is very small (on the order of 20 bars [290 psi]). Thus, it is possible that faulted reservoirs which are geopressured with potentially high differential pressures between fault-separated segments may be in a very nearly critical state to induce dilatant rather than shear fault behavior. Further, because the flow rate is related to the cube of the average crack aperture, an enormous volume of fluid can potentially migrate through such a dilated fault zone. We believe that the harmonic tremor observed at Brazoria is related plausibly to repeated dilatant opening of a fault and the fluid migration through the fault zone as illustrated in figure 32b. The behavior is induced by increasing the pressure differential along the fault until it exceeds some critical value. This could be accomplished by either reducing the hydrostatic load P1 on side 1 of figure 32a (drawdown), or increasing the hydrostatic load P2 on side 2 (injection). The fault would remain in an unstable dilatant state until the pressure differential drops below the critical value. At this time, the fault would again act as a permeability barrier. Although the critical pressure differential required to activate the harmonic dilatant fault behavior is unknown for the Brazoria reservior, there is some information which may help restrict the likely value.

-71-
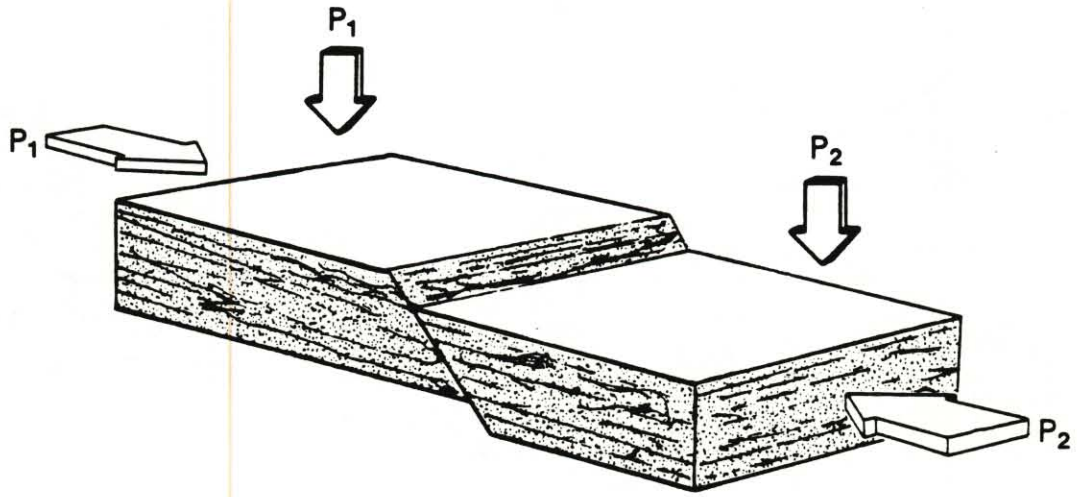
a. FAULTED RESERVOIR
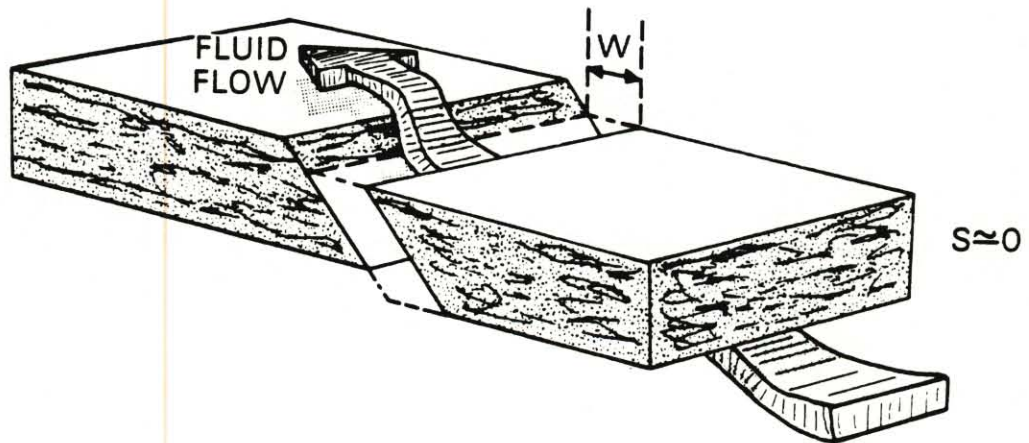
b. DILATANT FAULT BEHAVIOR PERMITTING
   FLUID FLOW
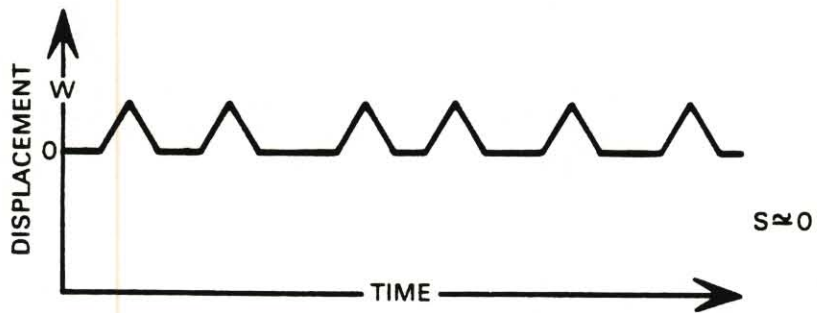
c. DILATANT DISPLACEMENT TIME HISTORY

FIGURE 32. HYPOTHETICAL DILATANT FAULT BEHAVIOR

G 12324

-72-

Figure 33 illustrates the distribution of faults and the contoured depth of the T5 horizon as mapped by the Texas Bureau of Economic Geology for the Brazoria geopressured well site. Note that the north south trending fault along the western edge of the map separates a down dropped western portion of the reservoir from the eastern portion. This fault is apparently seismically active because a large number of microearthquakes have been located in its vicinity. If fluid is to migrate from the western downdropped position of the reservior to the eastern portion, assuming the fault is normally a permeability barrier, it must do so by the circuitous path illustrated by the lower arrow. If, on the other hand, periodically the fault can conduct fluid when the pressure differential is right, then the shorter migration path of fluid from one portion of the reservoir to the other is illustrated by the upper arrow. Although we do not know from currently available data if this is the case, the argument is certainly plausible.
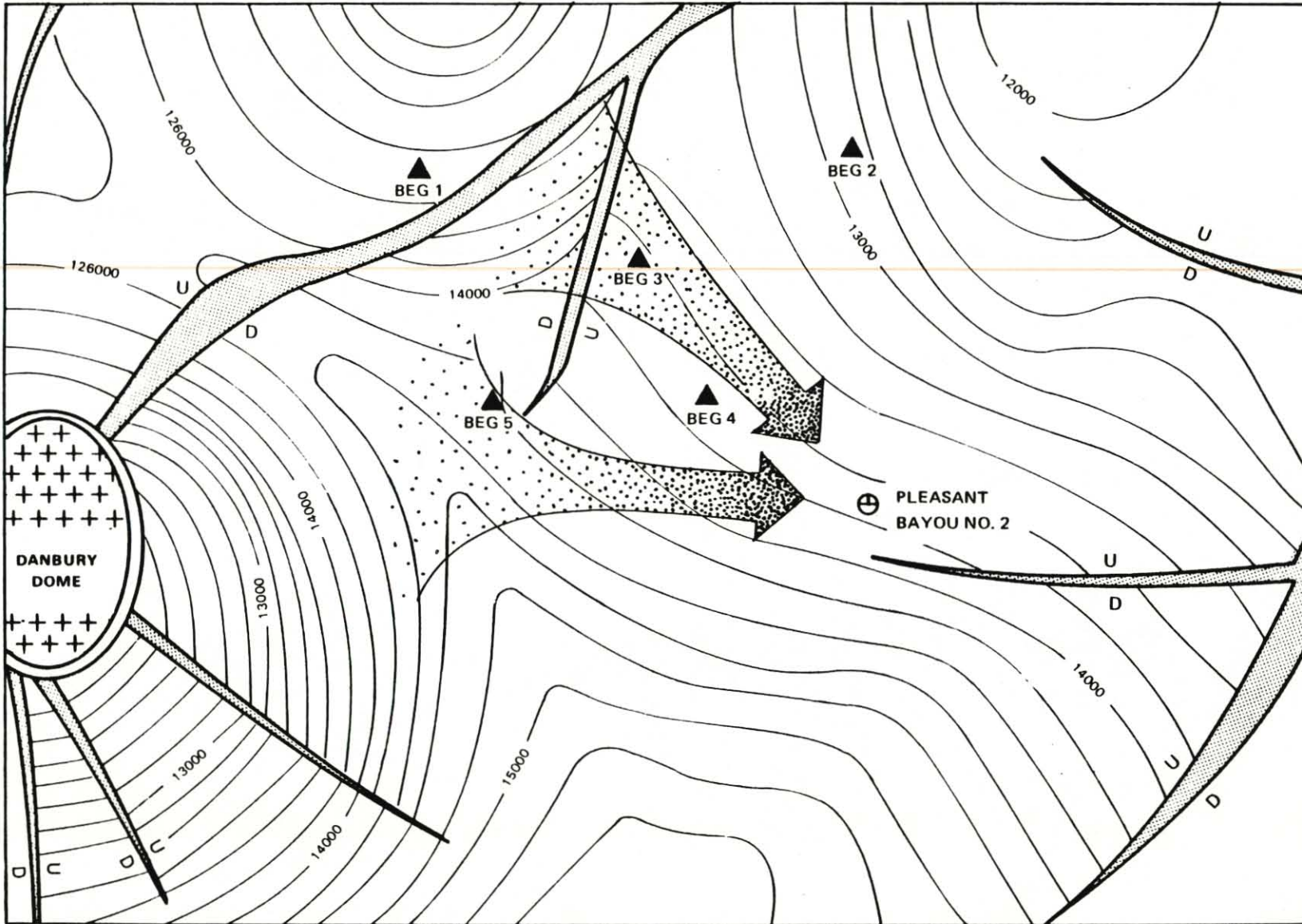
FIGURE 33. POSSIBLE FLUID MIGRATION PATHS IN THE FAULTED GEOPRESSURED BRAZORIA RESERVOIR

G 12427

Appendix I

Brazoria Louisiana Seismic Array Monthly
Develocorder Record Performance – January, 1981

Station	BEG1	BEG2	BEG3	BEG4	BEG5
Operational efficiency	98%	77%	96%	77%	98%
Total operational hours	732	573	714	574	730
Total hours of down time	12	171	30	170	14
Down time due to routine changing procedures	6	6	6	6	6
Down time due to recording system failure	5	5	5	5	5
Down time due to telemetry failure	1	0	1	0	3
Down time due to station failure	0	160 *	18 **	159	0
Other - *See explanation	0	0	0	0	0

Explanation

*   High noise level developed, then no data.

**   Recharging batteries at site.

Brazoria Louisiana Seismic Array Monthly
Develocorder Record Performance - February, 1981

Station	BEG1	BEG2	BEG3	BEG4	BEG5
Operational efficiency	99%	99%	99%	99%	99%
Total operational hours	665	665	665	665	665
Total hours of down time	7	7	7	7	7
Down time due to routine changing procedures	6	6	6	6	6
Down time due to recording system failure	0	0	0	0	0
Down time due to telemetry failure	0	0	0	0	0
Down time due to station failure	0	0	0	0	0
Other - *See explanation	1	1	1	1	1

Explanation

* Routine maintenance

Brazoria County, Texas Seismic Array Monthly
Develocorder Record Performance Log — March

Station	BEG1	BEG2	BEG3	BEG4	BEG5
Operational efficiency	98%	85%	95%	98%	84%
Total operational hours	726	630	709	726	627
Total hours of down time	18	114	35	18	117
Down time due to routine changing procedures	6	6	6	6	6
Down time due to recording system failure	12	108	29	12	111
Down time due to telemetry failure	0	0	0	0	0
Down time due to station failure	0	0	0	0	0
Other *See explanation	0	0	0	0	0

Explanation

Brazoria County, Texas Seismic Array Monthly
Develocorder Record Performance Log - April

Station	BEG1	BEG2	BEG3	BEG4	BEG5
Operational efficiency	99%	96%	99%	99%	99%
Total operational hours	713	691	713	713	713
Total hours of down time	7	29	7	7	7
Down time due to routine changing procedures	7	7	7	7	7
Down time due to recording system failure	0	0	0	0	0
Down time due to telemetry failure	0	22	0	0	0
Down time due to station failure	0	0	0	0	0
Other *See explanation	0	0	0	0	0

Explanation

Brazoria County, Texas Seismic Array Monthly
Devielocorder Record Performance Log - May, 1981

Station	BEG1	BEG2	BEG3	BEG4	BEG5
Operational efficiency	94%	51%	94%	94%	94%
Total operational hours	699	377	699	699	698
Total hours of down time	45	367	45	45	46
Down time due to routine changing procedures	10	10	10	10	10
Down time due to recording system failure	35	35	35	35	36
Down time due to telemetry failure	0	322	0	0	0
Down time due to station failure	0	0	0	0	0
Other	0	0	0	0	0

Explanation

Batteries needed charging at BEG2
Galvo contacts on BEG5 working intermittently

Brazoria County, Texas Seismic Array Monthly
Develocorder Record Performance Log – June, 1981

Station	BEG1	BEG2	BEG3	BEG4	BEG5
Operational efficiency	96%	96%	96%	94%	95%
Total operational hours	688	690	690	675	684
Total hours of down time	32	30	30	45	36
Down time due to routine changing procedures	8	8	8	8	8
Down time due to recording system failure	20	18	18	31	19
Down time due to telemetry failure	4	4	4	6	9
Down time due to station failure	0	0	0	0	0
Other	0	0	0	0	0

Explanation

Batteries needed charging at BEG2
Galvo contacts on BEG5 working intermittently

Brazoria County, Texas Seismic Array Monthly
Develocorder Record Performance Log – July, 1981

Station	BEG1	BEG2	BEG3	BEG4	BEG5
Operational efficiency	94%	70%	94%	94%	94%
Total operational hours	699	519	699	699	699
Total hours of down time	45	225	0	0	0
Down time due to routine changing procedures	10	10	10	10	10
Down time due to recording system failure	35	35	35	35	35
Down time due to telemetry failure	0	0	0	0	0
Down time due to station failure	0	0	0	0	0
Other See explanation	0	180	0	0	0

Explanation

Extreme noise on BEG2 for fifteen days occurs only during regular, weekly working hours.

Brazoria County, Texas Seismic Array Monthly
Develocorder Record Performance Log - August, 1981

Station	BEG1	BEG2	BEG3	BEG4	BEG5
Operational efficiency	98%	29%	98%	96%	98%
Total operational hours	731	219	731	713	731
Total hours of down time	13	13	13	34	13
Down time due to routine changing procedures	11.5	11.5	11.5	11.5	11.5
Down time due to recording system failure					
Down time due to telemetry failure	1.5	1.5	1.5	22.5	1.5
Down time due to station failure	0	0	0	0	0
Other See explanation	0	512	0	0	0

Explanation

Drilling within one kilometer of BEG2 creates a background noise level ten times higher than normal at that station. This totally obscures all signals at least 64% of the time. It is unknown how long this activity will continue.

Brazoria County, Texas Seismic Array Monthly
Develocorder Record Performance Log - September, 1981

Station	BEG1	BEG2	BEG3	BEG4	BEG5
Operational efficiency	89%	47%	89%	87%	89%
Total operational hours	639	338	637	626	639
Total hours of down time	81	97	83	94	81
Down time due to routine changing procedures	7	7	7	7	7
Down time due to recording system failure	74	74	74	74	74
Down time due to telemetry failure		16	2	13	
Down time due to station failure	0	0	0	0	0
Other See explanation		285			

Explanation

      High noise level on BEG2 due to continued drilling operations.

Brazoria County, Texas Seismic Array Monthly
Develocorder Record Performance Log – October, 1981

Station	BEG1	BEG2	BEG3	BEG4	BEG5
Operational efficiency	95%	90%	95%	93%	95%
Total operational hours	706	667	706	691	706
Total hours of down time	38	77	38	53	38
Down time due to routine changing procedures	37	37	37	37	37
Down time due to recording system failure	1	25	1	1	1
Down time due to telemetry failure		15		15	
Down time due to station failure					
Other See explanation					

Explanation

Brazoria Louisiana Seismic Array Monthly
Develocorder Record Performance - November, 1981

Station	BEG1	BEG2	BEG3	BEG4	BEG5
Operational efficiency	86%	86%	86%	86%	86%
Total operational hours	619	619	619	619	619
Total hours of down time	101	101	101	101	101
Down time due to routine changing procedures	11	11	11	11	11
Down time due to recording system failure	55	55	55	55	55
Down time due to telemetry failure	0	0	0	0	0
Down time due to station failure	0	0	0	0	0
Other - *See explanation	35	35	35	35	35

Explanation

* Routine maintenance: changing of develocorder galvo bank; readjusting gains and settings; polarity checks; battery charging.

TECHNICAL REPORT NO. 82-2

MICROSEISMIC MONITORING OF CHOCOLATE BAYOU TEXAS:
THE PLEASANT BAYOU NO. 2 GEOPRESSURED/GEOTHERMAL
ENERGY TEST WELL PROGRAM

1981 ANNUAL PROGRESS REPORT SUPPLEMENT:
RELATIONSHIP OF SEISMICITY TO PHASE I AND
PHASE II PRODUCTION TESTS

TELEDYNE GEOTECH
3401 Shiloh Road
Garland, Texas 75041

THE PHASE I PRODUCTION TEST

A short-term brine production test of the Pleasant Bayou No. 2 well (Phase I test) extended from 16 September through 31 October 1980. Analyses of the data to determine reservoir characteristics have been reported by Hartsock (1981) and Garg, Riney, and Fwu (1981). The production histories published by these two analysis groups are mutually inconsistent. Since the test monitoring was performed by Gruy and Associates, we have included only the published bottom hole pressure and production rate history of Hartsock (1981) (figure 1) to illustrate the Phase I production characteristics. Specific perturbations to the pressure log are numerically identified and keyed to table 1. Figure 1 illustrates that there were essentially three significant pressure declines and two pressure increases during the performance period. These correspond to times when flow rate was altered dramatically. Thus, for example, the production rate reduction from 15,324 B/D to 13,386 B/D did not constitute a significant bottom hole pressure perturbation.

The total volume of brine produced during the Phase I test was 537,300 barrels. Prior to this short-term (47 days) test, 274,000 barrels of brine had been produced from the Pleasant Bayou No. 2 well between 15 November and 3 December 1979.

THE PHASE II PRODUCTION TEST

On 2 July 1981, brine production was reinitiated in what was expected to be the Phase II long-term flow test. Because of a variety of problems with instrumentation and the Pleasant Bayou wells, the high-volume, long-term flow test was aborted on 18 July 1981.

The total volume of brine produced in the Phase II test of 2-18 July 1981 was 220,904 barrels. A plot of the brine and gas production versus flow time is illustrated in figure 2. The actual production rate history for the Phase II test is illustrated in figure 3. This figure clearly demonstrates the difficulties encountered during the test which required four significant shut-ins before the test was aborted. The corresponding production well and disposal well bottom hole pressure histories are illustrated in figures 4 and 5 respectively. Although the Phase II test of July 1981 was not successful, forty-one percent as much brine was produced in the 254 hours of flow time as was produced in the 1116 hours of Phase I flow time. Thus, the Phase II test may be more significant as a formation strain perturbation than the Phase I test.

-1-
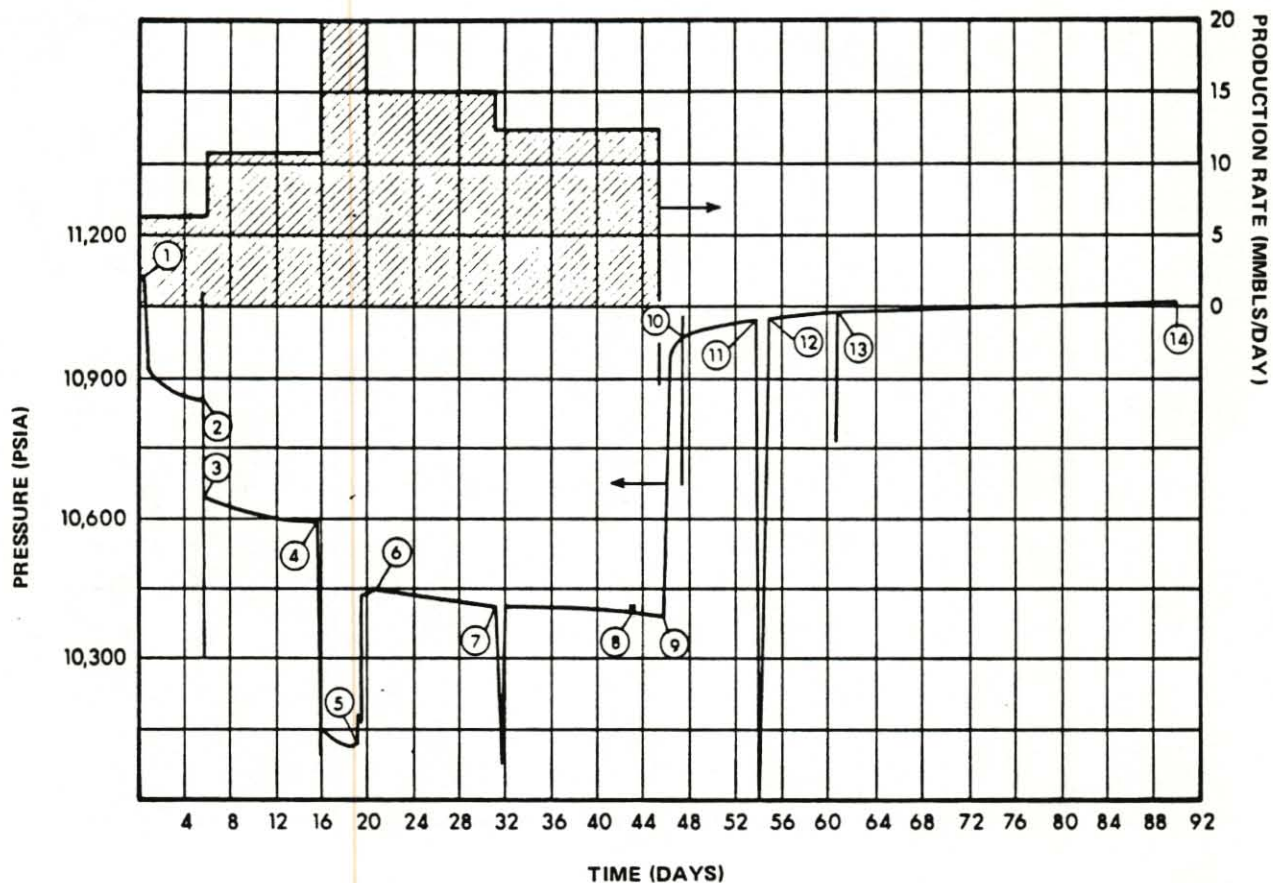
Table 1. Sequence of Events in Phase 1 Testing, Pleasant Bayou No. 2 Well

Event no.*	Date	Time hrs	Event	Event no.*	Date	Time, hrs	Event
1	9-16-80	1130	Opened well for Phase I test at 6,624 B/D	7	10-17-80	1550	Lost signal in surface recording system
2	9-21-80	1710	Well shut in to repair adjustable choke	8	10-29-80	2240	Abnormal pressure-production response
3	9-21-80	1932	Opened well for second flow rate at 10,896 B/D	9	10-31-80	1532	Well shut in to monitor pressure buildup
4	10-01-80	1102	Increased flow rate to 19,200 B/D	10	11-02-80	0940	Lost signal from HP gauge. Moved gauge and regained signal
5	10-05-80	0632	Reduced rate to 15,324 B/D to reduce injection pressure	11	11-08-80	1700	Lost signal from HP gauge. Pulled gauge, repaired, and re-ran.
6	10-08-80	1230	Reduced rate to 13,386 B/D to reduce injection pressure	12	11-10-80	0511	Gauge on bottom
				13	11-15-80	1800	Erratic pressure readings for one hour
				14	12-15-80	1304	Pulled Hewlett-Packard bottomhole pressure gauge

*Refer to Fig. 1.

FIGURE 1. BOTTOMHOLE PRESSURE VS. TIME, PHASE I TEST, PLEASANT BAYOU NO. 2 WELL

G 13032
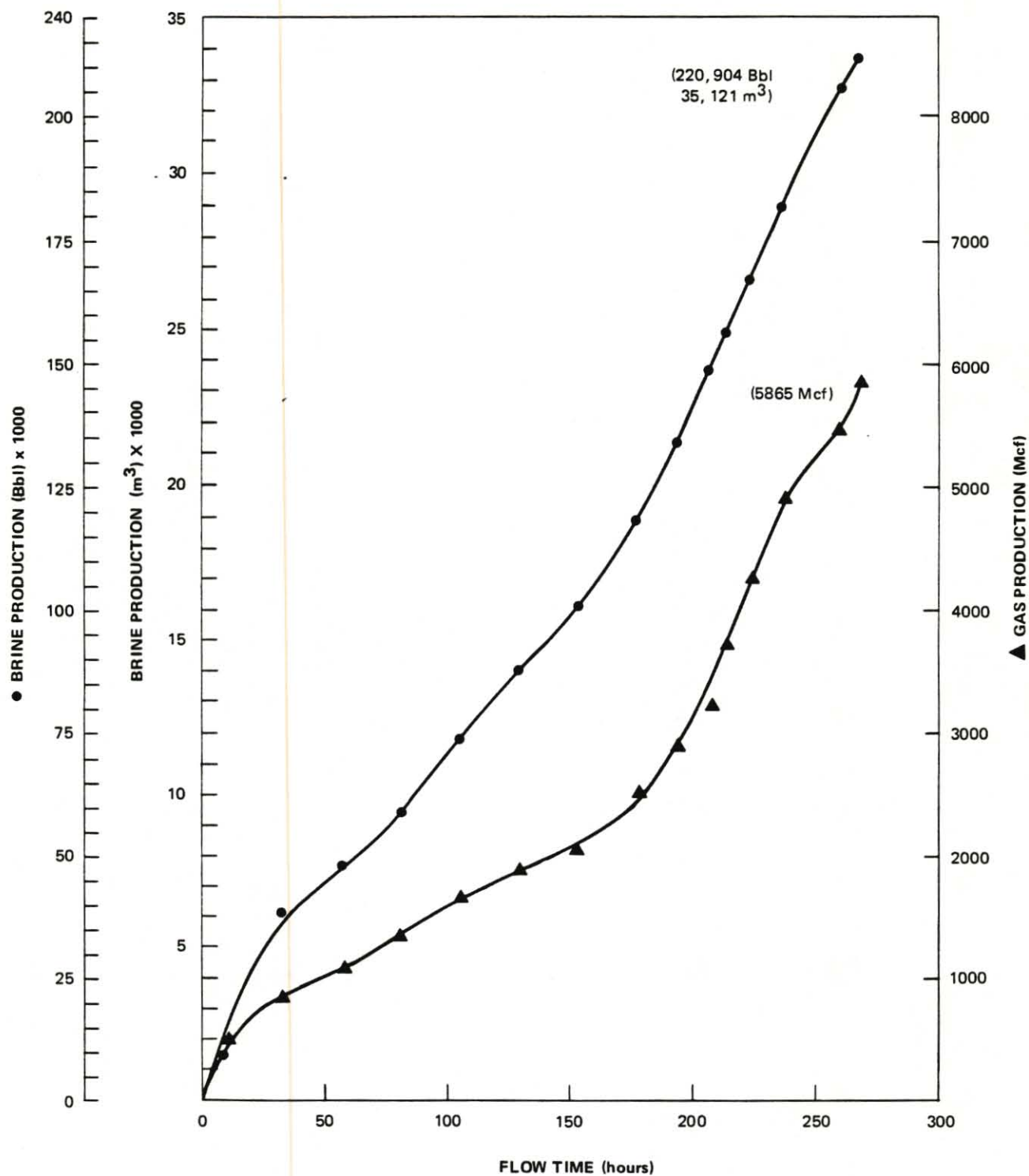
FIGURE 2. PHASE II PRODUCTION FROM PLEASANT BAYOU NO. 2 FOR THE PERIOD 2-18 JULY 1981
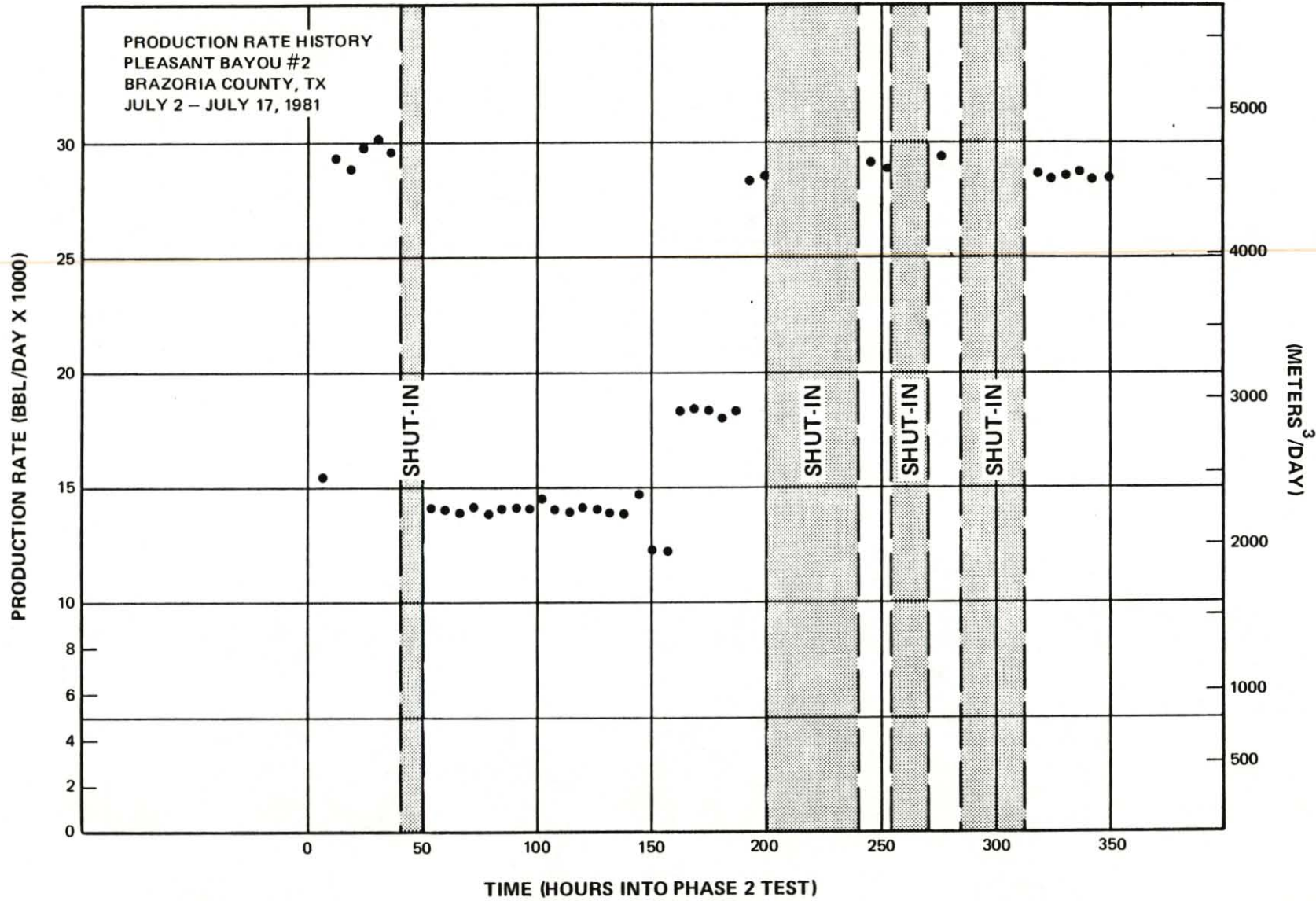
FIGURE 3. PLEASANT BAYOU PHASE II TEST PRODUCTION RATE HISTORY

-4-

G 12962
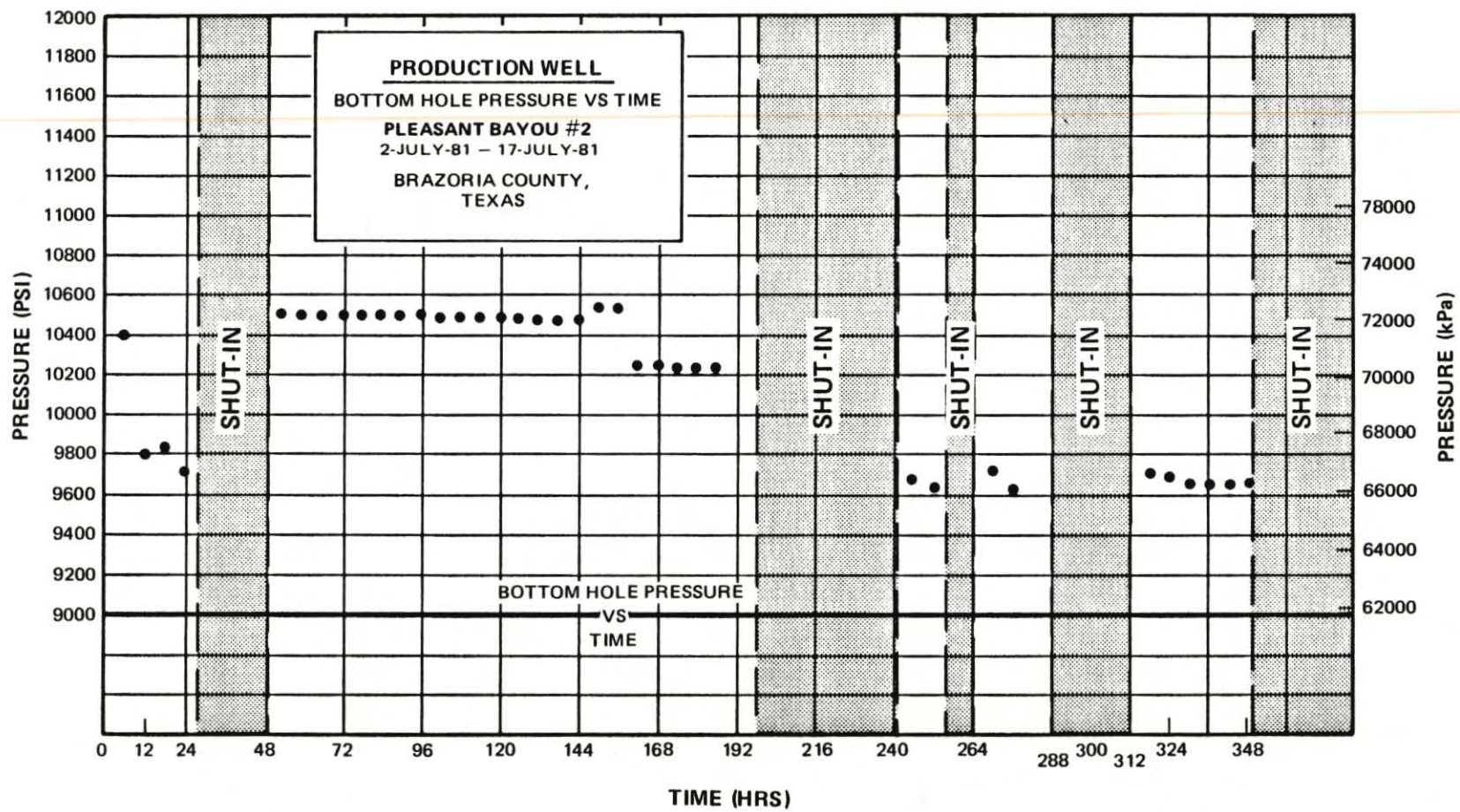
FIGURE 4. PLEASANT BAYOU PHASE II TEST PRODUCTION WELL BOTTOM HOLE PRESSURE VERSUS TIME

G 12967
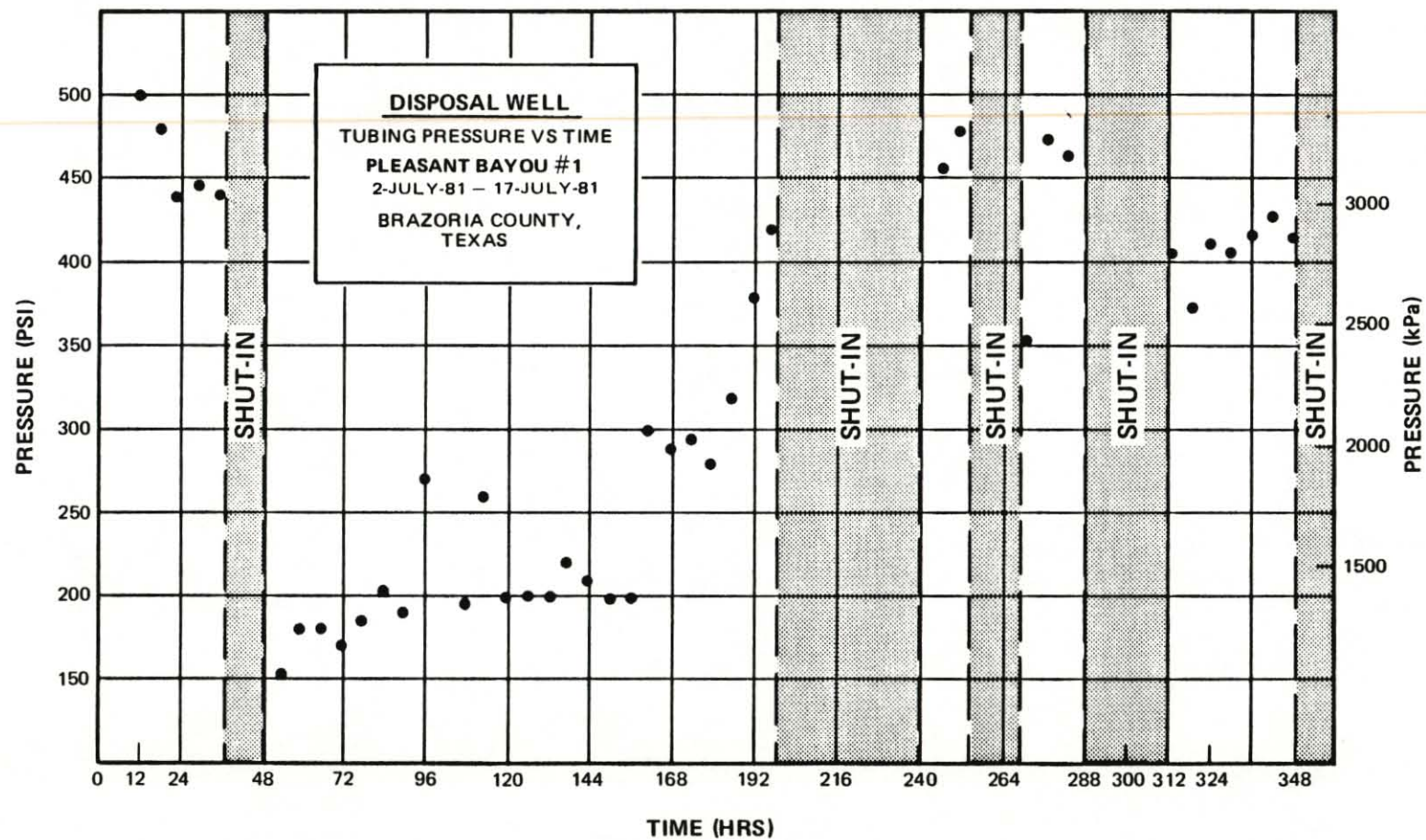
FIGURE 5. PLEASANT BAYOU PHASE II TEST DISPOSAL WELL INJECTION PRESSURE VERSUS TIME

G 12968

THE TEMPORAL AND SPATIAL DISTRIBUTION OF SEISMICITY AT PLEASANT BAYOU
DURING 1981

The temporal distribution of seismicity at Pleasant Bayou since the initiation
of the Phase I test is illustrated in figure 6. The times of the Phase I and
aborted Phase II tests are illustrated in figure 6 by brackets. Times when
flow rate was altered within each test are indicated by arrows. The seismi-
city is displayed as a histogram of the number of events per five-day incre-
ment versus time.

Qualitative examination of figure 6 reveals that the seismicity at Pleasant
Bayou is distributed unequally with time. There is only one event within the
first 230 days following the initiation of the Phase I test program. On the
other hand, there are twenty-six events clustered in the second 230 days.
The seismic activity in the period from 230 days to 420 days following the
initiation of the Phase I test is divisible similarly into two periods of
activity separated by thirty-five days of inactivity. Interpretation of a
cause/effect relationship between geopressured-geothermal well brine produc-
tion and/or disposal and earthquake activity from these data is tenuous at
best. It is obvious that, following both the Phase I and aborted Phase II
tests, there is a period characterized by no seismicity. This is par-
ticularly apparent for the Phase II test since it constitutes a gap in
ambient activity of one to two events per five-day period. Defining periods
of enhanced seismicity relative to brine production periods is not quanti-
tatively meaningful from these data. If, for example, the seismicity
beginning 230 days following the Phase I test is suggested to be related to
the well production, there is no similar clustering of activity 230 days
following the aborted Phase II test. In addition, considering that the
seismicity supposedly related to the Phase I test is perturbed by the Phase
II test, the cause/effect relationship is contaminated and unclear. Only the
activity prior to 2 July 1981 can be considered free of possible contamination
by the Phase II test.

The spatial distributions of the seismicity at Pleasant Bayou for 1981 are
illustrated in figures 7 and 8 for events located using body waves (P and S)
and surface waves (L_R) respectively. An important observation derived from
comparison of figures 7 and 8 is that events located using both body and sur-
face wave inversion techniques cluster in the same region. This strongly
suggests that these two populations of microearthquakes are likely related
and do not reflect significantly different sources. The two event popula-
tions may reflect different source depths, but depth resolution for the body
wave inversions is extremely poor, and nonexistent for the surface wave
inversions, so this is only a speculative conclusion. Since there is no
obvious reason to separate the body wave and surface wave event populations,
they are treated as a single seismicity distribution.

-7-
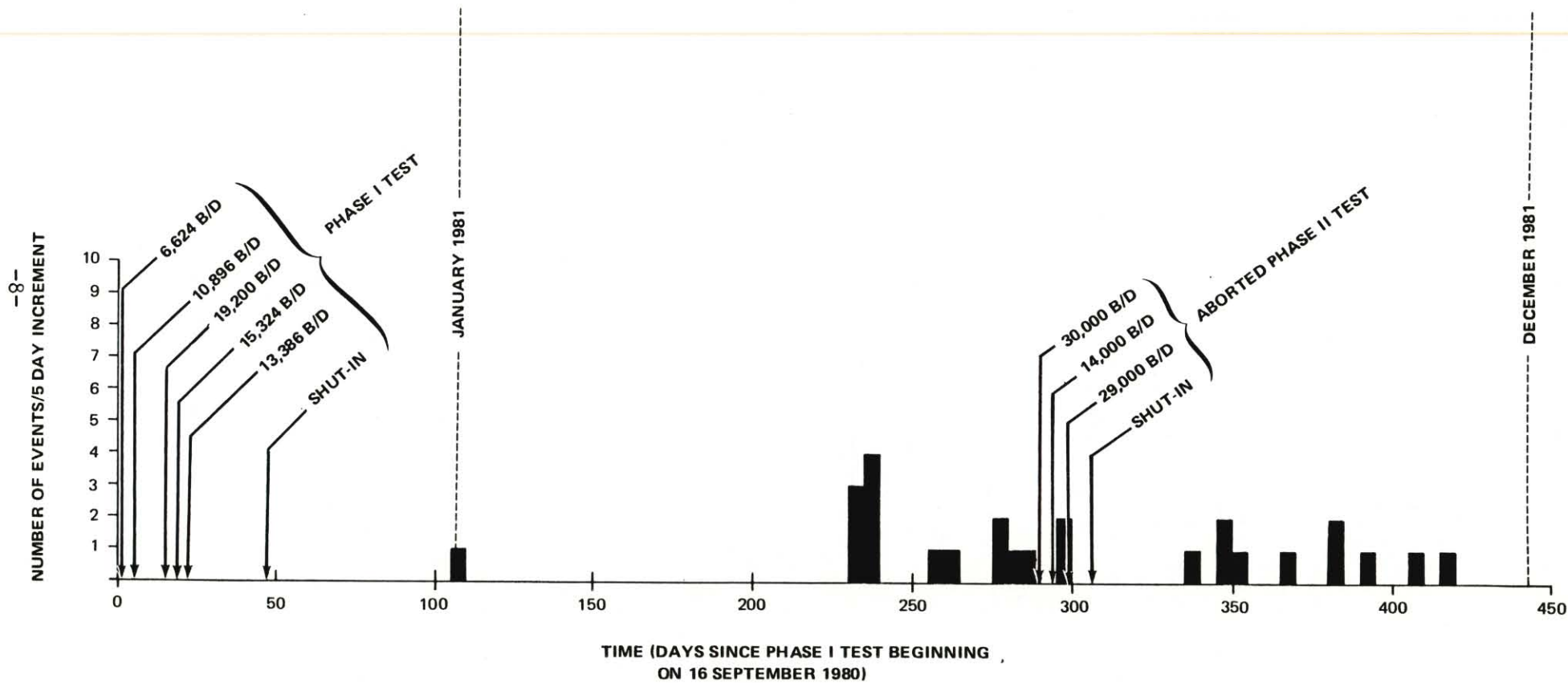
FIGURE 6. TEMPORAL DISTRIBUTION OF SEISMICITY AT PLEASANT BAYOU DURING 1981

Supplement TR 82-2

G 13030
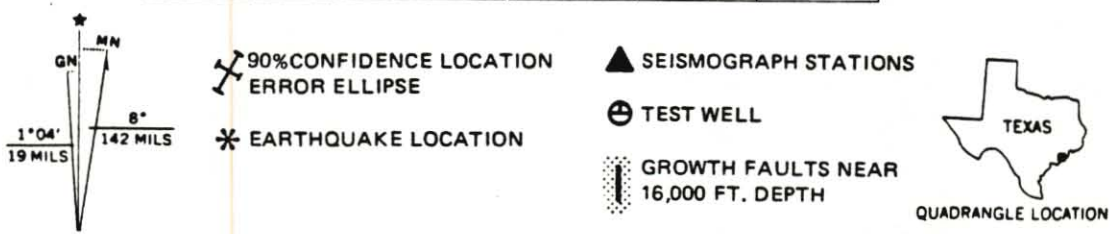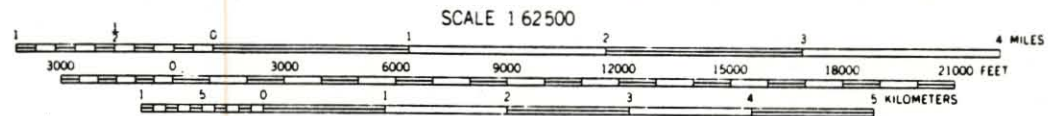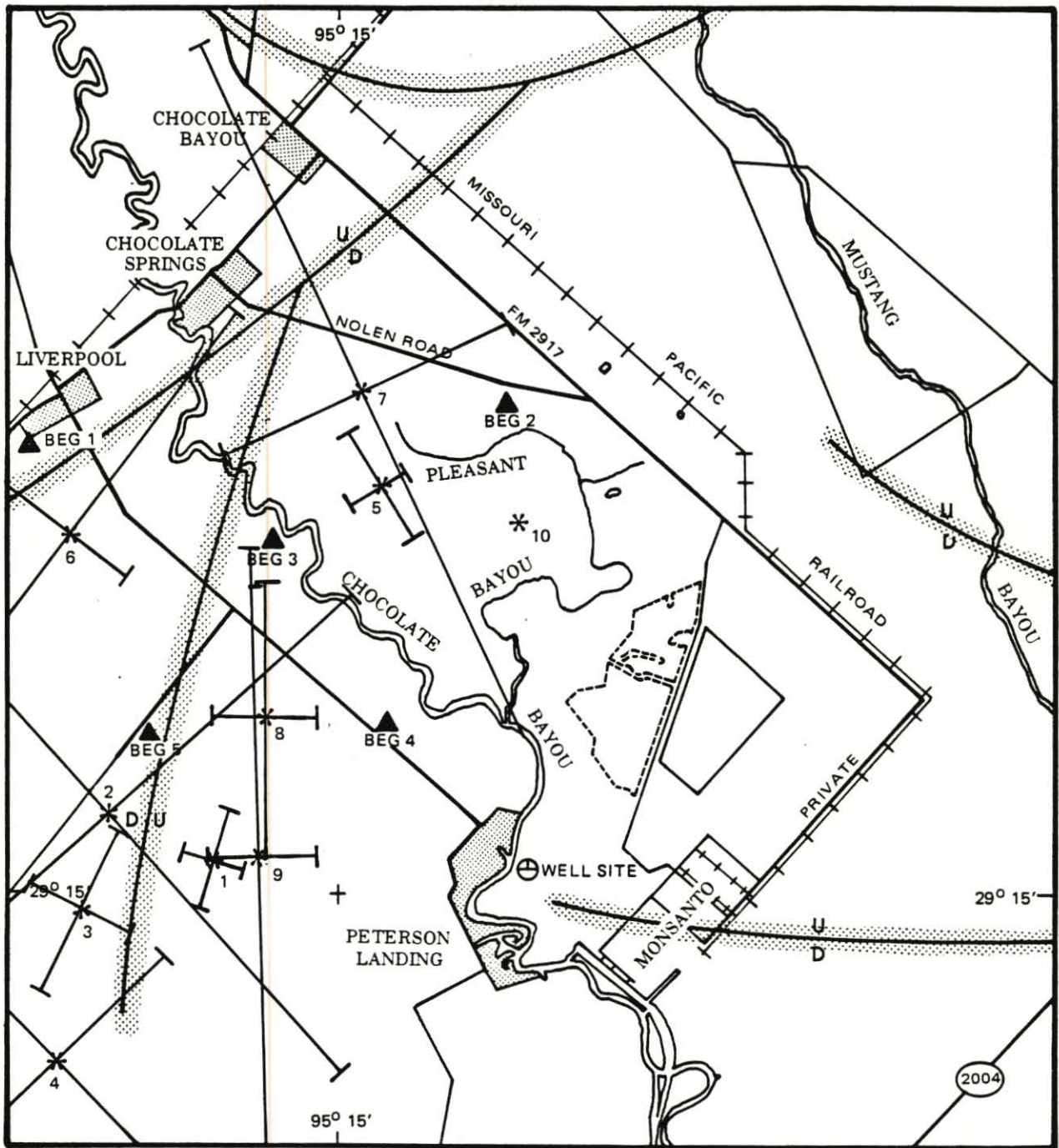
FIGURE 7. RELOCATED EARTHQUAKES FOR 1981 (USING BODY WAVES)
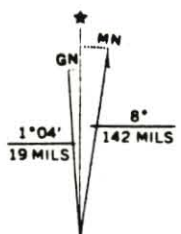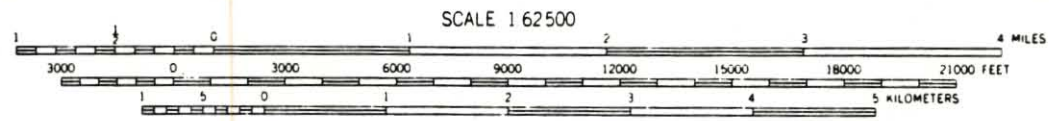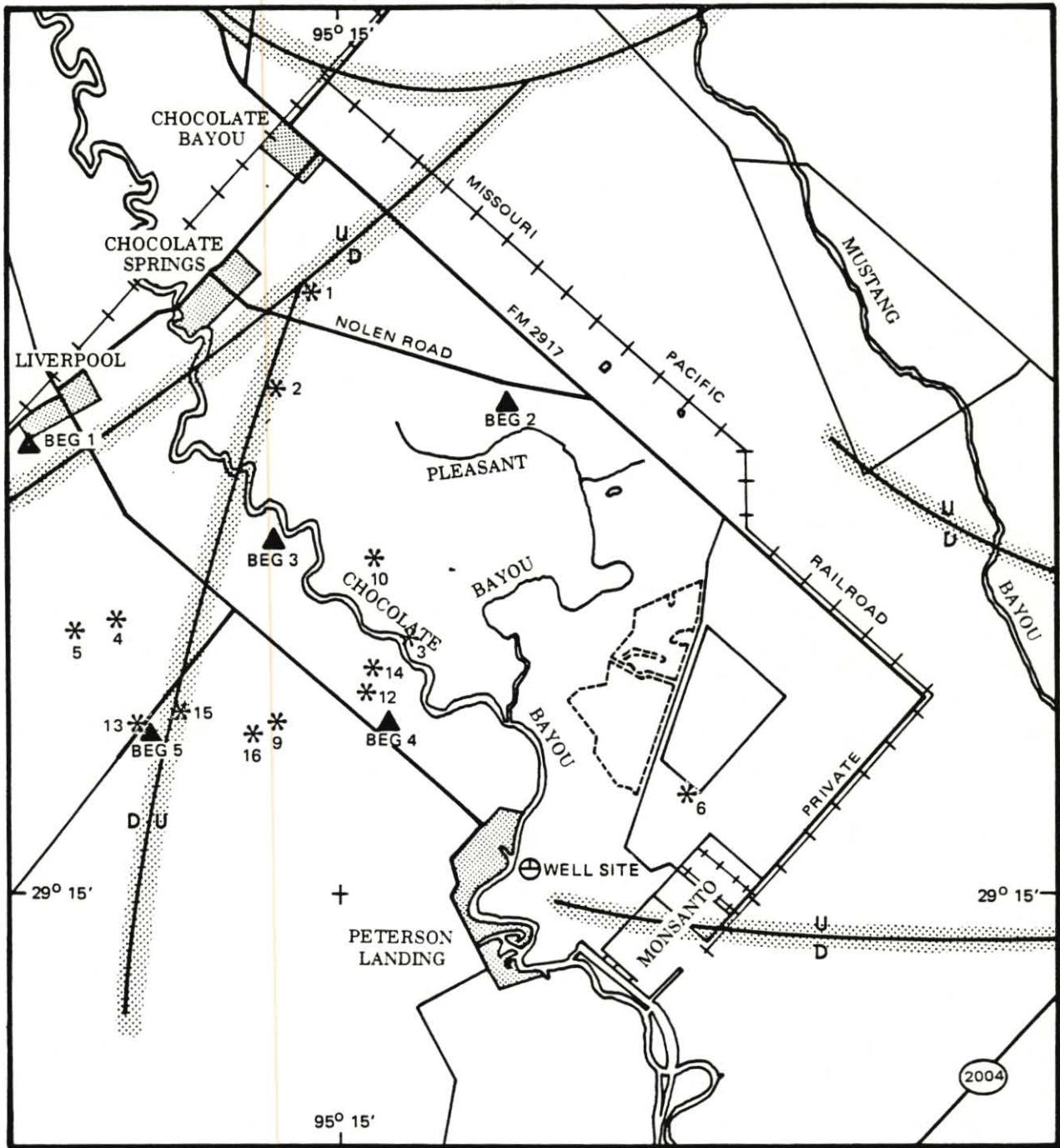
G 11907 L

-9-

FIGURE 8. 1981 EVENTS RELOCATED USING SURFACE WAVES

G 11907K

The distance between the centroid of the seismicity population and the
Pleasant Bayou No. 2 and No. 1 wells is approximatley 3600 meters. The tem-
poral centroid of the first seismicity cluster is approximately 265 days
after the Phase I test. If this seismicity is related to the Phase I test,
then it can be concluded that the strain pulse diffusion rate is approximately
fourteen meters per day. Whether or not this number is meaningful is
definitely questionable. It is apparently larger than expected fluid dif-
fusion rates for either the production or injection horizons but not by an
order of magnitude. Thus, the seismicity observed in 1981 may be related to
the geopressured-geothermal well test of 1980. Alternatively, the seismicity
may be a random process unrelated to the well tests at all. At this time,
the data are insufficient to exclude this possiblility.

In summary, the results of the microseismicity monitoring program at the
Pleasant Bayhou geopressured-geothermal well are inconclusive. The possibil-
ity that high-volume production and/or disposal of brines can result in
enhanced seismic activity is unknown because results from the Phase I and
aborted Phase II tests are neither mutually consistent nor exclusive.
Seismic activity at Pleasant Bayou following the Phase I test is strongly
distributed toward the latter half of 1981 and is not uniformly distributed
with time. At this time, it is unknown if the seismicity is related to the
test production programs. If the seismicity is related, it is unknown
whether the seismicity is related to withdrawal or reinjection procedures.
Because of the character of the recorded microearthquakes, we believe that
the events are of shallow origin and, therefore, more likely associated with
injection rather than withdrawal of the brines. This is a fundamentally
important question to be resolved which can be addressed most effectively
using numerical modeling procedures. Hopefully, additional testing, moni-
toring and analyses will result in more definitive characterization of the
potential seismic hazard associated with development of this alternative
energy resource.

REFERENCES

Hartsock, J. H. (1981), 'Test Prognosis and Actual Test Performance of the Pleasant Bayou No. 2 Well', in Proceedings of the Fifth Conference Geopressured-Geothermal Energy: U.S. Gulf Coast, Edited by D. G. Bebout and A. L. Bachman, Louisiana State University, Baton Rouge, Louisiana pp 91-95.

Garg, S.K., T. D. Riney, and J. M. Fwu (1981), 'Analysis of Phase I Flow Data from Pleasant Bayou No. 2 Geopressured Well', in Proceedings of the Fifth Conference Geopressured-Geothermal Energy: U.S. Gulf Coast, Edited by D.G. Bebout and A.L. Bachman, Louisiana State University, Baton Rouge, Louisiana, pp 97-100.

Supplement TR 82-2